The stem cell transcription factor SOX2 is essential for astrocyte maturation and controls animal hyperactive behavior

Sheng Zhang
University of California, Davis https://orcid.org/0000-0002-0692-8999
Zhaohui Lan
University of California, Davis
Yan Wang
University of California, Davis
Bokyung Kim
University of California, Davis
Fuzheng Guo (fzguo@ucdavis.edu)
University of California, Davis https://orcid.org/0000-0003-3410-8389

Article

Keywords: SOX2, Sox2-deficiency, astrocyte, brain development and behavior

Posted Date: July 30th, 2020

DOI: https://doi.org/10.21203/rs.3.rs-43277/v1

Title- The stem cell transcription factor SOX2 is essential for astrocyte maturation and controls animal hyperactive behavior

Authors and affiliations: Sheng Zhang, Zhaohui Lan, Yan Wang, Bokyung Kim, and Fuzheng Guo

Institute for Pediatric Regenerative Medicine, Shriners Hospitals for Children, Northern California; Department of Neurology, School of Medicine, University of California, Davis, CA 95817

Corresponding author: Fuzheng Guo, Shriners Hospitals for Children / School of Medicine, UC Davis, c/o Rm601A, 2425 Stockton Blvd, Sacramento, CA. Email: fzguo@ucdavis.edu
ORCID: 0000-0003-3410-8389

Acknowledgements: We thank Dr. Cagla Eroglu (Duke University) for guiding synapse density quantification, Dr. Jeffrey Rothstein (Johns Hopkins University) for generously providing anti-GLT-1 antibody, and Dr. John Gray (UC Davis) for assisting electrophysiological recordings. This study is supported by NIH (R21NS109790, R01NS094559 to F.G.) and Shriners Hospitals for Children (F.G., S.Z.).

Competing interests: none

8 figures, 8 supplementary figures, 8 supplementary tables, and 2 supplementary videos

Abstract

Children with *SOX2*-deficiency develop anophthalmia/microphthalmia and display neurological impairment. Here we report an essential role for astroglial SOX2 in brain anomalies and neurological defects. *Sox2*-deficiency inhibited postnatal astrocyte maturation without affecting astroglial proliferation and population expansion. Mechanistically, we found that SOX2 directly bound to a cohort of astrocytic signature genes such as those involving in glutamate transport and that *Sox2*-deficiency remarkably reduced glutamate transporter expression and compromised astrocyte function of glutamate uptake. Behaviorally, astroglial *Sox2*-deficient mice developed hyperactivity in locomotion while their motor skills, social capability, and learning abilities were unaffected. We found that astroglial *Sox2*-deficiency results in elevated glutamatergic synapse formation and elevated excitability of striatal medium spiny neurons,

which has been shown to trigger hyperactive locomotion. Our study provides new insights into the biological mechanisms underlying brain defects in children with *SOX2* mutations and unveils a novel connection between astrocyte SOX2 and brain development and behavior.

Introduction

Loss-of-function mutations in *SOX2* gene, a key determining factor of stem cell properties, are found in about 10-20% of patients with anophthalmia or microphthalmia, a rare disorder of abnormal eye development (OMIM 206900). An increasing amount of animal studies have suggested that SOX2 in retinal cells including retinal neural stem/progenitor cells (1-3) and their progeny cells (4-6) plays essential roles in eye development, providing cellular and molecular insights into the ocular defects of *SOX2*-deficiency patients.

Children with *SOX2*-deficiency also develop extra-ocular CNS symptoms with highly variable phenotypic expression and severity such as brain developmental anomalies, seizures, and behavioral impairments, yet the underlying mechanisms remains incompletely defined. In the CNS, SOX2 is highly expressed in neural precursors and neural stem cells (NSCs) and it plays an essential role in NSC maintenance and differentiation (7). Previous studies show that constitutive SOX2 disruption in murine neural precursors and NSCs causes brain developmental defects in the embryonic and postnatal brain such as malformation of ventral telencephalon and hippocampus (8-10). Recent animal studies including our own have demonstrated that SOX2 in oligodendroglial lineage cells controls CNS myelin formation and motor function (11-14), suggesting that *SOX2* deficiency in glial cells may also involve in the brain anomalies and behavioral defects in *SOX2*-deficient children.

Astrocytes, the most abundant glial cells in the CNS, express high level of SOX2 in the developing and adult CNS (11, 13, 15, 16). Whether astroglial *SOX2*-deficiency contributes to neural developmental defects and/or behavioral impairments remains elusive. Previous study using *Cag-CreER*^{T2}:*Sox2*$^{fl/fl}$ mice has reported that SOX2 deletion does not affect astrocyte development in the spinal cord (11). In contrast, SOX2 is recently reported to regulate astrocyte maturation in the retina of *hGFAP-Cre:Sox2*$^{fl/fl}$ mice (17). However, *hGFAP-Cre* mediates gene disruption in embryonic multi-potential NSCs, NSC-derived glial/neuronal cells, and retinal Muller glia as indicated by reporter gene expression (18). Astroglial-specific SOX2 deletion paradigms are necessary to study the role of SOX2 in astrocyte maturation *in vivo*. Furthermore, much of our current knowledge of SOX2 in astrocyte development is largely based on GFAP

immunostaining (11, 17), which displays intrinsic limitations for astrocyte visualization despite its importance in assessing astrocyte maturation. The direct delineation of the role of SOX2 in postnatal astrocyte development and animal behavior is still very limited, and how SOX2 regulates astrocyte maturation is largely unknown. In this study, by employing cell-specific *Cre-loxP* mouse genetics in combination of histological, molecular, and morphological assessment, unbiased bioinformatic analysis, electrophysiological recording, and behavioral evaluation, we for the first time demonstrate that SOX2 is required for astrocyte maturation during postnatal CNS development and controls hyperactive locomotory function in mice. Astroglial *Sox2*-deficiency results in altered synapse formation and enhanced excitability of neurons in the corticostriatal circuit, which has been shown to trigger hyperactive animal behavior. Our findings suggest SOX2 functional mutations in postnatal astrocytes may also contribute to brain anomalies and neurological defects in *SOX2*-deficient children.

Results

SOX2 regulates astroglial molecular maturation and is dispensable for astroglial proliferation

Previous studies including our own have reported that SOX2 is highly enriched in astrocytes in the developing brain and spinal cord (11, 13) (Suppl Fig. 1a). By analyzing the *Sox2-CreER*^{T2}:*Sox2*$^{fl/+}$ mice (*Sox2-CreER*^{T2}, a knock-in transgene) generated in our recent study (13), we unexpectedly found that SOX2 conditionally knockout (cKO) in SOX2^{+} cells (Suppl Fig. 1b-c) significantly decreased the CNS expression of the mature astrocyte marker GFAP at both mRNA and protein levels (Suppl Fig. 1d-g), suggesting that SOX2 may play a crucial role in postnatal astrocyte maturation.

Since *Sox2-CreER*^{T2} mediates SOX2 deletion in all SOX2-expressing cells, which include astrocytes, oligodendrocytes, and NSCs, we sought to use astrocyte-specific SOX2 disruption. To this end, we generated *mGfap-Cre:Sox2*$^{fl/fl}$ transgenic mice (mGfap:Sox2 cKO) (Fig. 1a). We analyzed the spinal cord at postnatal day 14 (P14) because *mGfap-Cre*-mediated gene recombination is specific to astrocytes in the spinal cord and the recombination efficiency gradually reaches to ~80% by P14 (19). Consistently, SOX2 was ablated in ~84% of astrocytes labeled by brain lipid basic protein (BLBP) in the spinal cord of mGfap:Sox2 cKO mice at P14 (Fig. 1b). We found that the mRNA levels of astrocyte-enriched genes (*Id3, Id4, Wnt7a*, *Nwd1*, and *Sparcl1*) were significantly reduced in mGfap:Sox2 cKO mice (Fig. 1c). GFAP, which is otherwise upregulated upon astrocyte maturation, was significantly downregulated in

mGfap:Sox2 cKO mice, as demonstrated by mRNA in situ hybridization (Fig. 1d) and Western blot (Fig. 1e) assays. The number of astrocytes was not significantly different between mGfap:Sox2 cKO and control mice ($SOX9^+ALDH1L1^+$ cell density, 666 ± 33 /mm^2 Ctrl vs 607 ± 23 /mm^2 cKO, n=8 each group, P = 0.1718, mean ± s.e.m.), indicating that GFAP downregulation is less likely due to fewer astrocytes in mGfap:Sox2 cKO mice. Astrocyte maturation is concomitant with process extension; we therefore quantified the density of astrocyte major processes labeled by GFAP and ALDH1L1. Our data showed that the percent of GFAP- or ALDH1L1-occupying area among total assessed area was significantly decreased in mGfap:Sox2 cKO compared with non-Cre littermates (Fig. 1f and Fig. 1g). These data indicate that SOX2 disruption perturbs postnatal astrocyte maturation.

Next, we used time-conditional SOX2 disruption of *Aldh1l1-CreER^{T2}:Sox2$^{fl/fl}$* (Aldh1l1:Sox2 cKO) mice to study the role of SOX2 in astroglial proliferation and population expansion. Tamoxifen injections to neonatal mice at P1, P2, and P3 yielded a greater than 90% of SOX2 deletion efficiency among $BLBP^+$ astrocytes throughout different CNS regions (Fig. 2a-c). Astrocytes expand their cell population predominantly during the first two postnatal weeks by local proliferation in the cortex (20). To determine the effect of SOX2 disruption on astrocyte proliferation, we injected EdU into Aldh1l1:Sox2 cKO and control mice 2 hours before analysis at P8 (Fig. 2a) and found that the density of EdU^+BLBP^+ proliferating astrocytes (Fig. 2d) was not significantly different between Ctrl and cKO groups in the cerebral cortex and the spinal cord (Fig. 2e). Consistently, the density of total $SOX9^+BLBP^+$ astrocytes was also similar in the cortex and spinal cord between Aldh1l1:Sox2 cKO and control mice (Fig. 2f). These data suggest that SOX2 plays a minor role in controlling astrocyte proliferation and population expansion.

In agreement with defected astrocyte maturation in mGfap:Sox2 cKO in the spinal cord, the mRNA levels of astrocyte-enriched genes (*Gfap, Sox9, Id3, Gli3, Nwd1*, and *Sparcl1*) were significantly reduced in the forebrain of Aldh1l1:Sox2 mice (Fig. 2g). Of note, SPARCL1, which plays a crucial role in astrocytic regulation of synaptogenesis (21), was significantly reduced (Fig. 2h) in fate-mapped $GFAP^+EYFP^+$ astrocytes in Aldh1l1:Sox2 cKO mice compared with non-Cre control mice (Fig. 2i). Collectively, these data suggest that SOX2 regulates molecular maturation of postnatal astrocytes and is dispensable for astrocyte proliferation in the brain and the spinal cord.

SOX2 regulates astrocyte morphological maturation

Reduced GFAP and ALDH1L1-occupying area (Fig. 1e-g) suggests that *Sox2*-deficient astrocytes may develop less complex morphology compared with *Sox2*-intact ones. We crossed

membrane-bound GFP (mG) reporter (22) onto Aldh1l1:Sox2 cKO background to study the role of SOX2 in astrocyte morphological maturation. To this end, we generated *Aldh1l1-CreER*^{T2}:*Sox2*$^{fl/fl}$:mTmG (Sox2 cKO) and *Aldh1l1-CreER*^{T2}: *Sox2*$^{fl/+}$:mTmG (Sox2 Ctrl) mice. Given that astrocytic fine processes are formed primarily during the third postnatal week in the cortex (23), we deleted SOX2 at P8 and P9 and analyzed astrocyte morphology maturation at P19 (Fig. 3a). High-power confocal imaging demonstrated that mG is primarily distributed in fine processes and barely detectable in cell somas (Fig. 3b, upper). We employed IMARIS to perform 3D reconstruction of mG-labeled astrocytes (Fig. 3b, lower). Our data showed that the surface area (Fig. 3c) and volume (Fig. 3d) of *Sox2*-deficient astrocytes were significantly decreased compared with those of *Sox2*-intact astrocytes. We next used IMARIS to trace mG$^+$ processes of individual astrocytes (Fig. 3e) and found a significant reduction in the total process length (Fig. 3f), process surface area (Fig. 3g), and process volume (Fig. 3h) of *Sox2*-deficient astrocytes compared with *Sox2*-intact astrocytes. Together, our analysis indicates that *Sox2*-deficient astrocytes develop less complex morphology - smaller domain volume and surface area and less complexity of astrocytic processes inside individual astrocyte domains.

Astrocytes extend end-feet wrapping the blood vessels and participate in the functional maturation of the blood brain barrier (BBB) and blood spinal cord barrier (BSCB). We employed Evans blue dye tracing and endogenous blood-born macromolecule identification (24) to determine the effect of SOX2 disruption on the barrier integrity. We found that both Evan blue (Suppl Fig. 2a, b) and endogenous albumin (Suppl Fig. 2c, d) were absent from the neural parenchymal tissues in the CNS of mGfap:Sox2 cKO mutants, similar to that of non-Cre Ctrl mice with functional barriers. These data suggest that SOX2 plays a minor role in regulating astrocyte's barrier-forming function in the CNS.

SOX2 regulates astrocyte passive membrane properties

Compared with their immature counterparts, mature astrocytes displays characteristic low input resistance and capacitance and hyperpolarized membrane potential (25, 26). To determine the effect of SOX2 disruption on astrocyte membrane properties, we patch-clamped astrocytes in acute brain slices prepared from *Aldh1l1-CreER*^{T2}*:Sox2*$^{fl/fl}$ (Aldh1l1:Sox2 cKO) and non-Cre Ctrl mice. We disrupted SOX2 at P14 and P15 by tamoxifen injections and performed whole-cell recordings at P30-P35 (Fig. 4a) when most astrocytes are electrophysiologically mature in the normal CNS (26). We confirmed that SOX2 was disrupted in cortical astrocytes, as evidenced by lack of SOX2 expression in GFAP$^+$ astrocytes (Fig. 4b). For astrocyte recordings,

we used astrocyte-specific fluorescent dye Sulforhodamine 101 (SR101) (27) to visualize the cell bodies of cortical astrocytes in acutely prepared brain slices (Fig. 4c). Stepped voltage clamping (Suppl Fig. 3a) demonstrated that astrocytes in Aldh1l1:Sox2 cKO and non-Cre Ctrl mice displayed a nearly linear relationship between the current responses and applied voltages (I-V curve) (Suppl Fig. 3b-c). Interestingly, we found that the membrane capacitance was significantly reduced in *Sox2*-deficient astrocytes compared with *Sox2*-intact astrocytes (Fig. 4d), which is in agreement with the simpler morphology we documented (Fig. 3). Furthermore, *Sox2*-deficient astrocytes displayed significant increase in the membrane resistance (Fig. 4e) and a slightly more positive resting membrane potential (Fig. 4f). These data suggest that SOX2 promotes astrocyte maturation by regulating the passive membrane properties.

The characteristic passive conductance of astrocyte membrane is conferred mainly by the progressive expression of the inwardly rectifying K^+ channel Kir4.1 (28). The decreased slope conductance (Suppl Fig. 3c) and increased resistance (Fig. 4e) suggest that the passive conductance of *Sox2*-deficent astrocyte membrane is reduced. To explore the mechanism underlying SOX2-regulated membrane conductance, we assessed Kir4.1 expression. Western blot assay showed that SOX2 disruption remarkably reduced brain Kir4.1 expression to 37% of non-Cre Ctrl level (Fig. 4g-h). Double immunostaining with astrocytic nuclear marker SOX9 confirmed the reduction of Kir4.1 in cortical astrocytes (Fig. 4i-j). Our findings suggest that SOX2 promotes electrophysiological maturation of astrocytes presumably through regulating Kir4.1 expression.

SOX2 targets a cohort of genes that are crucial for astrocyte maturation and function

To gain molecular insights into the role of SOX2 in postnatal astrocyte maturation and function, we sought to identify SOX2-regulated target genes. We analyzed the SOX2 ChIP-seq dataset which was previously deposited to the Gene Expression Omnibus (GEO) data repository (GSE85213) (16). The dataset consists of raw reads of one input and three biological replicates of SOX2-immunoprecipitated chromatin from the adult murine cerebral cortex, where SOX2 is highly enriched in astrocytes, and, to a much lower level, in oligodendrocyte progenitor cells (OPCs) yet absent from neurons, microglia, or vascular cells (13, 14, 16). After mapping and peak-calling, 9,602 SOX2-bound sites were identified with FDR < 0.05 (Table S1), 33.6% of which were located at the upstream regions of the nearest genes and 35.8% at intronic regions (Fig. 5a). Among the 9602 SOX2-bound sites, 1059 were identified based on the peak fold-enrichment greater than 10, which were associated with 879 protein-coding and 37

microRNA-coding genes (Table S2). Motif analysis using MEME-ChIP (29) demonstrated that nearly all of these binding sites contained CAAAG sequence and its variants (*P* = 1.1e-551) (Fig. 5b) (Table S3), the canonical motif of the HMG-box transcription factor SOX2 (30, 31), indicating that these identified genomic regions are targeted by SOX2 with a very high confidence.

To provide insights into SOX2's function in astrocytes, we annotated the 1059 SOX2-bound sites using the tool GREAT (32). In agreement with a role of SOX2 in astrocyte morphological maturation, the products of SOX2-bound genes were primarily located in the ruffle, cell projection, and leading edge membranes (Fig. 5c), which are essential for astrocyte process extension during morphological maturation (33). GO analyses of molecular function (Fig. 5d) and biological process (Fig. 5e) revealed that amino acid (such as glutamate) transport activity was significantly overrepresented among SOX2-bound genes (Table S4). This is further supported by disease ontology analysis showing that epilepsy, a neurological condition in which astrocytic regulation of glutamate homeostasis is compromised (34), was significantly enriched (Fig. 5f). The SOX2-bound genes that are associated with both glutamate import and epilepsy were identified as *Kcnj10* (Kir4.1), *Slc1a2* (GLT-1), and *Slc1a3* (GLAST). In addition, SOX2 also bound to other characteristic astrocyte genes, for example, *Gfap, Apq4, Wnt7a, Ntrk2*, and *Sparcl1* (Fig. 5g-l), among which *Ntrk2* has been shown to promote astrocyte morphological maturation both *in vivo* and in *in vitro* (35).

To gain insights into the regulation of SOX2 binding, we analyzed the genomic occupancy of H3K27Ac, an epigenetic marker of active enhancers (36) and found that SOX2-bound regions were co-occupied by H3K27Ac at these genes (Fig. 5g-l), suggesting that SOX2 may activate these characteristic astrocyte-enriched target genes. To support this hypothesis, we found that *Sox2* deficiency significantly reduced the transcription of these genes in purified primary astrocytes (Fig. 5m). Taken together, unbiased ChIP-seq analysis reveals that SOX2 directly binds to a cohort of key astrocytic genes that are involved in astrocytic maturation and function.

To determine the functional significance of SOX2's genomic binding activity, we disrupted astroglial SOX2 and identified transcriptomic changes by RNA-seq. Our recent data show that *mGfap-Cre*-mediated gene recombination occurs specifically in astrocytes in the spinal cord (19), we therefore used RNA prepared from the adult spinal cord of mGfap:Sox2 cKO and non-Cre Ctrl mice for RNA-sequencing. We identified 2,342 downregulated and 1,984 upregulated differentially expressed genes (DEGs) in mGfap:Sox2 cKO (n=3) compared with non-Cre Ctrl

(n=3) mice (Suppl Fig. 4a) (Table S5). We intersected the 1059 SOX2-bound sites identified by ChIP-seq with the DEGs identified by RNA-seq and found that 30% (263/879) of SOX2-bound protein-coding genes were dysregulated, among which the majority (208/263, 79%) were downregulated whereas only 21% were upregulated (Table S2) in mGfap:Sox2 cKO compared with non-Cre control mice, suggesting that SOX2's genomic binding may act mainly as a transcriptional activator for its target genes in astrocytes.

Congruent with the role of SOX2 in postnatal astrocyte maturation, RNA-seq identified significant reduction in the mRNA of genes encoding the canonical markers of mature astrocytes (for example *Gfap, Aqp4, Aldh1l1*, and *Glul*) and the newly identified markers of mature murine astrocytes (for example *Tril, Tmem47, Timp3*, and *Asrgl1*) (37) (Fig. 5n). Astrocyte functional genes were also significantly decreased in SOX2-defciency mice, for example, glutamate transport genes *Slc1a2* and *Slc1a3* (38), synaptogenesis regulatory genes *Sparcl1* and *Megf10* (21, 39), astrocytic morphogenesis-promoting gene *Ntrk2* (35), and K^+-buffering gene *Kcnj10* (28) (Fig. 5n). Most of these mature astrocyte-enriched genes and key functional genes were directly targeted by SOX2 (Fig. 5n, asterisks). Western blot assay demonstrated the decrease in the protein level of GFAP and SPARCL1 (Fig. 5o), and Kir4.1 (gene symbol *Kcnj10*) (cf Fig. 4g-j) in the adult forebrain, suggesting a CNS region-independent role of SOX2 in regulating astrocyte signature gene expression. GO analysis of down-regulated genes revealed that axonal/dendritic/forebrain development, regulation of cell morphogenesis, and locomotory behavior were among the top over-represented biological processes (Fig. 5p, Table S6). In contrast, mitochondrial respiratory chain complex assembly and ATP metabolic process were over-represented among upregulated genes (Suppl Fig. 4b, Table S7), which was supported by the upregulation of genes encoding the mitochondrial respiratory chain (Complex I, III, IV), and ATP synthase (Complex V) (Suppl Fig. 4c, Table S8). Taken together, bioinformatic analysis of RNA-seq indicates that SOX2 disruption elicits a comprehensive molecular change during postnatal CNS development.

SOX2 regulates GLT-1 expression and astrocyte glutamate uptake

The regulation of glutamate transport identified by unbiased ChIP-seq and RNA-seq analysis prompted us to hypothesize that SOX2 regulates glutamate transporter expression and glutamate uptake in astrocytes. In the CNS, glutamate transporter 1 (GLT-1, gene *Slc1a2*) and glutamate-aspartate transporter (GLAST, gene *Slc1a3*) are the major astrocytic transporters which take up over 90% of glutamate and maintain optimal extracellular glutamate levels, thus

preventing neuronal over-excitation (38). We found that the cis elements of the mouse *Slc1a2* and *Slc1a3* had multiple SOX2-binding sites (Table S1) and that the SOX2-bound sites were also occupied by active epigenetic marker H3K27Ac (Fig. 6a, b). Since GLT-1 is the major glutamate transporter of mature astrocytes in the adult brain (40), we focused on the GLT-1 regulation by astroglial SOX2. ChIP-qPCR assay confirmed the physical binding of SOX2 at the cis elements of *Slc1a2* in purified primary astrocytes (Fig. 6a, c). To gain insights into the SOX2-GLT-1 regulation *in vivo*, we disrupted SOX2 specifically in astrocytes during the first postnatal week (Fig. 6d) and assessed GLT-1 expression in the forebrain at P21 by Western blot (Fig. 6e). Our results demonstrated a ~5-fold reduction in GLT-1 protein level in Aldh1l1:Sox2 cKO brain (Ctrl: 1.00 ± 0.19 vs cKO 0.19 ± 0.04, mean ± s.e.m.) (Fig. 6f). The diminution of GLT-1 expression was further confirmed by histological DAB staining (Fig. 6g-h). *In vitro* primary *Sox2*-deficient astrocytes proliferated normally and grew in a similar manner to *Sox2*-intact astrocytes (Fig. 6i), yet expressed lower level of GLT-1 and GLAST compared with *Sox2*-intact astrocytes (Fig. 6j). These results suggest that *Sox2*-deficient astrocytes may have compromised ability of extracellular glutamate uptake. To test this hypothesis, we performed glutamate uptake experiment by incubating DIV21 (21 days *in vitro*) $GFAP^+$ mature astrocytes (Fig. 6i) with added glutamate in the medium. Our results demonstrated that *Sox2*-deficient astrocytes displayed reduced ability of glutamate removal from the medium at 1.5 h and 4 h (Fig. 6k). Collectively, our data suggest that SOX2 regulates the expression of astrocytic glutamate transporters and its deficiency compromises the astrocytic function of extracellular glutamate removal.

Astroglial *Sox2*-deficiency does not perturb the development of motor skills, social behavior, and cognition.

Given the cellular, morphological, electrophysiological, and functional alterations of *Sox2*-deficient astrocytes, we sought to determine the behavioral output of astrocytic Sox2-deleted mice. We found that mGfap:Sox2 cKO and non-Cre Ctrl mice had comparable eye blinks when a cotton swab was brought close to the eyes and displayed similar response to light and dark (data not shown), both of which indicate that astroglial-specific *Sox2*-deficiency does not perturb animal's vision. We then used accelerating Rotarod and video-tracked CatWalk to test animal motor coordination and walk gait, respectively, and found no difference in the quantitative aspects of these two test regimes between Sox2 cKO and Ctrl groups (Suppl Fig. 5). We next employed Barnes maze to measure the effect of astroglial *Sox2*-deficiency on animal's cognition of spatial learning and memory (41) and found no alteration in the ability of spatial learning and memory of adult mGfap:Sox2 cKO and Aldh1l1:Sox2 cKO mice compared to their

non-Cre Ctrl mice (Suppl Fig. 6). Three-chamber social test was used to evaluate the social ability (sociability) and short-term social memory and novelty (Suppl Fig. 7a) and no perturbation effect of SOX2 disruption was observed in astroglial *Sox2*-deficient animals compared with non-Cre Ctrl mice (Suppl Fig. 7b-e). Collectively, the above behavioral testing paradigms indicate that astroglial SOX2 plays a minor role in the development of motor skills, cognitive ability of spatial learning and memory, and social ability and novelty.

Astroglial *Sox2*-deficient mice develop hyperactivity

Although Barnes maze test demonstrated a normal ability of spatial learning and memory, we unexpectedly found that both constitutive mGfap:Sox2 cKO and inducible Aldh1l1:Sox2 cKO exhibited a significant increase in the total travel distance and velocity compared with their respective non-Cre Ctrl mice (Fig. 7a, b), indicating that astroglial *Sox2*-deficiency results in hyperactive locomotory behavior.

To strengthen the hyperactive locomotion, we employed open field test, a classical paradigm widely used to assess locomotory activity (42). We found that adult mGfap:Sox2 cKO mice traveled significant longer distance (Fig. 7c,d) and were more active (Fig. 7e) in the open field than non-Cre Ctrl mice. The hyperactive behavior was further corroborated by testing adult Aldh1l1:Sox2 cKO mutant at 2-month old, which traveled longer distance (Fig. 7f, g) and spent more time moving around in the open field than control mice (Fig. 7h). In a separate experiment of open field test, we found that adult Aldh1l1:Sox2cKO mice were hyperactive in the vertical dimension, as evidenced by significant more bouts of sudden jumps during the testing sessions (Fig. 7i) (Video S1, Video S2). Furthermore, the hyperactive locomotory behavior was observed at 5-month old Aldh1l1:Sox2 cKO mice which had been treated with tamoxifen at P14-P16 (Suppl Fig. 8), suggesting that astroglial SOX2 is required for controlling hyperactive locomotion not only during CNS development but also throughout the adult life.

To strengthen the conclusion of hyperactivity of astroglial *Sox2*-deficient animals, we used Home Cage test paradigm to monitor the locomotory activity in a natural environment. In line with the open field results, our data showed that adult Aldh1l1:Sox2 cKO mice traveled longer distance (Fig. 7j, k) and spent more time moving (Fig. 7i). Taken together, these data convincingly demonstrate that astroglial *Sox2*-deficienct animals develop hyperactive motor function and suggest that astroglial SOX2 is required for controlling animal locomotory activity.

Astroglial SOX2 disruption results in elevated excitability of neurons in the corticostriatal circuit.

The compromised astrocytic glutamate uptake and hyperactive locomotion suggest that the synaptic events of neurons in the motor circuitry may be altered in astroglial *Sox2*-deficient mice. The corticostriatal circuit plays an essential role in motor control and its defect is linked to various neurodevelopmental disorders inducing attention-deficit hyperactivity disorders (43). Recent data have established that activating striatal medium spinal neurons (MSNs), the most abundant cell type in the striatum taking up about 95% of all striatal neurons (44), elicits hyperactive locomotory behavior in mice (45). GO analysis of our RNA-seq data suggest that locomotory behavior and synaptic development may be altered in astroglial *Sox2*-deficiency mice (Fig. 5p), so we first sought to quantify synapse density. Since the cortical projection onto striatal medium spiny neurons (MSNs) is glutamatergic (Fig. 8a), we used an IHC-based approach (46) to quantify glutamatergic synapse numbers in the dorsal striatum. To this end, we employed vesicular glutamate transporter 1 (VGLUT1) and postsynaptic density 95 (PSD95) as pre-synaptic and post-synaptic markers, respectively, and used NIH Image J to quantify the co-localization in high-power confocal images (Fig. 8b). Our data showed an increased density of co-localized puncta in the dorsal striatum of Aldh1l1:Sox2 cKO mice compared with control mice (Fig. 8c), suggesting that astroglial SOX2 controls cortical synaptic projections onto dorsal striatal MSNs. Next, we patch-clamped dorsal striatal MSNs in acutely prepared sagittal brain slices and recorded the spontaneous synaptic currents, miniature excitatory postsynaptic currents (mEPSCs) (Fig. 8d). We found that the frequency of MSNs mEPSCs, which was recorded in the presence of tetrodotoxin (sodium channel blocker) and picrotoxin (GABA receptor antagonist), was approximately 3-fold higher in Aldh1l1:Sox2 cKO mice (2.91 ± 0.62 events / sec) than that in non-Cre littermate control (0.97 ± 0.18 events / sec) (Fig. 8d, e), yet the amplitude was comparable (Fig. 8f), which is suggestive of an increased number of functional synaptic input onto striatal MSNs. We also found that the frequency (Fig. 8g) but not amplitude (Fig. 8h) of mEPSCs was significantly increased in the cortical layer V neurons projecting onto striatal MSNs.

c-Fos is an immediate early gene that is expressed in neurons following membrane depolarization, therefore its immunohistochemical signals can be used as a marker for neuronal activation (47-49). Our RNA-seq data showed that c-Fos transcript was significantly increased in astroglial *Sox2*-deficient mice (Table S5). To determine whether the protein is elevated in MSNs, we co-immunostained c-Fos and neuronal marker NeuN and found that the density of

C-Fos-positive striatal MSNs (Fig. 8i) were significantly increased in astroglial *Sox2*-deficient mice compared with non-Cre Ctrl mice (Fig. 8j). Collectively, our data suggest that astroglial SOX2 disruption results in elevated excitability of striatal MSNs, which has been shown to mechanistically underlie hyperactive locomotory behavior in mice (45).

Discussion

How astrocytes are specified and differentiated from radial glia during embryonic CNS development has been extensively investigated. However, little is known about the molecular mechanisms underlying postnatal astrocyte maturation (37, 50). Although it has been recognized for a long time that astrocytes express highly level of the stem cell transcription factor SOX2 (15, 51), its role in brain development and animal behavior remains enigmatic. In this study, by combining astroglial-specific SOX2 disruption with a series of molecular, morphological, electrophysiological, bioinformatic, and behavioral assessments, we provide experimental evidences demonstrating that SOX2 is essential for astrocyte maturation in the CNS. Astroglial SOX2 disruption impairs the expression of glutamate transporters, compromises the efficiency of glutamate uptake by astrocytes, increases the excitability of neurons in the motor circuitry, and leads to hyperactive locomotion. Our findings suggest that SOX2 functional deficiency in astroglial lineage also contributes to brain developmental and neurological impairment of *SOX2*-mutated individuals.

SOX2 heterozygous mutation is sufficient to cause ocular and extra-ocular neurological deficits in humans (52) but not in laboratory rodents (2, 53, 54). The human-mouse disparity in phenotypes is more likely due to a differential sensitivity of SOX2 between the species than an additional novel role of SOX2 that is specific to humans (55). In support of the differential sensitivity of SOX2, mice with germline SOX2 reduction to <40% of wild type level develop eye malformations (2) and brain abnormalities (10). In our study, we did not find any differences in astrocyte maturation and behavioral output of astroglial-specific heterozygous mutants (expressing ~50% of wild type SOX2 level). We therefore used homozygous mutants as an animal model to study the role of astroglial SOX2 in CNS development.

Heterozygous *SOX2*-deficient children develop cognitive disability, motor problems, and seizures. However, the cellular basis underlying the neurological dysfunction is incompletely defined. It appears that SOX2 expression in different population of neural cells controls different behavioral outputs. Previous animal study reported that mice with *Sox2*-deficiency in early neural precursor cells exhibit seizures and motor dysfunction of cycling movements (10). SOX2

disruption in Nestin-expressing NSCs causes a more restricted neurogenic defect and a progressive loss of the hippocampus (8), suggesting that SOX2 in NSCs may be responsible for cognitive disabilities given the importance of the hippocampus in cognition (56, 57). Recent studies demonstrated that mice with SOX2 deletion specifically in oligodendroglial lineage cells exhibit CNS hypomyelination and develop ataxia and motor coordination defects (13, 14). Our current findings demonstrate that SOX2 expression in astrocytes is dispensable in animal's motor skill development and learning and social ability. Very impressively, both mGfap:Sox2 cKO and Aldh1l:Sox2 cKO mice develop hyperactivity in locomotory behavior. Since SOX2 is conditionally disrupted in astrocytes yet spared in NSCs and oligodendroglial cells, our results suggest that astroglial SOX2 controls motor hyperactivity in mice. The dysregulated synapse density and elevated excitability of neurons in the corticostriatal motor circuitry provide possible explanations for the hyperactive locomotion in astroglial *Sox2*-deficient mice.

Previous study using Cag-CreER^{T2}:Sox2$^{fl/fl}$ mice reported that SOX2 plays a minor role, if any, in astrocyte maturation, evidenced by qualitative GFAP immunostaining (11). We initially employed a quantitative approach to assess GFAP expression in the Sox2-CreER^{T2}:Sox2$^{fl/+}$ mutants which were generated in our recent study of oligodendroglial myelination (13) and found a greater than 50% reduction of GFAP in *Sox2* mutant mice (Suppl Fig. 1). These contrasting data presumably reflect the methodological differences (qualitative vs quantitative) and prompt us to revisit the role of SOX2 in postnatal astrocyte development. Subsequent characterization of astroglial-specific *Sox2* cKO mutants points to a key role of SOX2 in regulating molecular maturation of postnatal astrocytes. Consistently, SOX2 deficiency results in a dramatic transcriptomic changes in the adult CNS evaluated by RNA-seq. These data suggest that SOX2 is essential for astrocyte molecular maturation. The downregulation of astrocyte signature genes in both spinal cord and brain indicates that SOX2 appears necessary for common molecular maturation in different CNS regions during postnatal CNS development.

The dispensability of SOX2 in astrocyte proliferation and population expansion (Fig. 2) is quite surprising given that local proliferation is the main mechanism underlying astrocyte population expansion in the murine brain (20, 58). In the CNS, SOX2 is a stereotypical transcription factor of NSCs and neural precursor cells and plays an essential role in the proliferation of NSCs and neural precursor cells (8, 10) and OPCs (13). The molecular mechanisms underlying postnatal astrocyte proliferation remain elusive and seem to be SOX2-independent. Alternatively, the functional redundancy of between SOX2 and SOX1/3 (12) may be accountable for normal proliferation of *Sox2*-deficient astrocytes. In contrast, a recent

study reported that SOX2 disruption in adult quiescent astrocytes inhibits their proliferation and activation in response to traumatic brain injury, which was assessed by BrdU labeling and GFAP expression (16). These data suggest that SOX2 regulation of astrocyte proliferation is context-dependent of CNS development vs injury. Even under CNS injured conditions, whether the SOX2 regulation of reactive astrocyte proliferation is specific to traumatic brain injury or generic to different types of CNS injured insults, such as inflammatory CNS injury, in which SOX2 is upregulated in all reactive astrocytes (15), remains enigmatic and warrants further study.

Consistent with molecular maturation, SOX2 is also necessary for morphological and electrophysiological maturation of astrocytes in the CNS. By utilizing membrane-bound reporter and morphological analysis, we found that *Sox2*-deficient astrocytes develop less complex process network and occupy smaller domain volume and surface area (Fig. 3). The less complex morphology is congruent with the decreased capacitance of *Sox2*-deficient astrocytes (Fig. 4d), which is directly proportional to the membrane surface area (59). Mature astrocytes are electrophiologically passive and characterized by very low input resistance (i.e. high conductance), low capacitance, and hyperpolarized resting membrane potential (25, 26). Such passive property is primarily attributed to a progressive increase in Kir4.1 channel expression during astrocyte maturation (28). Given its importance in astrocytic function, mild Kir4.1 reduction (by ~30%) is sufficient to enhance the excitability of striatal MSNs and elicit motor deficits in a mouse model of Huntington's disease (60). Interestingly, we reported that SOX2 not only physically binds to the cis-regulatory elements of the Kir4.1 gene (*Kcnj10*) but also functionally regulates Kir4.1 expression in primary astrocytes and *in vivo*. Strikingly, SOX2 disruption results in a >2-fold reduction of Kir4.1 expression in the brain (Fig. 4g-j). It is plausible that SOX2 disruption-elicited downregulation of astroglial Kir4.1 may contribute, at least in part, to the enhanced excitability of MSNs we observed.

Previous study suggests that SOX2 genomic binding is usually found around genes specifically expressed in the corresponding cells (61). Our SOX2 ChIP analysis identifies key signature genes as SOX2 targets in astrocytes, such as *Gfap, Aqp4, Sparcl1, Megf10, Slc1a2, Kchj10, Nfia, Ntrk2,* and *Grm3* (Fig. 5n, Table S1). Importantly, the binding of SOX2 to those signature genes is overlapped with the occupancy by the active epigenetic marker H3K27Ac, suggesting that SOX2 binding may activate these astrocytic signature genes. The activating effect of SOX2 on these signature genes is further supported by our RNA-seq analysis and by purified astrocyte culture. Unbiased GO analysis of SOX2-binding regions (Fig. 5e) points to a

key role of SOX2 in regulating astrocytic function of glutamate uptake. Astrocytes take up >90% extracellular glutamate after neuronal depolarization to avoid network overactivation and play an important role in maintaining a balance of excitation and inhibition (E/I balance) (34). Both GLT-1 and Kir4.1 are functionally essential for extracellular glutamate uptake by astrocytes (34, 62). Our data show that GLT-1 is also targeted by SOX2 in astrocytes and SOX2 disruption results in remarkable GLT-1 downregulation. Consistently, our functional analysis demonstrates that *Sox2*-deficient astrocytes display significantly compromised capability to uptake extracellular glutamate. These data suggest that SOX2 regulates functional maturation of postnatal astrocytes through directly targeting glutamate transporters, particularly GLT-1.

The current study demonstrates an essential role of SOX2 in postnatal astrocyte development and function. It has been reported that quiescent mature astrocytes express high level of SOX2 in the adult CNS (15, 16), yet the role of SOX2 in adult astrocyte homeostasis and function remains elusive. A recent study demonstrates that nuclear factor 1A (NFIA), a crucial transcription factor essential for astrocyte differentiation (63), is required for maintaining adult astrocytes function in a brain region-specific manner (64). Our data show that SOX2 directly targets NFIA (Table S1) and that SOX2 disruption impairs NFIA expression (Fig. 5n) during developmental, suggesting that SOX2 may act upstream of NFIA to regulate adult astrocyte function. Our unpublished data showed that SOX2 disruption in adult quiescent astrocytes significantly downregulated GFAP, as we observed during postnatal development, yet upregulated the expression of Vim, Lcn2, and Serpina3n, typical markers of astrocyte activation, indicating that SOX2 may maintain astrocyte homeostasis and function in the adult brain. We are currently studying the effects of SOX2 cKO specifically in adult quiescent astrocyte on astrocytic morphological and electrophysiological maintenance, calcium activity, neuronal synaptic transmission, and behavioral output.

In conclusion, using astroglial-specific SOX2 cKO mutants and a variety of approaches, we demonstrate that SOX2 plays an essential role in astrocyte developmental maturation and controls motor hyperactivity in mice. Together with the recent demonstration that SOX2 is required for CNS myelination and motor skill development (13), our data collectively suggest that glial SOX2 coordinates postnatal brain development and regulates animal motor skill and motor activity, thus providing new insights into explaining the brain abnormalities of *SOX2*-deficient children.

Materials and Methods

Animals and SOX2 conditional knockout (cKO)

All mice were housed at 12 hours light/dark cycle with free access to food and drink. All transgenic mice were maintained on a C57BL/6 background and approved by Institutional Animal Care and Use Committee at the University of California, Davis. *Aldh1l1-CreER^{T2}* (RRID: IMSR_JAX:029655), *mGfap-Cre* (RRID: IMSR_JAX:024098), *Sox2-CreER^{T2}* (RRID:IMSR_JAX:017593), Sox2$^{fl/fl}$ (RRID:IMSR_JAX:013093), and *Rosa26-EYFP (RRID: IMSR_JAX:006148)* were described in our previous studies (13, 14, 19). mTmG (RRID: IMSR_JAX:007676) mice were purchased from the Jackson Laboratory and described in previous study (22). All Cre transgene was maintained as heterozygosity. Animal genotype was determined by PCR of genomic DNA extracted from tail tissue according to our previous protocols. Both male and female mice were included. *Sox2$^{fl/fl}$* or *Sox2$^{fl/+}$* mice were used as non-Cre control mice in our study. In our study, we referred to the *mGfap-Cre:Sox2$^{fl/fl}$* mice as mGfap:Sox2 cKO mice, *Aldh1l1-CreER^{T2}:Sox2*$^{fl/fl}$ as Aldh1l1:Sox2 cKO mice. Both *Aldh1l1(or Sox2)-CreER^{T2}:Sox2*$^{fl/fl}$ and corresponding non-Cre littermate mice (*Sox2$^{fl/fl}$* or *Sox2$^{fl/+}$*) were treated subcutaneously with tamoxifen (or hydroxytamoxifen, OH-TM) according to our previous protocolss (19).

Tamoxifen and EdU injection

Tamoxifen (TM) (T5648, Sigma) and 4-hydroxytamoxifen (OH-TM) (H7904, Sigma) were prepared in a mixture of ethanol and sunflower seed oil (1:9, v/v). The stock solution of TM and OH-TM were 30 mg/ml and 10 mg/ml, respectively. All study mice including non-Cre Ctrl and knockout were received TM and OH-TM subcutanenously at a dose of 200 μg/g and 100 ug/g body weight, respectively. EdU (A10044.Thermo Fisher Scientific) was dissolved in 0.9% sterile saline at 10 mg/ml. To study the proliferation of astrocyte, EdU was intraperitoneally injected into Sox2 cKO and control littermates (100 μg/g) from postnatal day 1 to day 3.

Evans blue (EB) assessment of the blood brain (spinal cord) barrier

EB (E2129, Sigma) was freshly prepared by sterile PBS at concentration of 1 mg/ml. Ten-month old mGfap:Sox2 cKO and control animals were administrated EB through tail vain at a dose of 4 ml/kg body weight. Age-matched wild type mice insulted by experimental autoimmune encephalomyelitis (EAE) were also injected with EB. Mice were sacrificed at 30 min

post-injection. To fully remove EB from the bloodstream, EB-injected animals were perfused with 100 ml PBS. The brain and spinal cord were harvested for subsequent examination.

RNA-sequencing (RNA-seq) and bioinformatic analysis

Total RNA was prepared from the spinal cord of P80 *mGfap:Sox2*$^{fl/fl}$ (*n* = 3, 2 females and 1 male) and *Sox2*$^{fl/fl}$ littermate control mice (n=3, 2 females and 1 male). The quality of RNA samples was determined by the Bioanalyzer 2100 system (Agilent Technologies). The RIN (RNA integrity number) of all our RNA samples used for RNA-seq and qPCR was greater than 6.8. The library constructing and sequencing, and subsequent bioinformatic analysis were conducted according to the standard operating procedure by Novogene Inc. In brief, the library was prepared using the NEBNext Ultra Directional RNA Library Prep Kit (#E7420, New England BioLabs) for Illumina, and sequenced on the Illumina HiSeq 4000 sequencing platform. Paired-end clean reads were aligned to the mouse genome (mm10) using the STAR software package (v2.5) with mismatch=2. HTSeq v0.6.1 was used to count the read numbers mapped of each gene and FPKM of each gene was calculated based on the length of the gene and reads count mapped to that gene. Differential expression analysis between mGfap:Sox2 cKO and Non-Cre Ctrl was performed using the DESeq2 R package (2.1.6.3), and genes with an adjusted P-value <0.05 found by DESeq2 were assigned as differentially expressed genes (DEGs). Gene Ontology (GO) enrichment analysis of DEGs was implemented by the clusterProfiler R package (v2.34.3), in which gene length bias was adjusted. GO terms with adjusted P value less than 0.05 were considered significantly enriched. The high-throughput sequencing data from this study have been submitted to the NCBI Sequence Read Archive (SRA) under the accession number PRJNA644649.

Astrocyte morphology analysis

The data of Fig. 1f and Fig. 1g were quantified by NIH Image J. Ten-micron optical sections from confocal z-stack (Nikon C1) were projected into a flattened image. The parameter setting of z-stack confocal imaging was below: total optical thickness, 10 μm, step size, 0.5 μm, total number optical slices, 21. The volume-rendered confocal images were subsequently imported to NIH ImageJ 1.46r for quantifying the percentage of astrcoyte marker occupying area among total area. We used a customer-defined Image J Macro program acoording to our previous protocol for semi-automated quantification (19). At least three sections from each mouse were used for ImageJ quantification.

The data of Fig. 3 were quantified by IMARIS (Bitplane version 9.30). Briefly, z-stack images were obtained by Nikon C2 confocal using 60x oil-immersion objective lens. The parameter setting of z-stack confocal imaging is below: total optical thickness, 10 μm, step size, 0.5 μm, total number optical slices, 21. The orignal z-stack images from Nikon C2 were imported to IMARIS for 3D morphological reconstruction according to the software mannual. We mannually adjusted the sensitivity threshold to obtain generated 3D images machted with orignal mG^+ astrocytes from confocal images. To quantify astrocyte surface area and enclosed volume (domain), the Surface Tool of IMARIS was used to build the domains of mG^+ astrocytes. Cell soma was identified by S100β immunoreactive signals and automanally seclected base on the size point (<12 μm). The Classification/Filter function of IMARIS was used to remove the background noise.

To quantify astrocyte processes, the IMARIS Filament Tracing module was performed to detect an automatic intensity threshold, subtract background noise, and generate process of astrocyte computer reconstructions which machted with orignal images. IMARIS parameters were set to detect processes between 0.6 μm and 10.4 μm in diameter. The process length, area, and volume of mG^+ astrocytes were calculated automatically by IMARIS with same intensity threshold between Non-Cre Ctrl and Sox2 cKO groups.

Bioinformatic analysis of SOX2 ChIP-seq data

The dataset GSE85213 (16), which consists of raw sequence reads of one input sample and 3 biological replicate samples of SOX2 IP prepared from the adult cerebral cortex, was used for bioinformatics analysis. ChIP-seq raw reads of H3K27Ac in cultured mature astrocytes at DIV21 differentiation from NSCs, were retrieved from the dataset GSE96539 (65). We used the open source, web-based platform usegalaxy.org for ChIP-seq data analysis.

For SOX2 ChIP-seq analysis, the SRA accession (SRR4000651 input, SRR4000652 SOX2 IP-1, SRR4000653 SOX2 IP-2, SRR4000651 SOX2 IP-3) was used to retrieve the raw sequence reads. For H3H27Ac ChIP-seq analysis, the SRA accession (SRR5339737 input, SRR5339717 H3K27Ac) was used to retrieve the raw sequence reads. Bowtie 2 was used to align raw reads to the mouse reference genome mm10 and the resulting aligned reads were written into BAM files, which were subsequently filtered by minimal MAPQ quality score > 20 (filtered BAM files). Bigwig files were generated based on filtered BAM files using bamCoverage tool. MACS2 was used for peak calling with the following parameters: ChIP-seq Treatment File (IP-1, IP-2, and IP-3); ChIP-seq Control File (Input); effective genome size, 2150570000; band

width for picking regions to compute fragment size, 300; lower mfold bound, 5; upper mfold bound, 100; peak detection based on q-value (FDR) with minimal q-value cutoff for peak detection 0.05. The resulting NarrowPeak BED files were used for subsequent bioinformatic analysis. The gene annotation of the identified peaks to the closest transcription start sites (TSS) was conducted using the online tool annoPeakR (Table S1, Table S2). We used MEME-CHIP (http://meme-suite.org/tools/meme-chip) for motif analysis (Table S3) and GREAT v3.0 (http://great.stanford.edu/great/public-3.0.0/html/) for biological function annotation (Table S4).

Tissue preparation, in situ hybridization, and immunohistochemistry

Tissue process, in situ hybridization, and immunohistochemistry were performed according to our previous protocols (19). A 614bp digoxinin-conjugated complementary RNA (cRNA) probe (targeting *Gfap* mRNA) was prepared using SP6 RNA polymerase-mediated *in vitro* transcription. The DNA template for *in vitro* transcription was prepared using *Gfap* mRNA-specific forward primers 5'-GTGGATTTGGAGAGAAAGGTTG-3' and reverse primer 5'-GCGATTTAGGTGACACTATAGCTGGAGGTTGGAGAAAGTCTGT-3' (underlined is the core sequence recognized by SP6 RNA polymerase).

The folllowing antibodies used in our immunihistochemical study: SOX2 (Cat# sc-17320,RRID:AB_2286684,1:500,Santa Cruz biotechnology) ; BLBP (Cat# ABN14,RRID:AB_2494022,1:200,Millpore); GFAP(Cat# MAB36014, RRID:AB_11212597,1:500,Millpore); GFAP(Cat# Z0334,RRID:AB_10013382, 1:500, Agilent); ALDH1L1 (Cat# 75-164, RRID:AB_10671695,1:500, UCDAVIS); SOX9 (Cat# AF3075, RRID: AB_2194160,1:200, R&D system); SPARCL1(Cat# AF2836;: AB_2195097,1:300,R&D system); EYFP/GFP(Cat# ab13970,RRID:AB_300798,1:500,abcam); Kir4.1(Cat# APC-035, RRID: AB_2040120,1:400, Alomone labs) ;#Anti-GLT1 (1:5000, rabbit) antibody was generously provided by J.D. Rothstein (Johns Hopkins University, Baltimore, MD) ; VGLUT1(Cat# AB5905, RRID: AB_2301751, 1:500, Millipore); PSD95(Cat# 124011, RRID:AB_10804286, 1;500,Synaptic Systems); NeuN (Cat# MAB377, RRID:AB_2298772, 1:500, Millipore) ; C-fos(Cat# sc-52, RRID:AB_2106783,1:500, Santa Cruz Biotechnology); PDGFRα (Cat# AF1062，RRID: AB_ 2236897,1:200, R&D system); Albumin (Cat# A90-134, RRID:AB_67120, 1:500,Bethyl); Laminin(Cat# L9393, RRID:AB_477163, 1:500, Sigma-Aldrich).

Protein extraction and Western blot (including antibody information

Protein extraction and Western blot were conducted according to our previous protocols (19). The following primary antibodies were used for Western blot : Anti-β -actin(Cat# 3700, RRID:AB_ 2242334, 1:1000; Cell Signaling Technology); GAPDH (Cat# 2118, RRID:AB_561053,1:2000, Cell Signaling Technology) ; GFAP (Cat# MAB36014,RRID:AB_11212597,1:1000,Millpore); SPARCL1(Cat# AF2836;: AB_2195097,1:2000,R&D system); Kir4.1 (Cat# APC-035, RRID: AB_2040120, 1:1000, Alomone labs); Anti-GLT-1 (1:5000, rabbit) antibody was generously provided by J.D. Rothstein (John Hopkins University, Baltimore, MD). Multiple GLT-1 protein bands of ~62 kD, ~120 kDa, and ~250 kDa were observed in Western blot images, representing monomer, dimer, and tetromer of GLT-1 molecules as described in previous study (66).

RNA extraction, cDNA preparation, and real-time quantitative PCR (RT-qPCR)

RNA was prepared using commercial kit (Qiagen, #74804) according to the kit manual. cDNA was prepared according to the kit manual (Qiagen #20511). RT-qPCR was performed using Sybr Green-based approach. Gene expression was normalized to the internal housekeeping gene *Hsp90* and the relative expression in non-Cre control was assigned to 1. The qPCR primers used in the study were: *Sox2* (CCAGCGCATGGACAGCTA/ CCAGCGCATGGACAGCTA), *Gfap* (GTGTCAGAAGGCCACCTCAAG/ CGAGTCCTTAATGACCTCACCAT), *Nwd1 (*GATGAGCTATGAGAACTCCTGC/ GCATGAACAAACTGGACAGC*), Wnt7a (*ACGAGTGTCAGTTTCAGTTCC/ AATCGCATAGGTGAAGGCAG*), Slc1a2 (*CAACGGAGGATATCAGTCTGC/ TGTTGGGAGTCAATGGTGTC*), Slc1a3 (*CAAGACACTGACACGCAAGGAC/ CTTAACATCTTCCTTGGTGAGGC*), Id3 (*CGACCGAGGAGCCTCTTAG/ GCAGGATTTCCACCTGGCTA*), Id4 (*CAGTGCGATATGAACGACTGC/ GACTTTCTTGTTGGGCGGGAT*), Sparcl1 (*TGCAGACAGGATCTTGACAC/ TGGCCCCATTCCTTCAAG*), Sox9 (*AGTACCCGCATCTGCACAAC/ ACGAAGGGTCTCTTCTCGCT*), Gli3 (*GGCCTCCAGTACCACTTCAA/ CTGAGACCCTGCACACTCTG*), Aqp4(*ATCAGCATCGCTAAGTCCGTC/ GAGGTGTGACCAGGTAGAGGA*), Ntrk2(*TGTAGTGTGGCAGGTGATCCGGT/ GGAGCCCTGTGTGTGGCTTGTTT*), Kcnj10 (*ACAAAGTTTGGCTTCGGCAC/ TAGCGACCGACGTCATCTTG*),* and *Hsp90 (*AAACAAGGAGATTTTCCTCCGC/ CCGTCAGGCTCTCATATCGAAT).

Primary astrocyte culture

Primary mixed glial cells were prepared from P0-P2 neonatal mouse forebrains as previous study (19). After digestion and centrifugation, mixed glial cells were plated on poly-D-lysine (PDL)-coated T75 flasks in high glucose DMEM medium (Gibco,11965-092) with 10% heat-inactivated fetal bovine serum and 1% Penicillin/Streptomycin. Culture medium was changed every 2 days (total ~10 days) until astrocytes are confluent. Next, mixed glia cells were shaked for 1 hour at 37°C and 200 rpm on an orbital shaker (Cat# C491, Hanchen) to remove microglia. The supernatant containing microglia was discarded and T75 flasks were washed twice with PBS to remove remaining microglia. Then 20 ml fresh astrocyte culture medium was added into each flask, and flasks were continued by shaking for 6 hours at 37°C and 200 rpm to remove oligodendrocyte precursor cells (OPCs). The supernatant was discarded and the remaining confluent astrocyte layer was rinsed twice with PBS. Astrocytes were collected by 0.25% trypsin-EDTA digesting and cultured in DMEM with 10% FBS for 21 days for further study.

Astrocytes glutamate uptake

Glutamate uptake was perfromed using DIV21 primary astrocytes. Cells were washed with HBSS (with Ca^{2+} and D-glucose) and equilibrated with HBSS for 15 min at 37 degree in the 5% CO_2 incubator. Cells were treated with 100 μM glutamate (PHR1007, Sigma) freshly dissolved in HBSS (with Ca^{2+}). The glutamate-containing HBSS was collected for measuring glutamate concentration and cells were collected for preparing whole cell protein at 1.5 hours or 4 hours. Glutamate concentration was determined by using the commercial glutamate assay kit (MAK004, Sigma) according to the manufacture instructions. The concentration of whole cell protein was determined by BCA method. The glutamate uptake rate was normalized to total whole cell protein and calculated as the reduction of glutamate concentration (μM) in HBSS per microgram whole cell protein (μM/μg).

Synapse quantification at the histological levels

Frozen sections (12 μm) were immune-stained for the presynaptic marker VGLUT1 and postsynaptic marker PSD95 and imaged by Nikon C1 confocal with the following z-stack settings: optical thickness of 2μm and z-step size of 0.2μm. The maximally projected images from 5 consecutive optical slices (total depth, 0.2 μm x 5 optical slices = 1 μm optical thickness) were analyzed by Puncta Analyzer plug-in of NIH ImageJ. We used the protocol previously published by Dr. Eroglu (Duke University) (67) to quantify the synaptic puncta density. As described in the published protocol (67), we normalized the synapse puncta density to the percentage of non-Cre control mice.

Electrophysiology recording of astrocytes and neurons

Mice of 4-5 postnatal weeks were used for electrophysiological recordings. After anesthesia with Ketamine/Xylazine combination (100-200 mg/kg body weight for Ketamine and 5-16 mg/kg body weight for Xylazine injected intraperitoneally), mice were decapitated and the brain was rapidly removed and placed into ice-cold slicing solution oxygenated with 95% O2 and 5% CO2 (125mM NaCl, 3.5mM KCl, 25mM $NaHCO_3$, 1.25mM NaH_2PO_4, 0.1mM $CaCl_2$, 3mM $MgCl_2$, and 10mM Glucose). Sagittal brain slices (300 μm thickness) were sectioned on the vibratome (Leica #VT100S) in the ice-cold slicing solution and then transferred into a small basket in a container consisting of standard aCSF (125mM NaCl, 25mM $NaHCO_3$, 1.25mM NaH_2PO_4, 3.5mM KCl, 2mM $CaCl_2$, 1mM $MgCl_2$, and 10mM Glucose (295±5 mΩ; pH 7.3-7.4; oxygenated with 95% O_2 and 5% CO_2) for 30 min at 32 °C, and then recovered from preparation damage at room temperature for 1 h. To visualize astrocytes, brain slices were briefly incubated in the oxygenated standard aCSF supplemented with 0.6 μM astrocytic marker sulforhodamine 101 (SR101) for 30min.

Whole-cell patch-clamp recordings of cortical astrocyte and dorsal striatal medium spiny neurons (MSNs) were conducted using MultiClamp 700B amplifier, filtered at 3 kHz, and sampled at 10 kHz with DigiData 1440 (Molecular Devices). Brain slices were continuously perfused with aCSF with a flow rate of 2–3 ml/min bubbled with 95% O_2 and 5% CO_2. For cortical astrocyte recording, the glass pipette resistance was 5-6 mΩ. Input resistance and capacitance were measured in voltage-clamp mode with 500ms 5mV step pulse from -70 mV holding potential. The resting membrane potential was measured in current-clamp model (I=0). For neuron recording, MSNs were identified by bright-field Nikon Eclipse e600FN microscopy with a 40 water-immersion lens (numerical aperture 0.8) and infrared illumination. To measure the miniature excitatory postsynaptic current (mEPSCs), the glass pipette resistance was 3-5 mΩ, and MSNs were recorded in voltage-clamp mode at a holding potential of -70mV in the presence of 1μM (Tetrodoxin) TTX and 50 μM picrotoxin (GABA antagonist). pClamp 11.0.3 (Molecular Devices) was used for data acquisition and storage. Analysis of mEPSCs were performed using Minianalysis 6.0.7 software (Synaptosoft). At least 5 min of spontaneous activity was recorded from each cell with access resistance measured before and after the recording. Access resistance (Ra) was monitored following membrane rupture and dialysis, and recordings were abandoned if Ra>30 M. An event amplitude threshold was set at 10 pA above the baseline, and at least 300 events were analyzed per cell.

Behavioral assessment

Animals were habituated to the behavioral room for at least 30 min before the test began. Two months old non-Cre control and mGfap:Sox2 cKO mice were firstly tested for motor skills on Rotarod and CatWalk, followed by locomotion and cognition test by open field and Barnes maze, respetively, and then HomeCage spontanous locomotion and social interaction test by HomeCage activity and three-chamber evaluations, respectively. Some test paradigms were also conducted on tamoxifen inducible Aldh1l1:Sox2 cKO and non-Cre Ctrl mice at 2-month and 5-month old which had been administered tamoxifen (three injections, once a day) at P14-P16 to induce astroglial-specific Sox2 cKO.

Accelerating Rotarod test: Accelerating rotarod test was used for assessing animal motor coordinataion and motor performance according to our previous protocols (13, 14, 19, 68, 69). The initial speed of rorarod was 4rpm and the maximal speed was 40 rpm with 1.2rpm incremental every 10 seconds. Mice were trained on rotating rod for two consecutive days (4 trials each day with 60 min interval between trials) followed by data collection on the third day. The maximum duration of each trial was set to 300 second. The time on rod and maximal speed at which mice fell off the rod were recorded and averaged for 4 individual trials.

CatWalk gait analysis: The real-time video-tracked CatWalk XT system with automated data collection (Noldus Information Technology) was used to quantify animal waking gait. Each animals was trained for walking across the walkway 3 runs per day. For data collection, the camera gain was set to 20 and the detection threshold to 0.1. All runs through the walkway with a duration between 0.50 and 5.00 sec were considerred as successful runs. The average of 3 succesful runs was used for data plotting.

Open field locomotion test: Open field test was performed using a 42 x 42 x 37 cm Photobeam Activity System (PAS)-Open Field (San Diego instrument) which is equipped with a 16x16 PhotoBeam configuration and an automated data collection station. Animals were allowed for adaptation to the open field for 30 min prior to test. The test session was set to 30 min. The moving activity of animals in the open field during each session was real-time collected by PAS version 1.0. The PAS software package was used for calculating total travel distance and percent of active time (with 3-second cutoff) according to the manufacture instruction.

Barnes maze test: Spatial learning/memory and locomotion were examined by Barnes maze. Briefly, mouse was placed in the center of the maze (100 cm diameter) which containning

twenty holes (10 cm diamater). The test was perfomed in a noise-free room strong illumination(>300 LUX) and with visual cues for the escaping hole leading to the escaping (goal) box. Animals were training for locating the escaping box for five consecutive days (D1-D5) prior to formal testing on day 6 (D6). The animal acivity was monitored by a camera controlled by the Ethovision tracking software system (Ethovision XT.14, Noldus). Each animal was trained or tested for 2 trials/day with an interval of approximately 60 min.The maximal duration of each trial was 5 min unless the mice found the goal box. During the training days, mice were placed in the ceter of the maze and allowed for free exploration for 5 min after which they were gently guided to the goal box and kept there for 1 min. During the testing day, mice were allowed for exploration for 5 min with the escape box was relocated for 180 degree. The tracking program will be automatically terminated when the animal had all four paws inside the escaping box. Total erors before entering the escape box, latency to entering the goal box, total distance travelled (pathlength), and moving velocity on the maze were calculated using Ethovision XT.14 software.

Spontaneous HomeCage locomotion activity: The SmartCage™ system (L 30 x W 18 x H 12 cm) (AfaSci, Inc. Burlingame, CA, USA) was used for automated analysis of spontaneous activity in animal's home cages as described previously (70, 71). Animal was placed into the home cages and allowed to explore for 20 min. The homecage activity variables (travel distance and active time) were determined by photobeam breaks and were analyzed automatically using CageScore software (AfaSci).

Three-chamber social interaction test: Social interaction was assessed by using the SmartCage™ system (L 29.8 x W 18.0 x H 12.8 cm) (AfaSci, Inc. Burlingame, CA, USA) with two add-on metal-mesh enclosure (W 8 x L 6 x H 12 cm) at each end of the home cage (see Suppl Fig 7a), which has been shown equivalent to conventional “three-chamber” test in evaluating animal social interaction (71). The socail interaction test consists of three 10-min sessions (habituation,socialability, social novelty or memory) (Suppl Fig. 7a). During habituation, the subject mouse was allowed to move around for 10 minutes without social cues. During socialability test, Stranger 1 mouse was placed into one of the two enclosures. The subject mouse was then allowed to explore for 10 minutes. The social novelty and memory was tested by introducing the unfamilar Stranger 2 mouse and familiar Stranger 1 after 1 hour interval. The percentage of occupancy time with empty or stanger mouse were recored by the SmartCage System (AfaSci, Inc. Burlingame, CA, USA).

Statistical analyses: Both male and female mice were included in this study. All data were plotted as mean ± s.e.m with each dot or square representing one mouse. Data collection was conducted by lab members who were blinded to mouse genotypes. We used Shapiro-Wilk approach to test data normality. F test and Browne-Forsythe test were used to evaluate variance equality of two groups and three or more groups, respectively. Unpaired two-tailed Student's *t* test was used for statistically analyzing two groups of data where the *t*-values and the degree of freedom (df) were shown as $t_{(df)}$ in each graph. Two-way ANOVA followed by Tukey's post test was used for statistically analyzing the data of Suppl Fig. 6 and Suppl Fig. 7 where the F ratio, and DFn and DFd was presented as F(DFn, DFd) in the figure legends. All data graphing and statistical analyses were performed using GraphPad Prism version 8.0. The P-value was designated as * $P < 0.05$, ** $P < 0.01$, *** $P < 0.001$, ns, not significant $P > 0.05$.

Figures and Figure Legends

Figure 1 –SOX2 conditional knockout (cKO) inhibits astrocyte maturation in *mGfap-Cre:Sox2*$^{fl/fl}$ mice

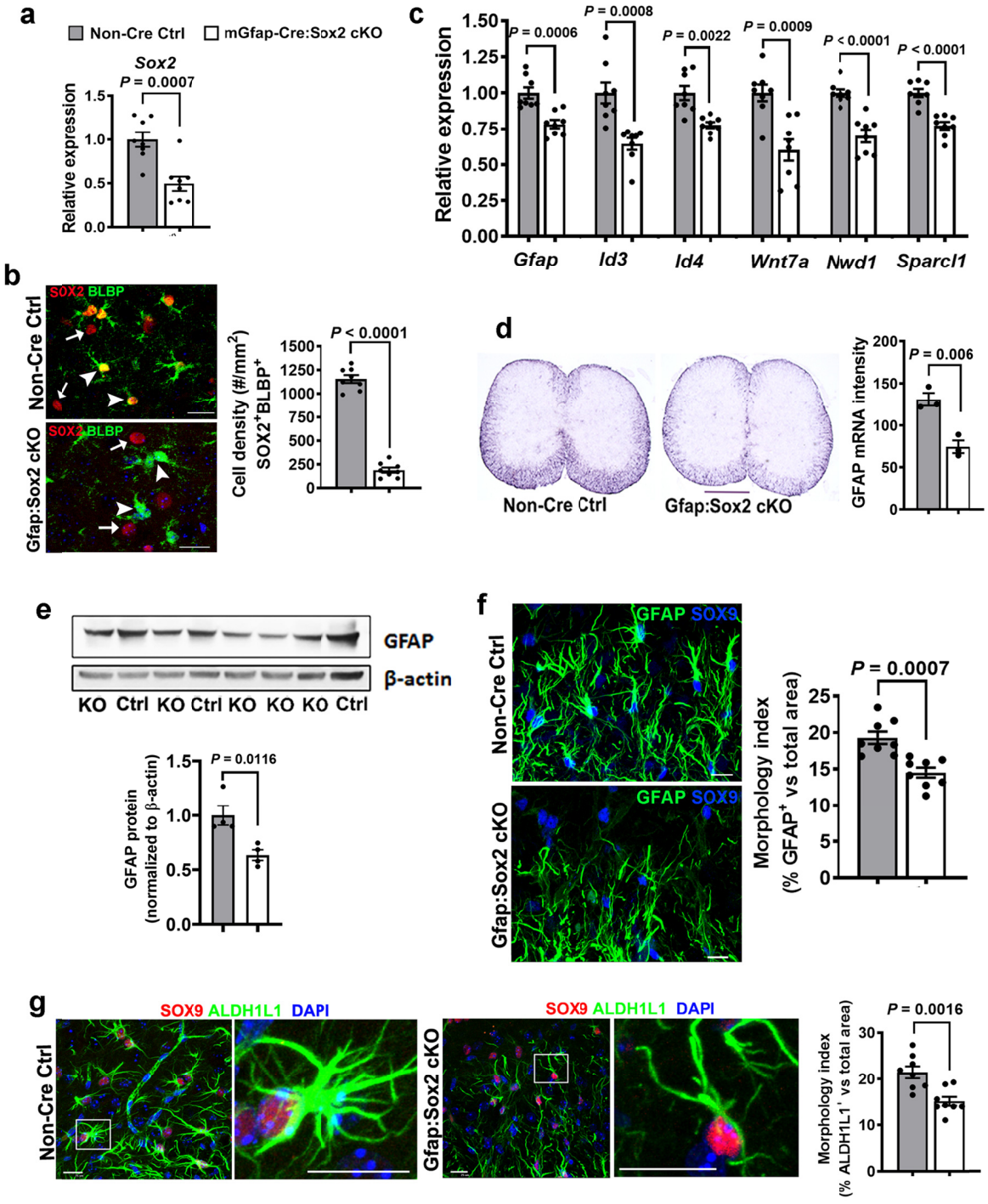

Data were collected from the spinal cord of two litters of *mGfap-Cre:Sox2*$^{fl/fl}$ (mGfap:Sox2 cKO) and non-Cre littermate control mice at P14.

a, RT-qPCR assay of *Sox2* mRNA. Two-tailed Student's t test, $t_{(14)}$=4.312.

b, immunohistochemistry (IHC) and quantification in the spinal cord. SOX2 is expressed in $BLBP^+$ astrocytes in Ctrl and is deleted in cKO (arrowheads). Arrows points to SOX2-expressing non-astrocytic cells. Two-tailed Student's t test, $t_{(14)}$=19.44. Scale bar = 20 μm.

c, RT-qPCR assay of astrocyte-enriched genes. Two-tailed Student's t test, $t_{(14)}$ = 4.448 *Gfap*, $t_{(14)}$ = 4.228 *Id3*, $t_{(14)}$ = 4.181 *Id4*, $t_{(14)}$ = 4.220 *Wnt7a*, $t_{(14)}$ = 5.826 *Nwd1*, and $t_{(14)}$ = 6.013 *Sparcl1*.

d, *Gfap* mRNA in situ hybridization (ISH) and quantification. Two-tailed Student's t test, $t_{(4)}$ = 5.313. Scale bar=500μm.

e, Western blot and quantification of GFAP protein level. Two-tailed Student's t test, $t_{(6)}$ = 3.584.

f, representative images of GFAP and astrocyte nuclear marker SOX9 and the percentage of $GFAP^+$ area among total assessed area. Two-tailed Student's t test, $t_{(14)}$ = 4.348. Scale bar = 10 μm.

g, representative images of astrocytic process marker ALDH1L1 and SOX9 and the percentage of $ALDH1L1^+$ area among total assessed area. Two-tailed Student's t test, $t_{(14)}$ = 3.889. Scale bar = 10 μm.

Figure 2 –SOX2 cKO inhibits molecular maturation without perturbing astrocyte proliferation in the early postnatal CNS.

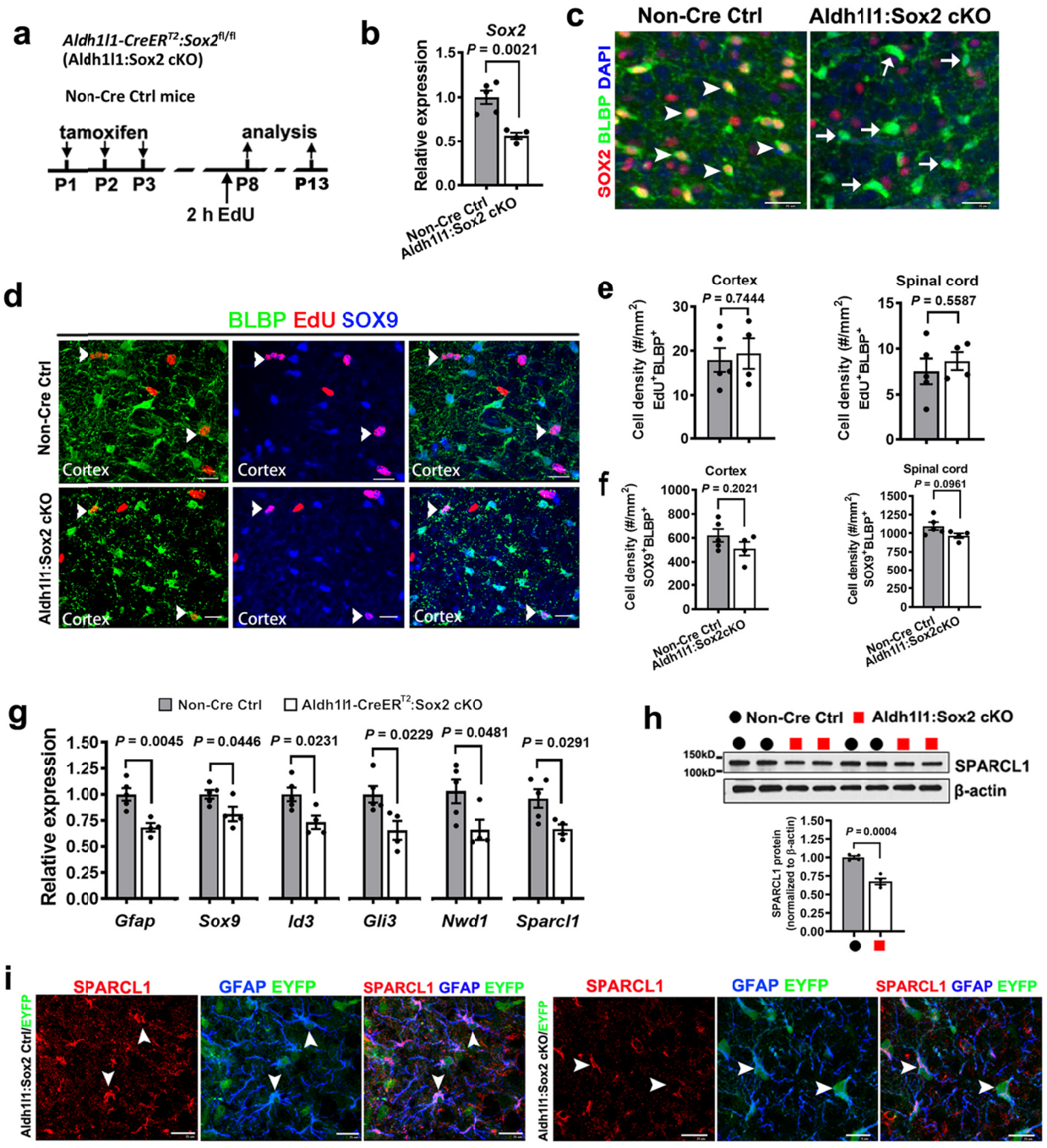

a, experimental design. Neonatal mice carrying *Aldh1l1-CreER*^{T2}*:Sox2*$^{fl/fl}$ (Aldh1l1:Sox2 cKO) and Sox2$^{fl/fl}$ or Sox2$^{fl/+}$ (non-Cre Ctrl) were injected with tamoxifen at P1, P2, and P3 (once a day), and analyzed at P8 (**b-f**) and P13 (**g-i**). Two hours before sacrifice at P8, thymidine analogy EdU was administered for astrocyte proliferation assay.

b, RT-qPCR assay of *Sox2* mRNA in the spinal cord. Two-tailed Student's t test, $t_{(14)} = 4.742$.

c, confocal images showing SOX2 expression in $BLBP^+$ astrocytes in the cerebral cortex of non-Cre control mice (arrowheads, left) and absent in Aldh1l1:Sox2 cKO mice (arrows, right). Scale bar = 25 um.

d, representative confocal images of BLBP, SOX9, and EdU immunostaining in the cerebral cortex. Arrowheads point to triple positive astrocytes. Scale bar = 20 um.

e, density of EdU^+BLBP^+ proliferating astrocytes. Two-tailed Student's t test, $t_{(7)} = 0.3392$ cerebral cortex and $t_{(7)} = 1.922$ spinal cord.

f, density of $SOX9^+BLBP^+$ astrocytes. Two-tailed Student's t test, $t_{(7)} = 1.407$ cerebral cortex and $t_{(7)} = 3.481$ spinal cord.

g, expression of astrocyte-enriched genes in the forebrain. Two-tailed Student's t test, $t_{(7)} = 4.110$ *Gfap*, $t_{(7)} = 2.440$ *Sox9*, $t_{(7)} = 2.896$ *Id3*, $t_{(7)} = 2.902$ *Gli3*, $t_{(7)} = 2.391$ *Nwd1*, and $t_{(7)} = 2.736$ *Sparcl1.*

h, Western blot images and quantification of mature astrocyte enriched protein SPARCL1 in the forebrain. Two-tailed Student's t test, $t_{(6)} = 6.996$.

i, Triple IHC of SPARCL1, SOX9, and EYFP in the cerebral cortex of *Aldh1l1-CreER^{T2}:Rosa26-EYFP* and Aldh1l1-CreER^{T2}:Sox2$^{fl/fl}$:Rosa26-EYFP mice at P13.

Figure 3 – SOX2 regulates astrocyte morphological maturation.

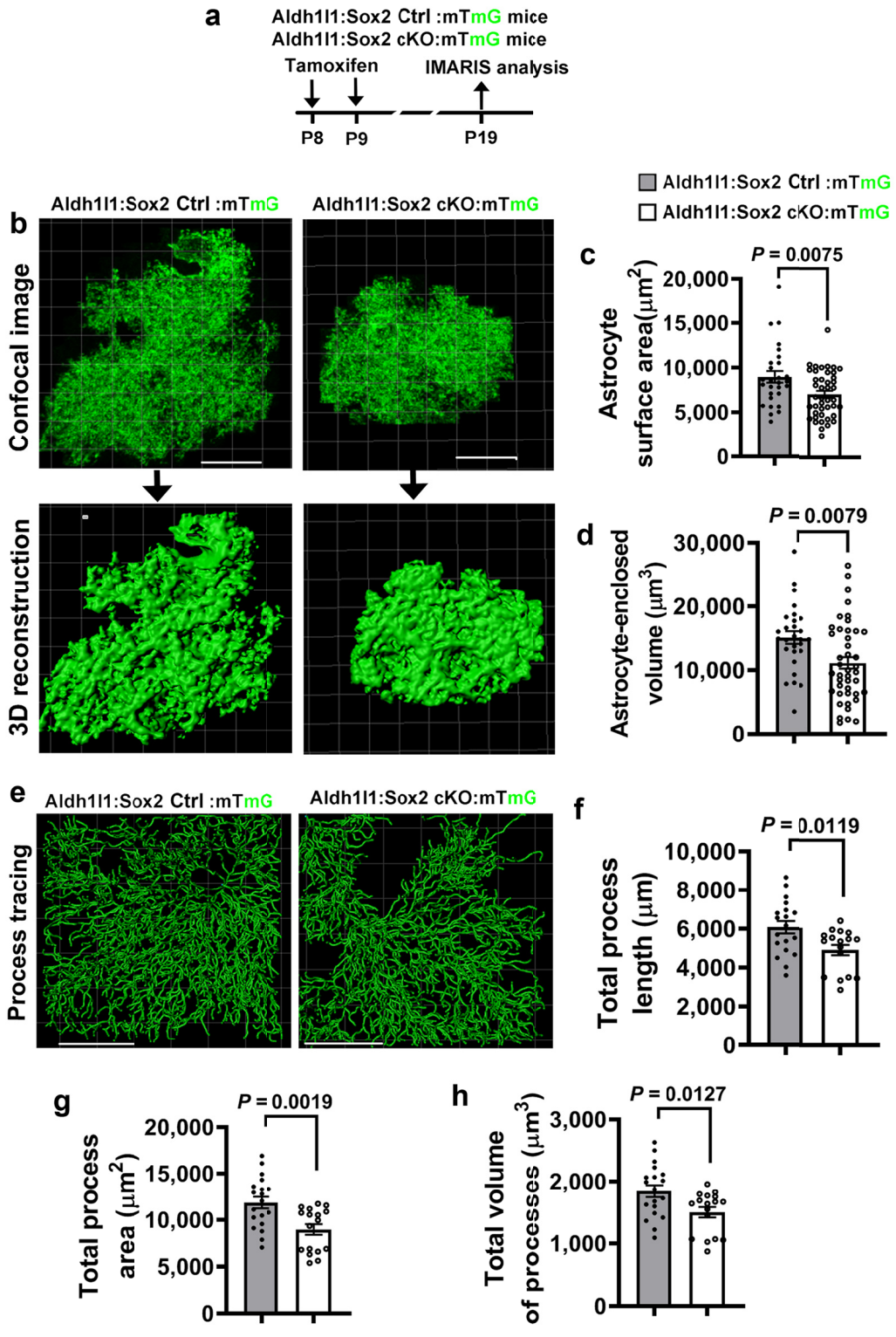

a, experimental design.

b, maximal projection of confocal images showing mG-expressing astrocytes (upper) and 3D reconstruction of mG signals by IMARIS (lower). Scale bar = 20μm.

c-d, surface area (**c**) and enclosed volume (**d**) of mG-positive astrocytes. Two-tailed Student's t test, $t_{(69)} = 2.753$ surface area, $t_{(69)} = 2.737$ volume. n=28 astrocytes from 3 Aldh1l1:Sox2 WT:mTmG mice and 43 astrocytes from Aldh1l1:Sox2 cKO:mTmG mice.

e, automatic tracing of mG^+ astrocyte processes by the Filament Tool of IMARIS. Scale bar = 20μm.

f-h, length (**f**), surface area (**g**), and volume (**h**) of mG^+ processes of astrocytes. Two-tailed Student's t test, , $t_{(34)} = 2.658$ length, $t_{(34)} = 3.376$ area, and $t_{(34)} = 2.632$ volume. n=17 and 19 astrocytes from 3-4 Aldh1l1:Sox2 WT:mTmG and Aldh1l1:Sox2 cKO:mTmG mice.

Figure 4 – SOX2 disruption impairs astrocyte electrophysiological properties

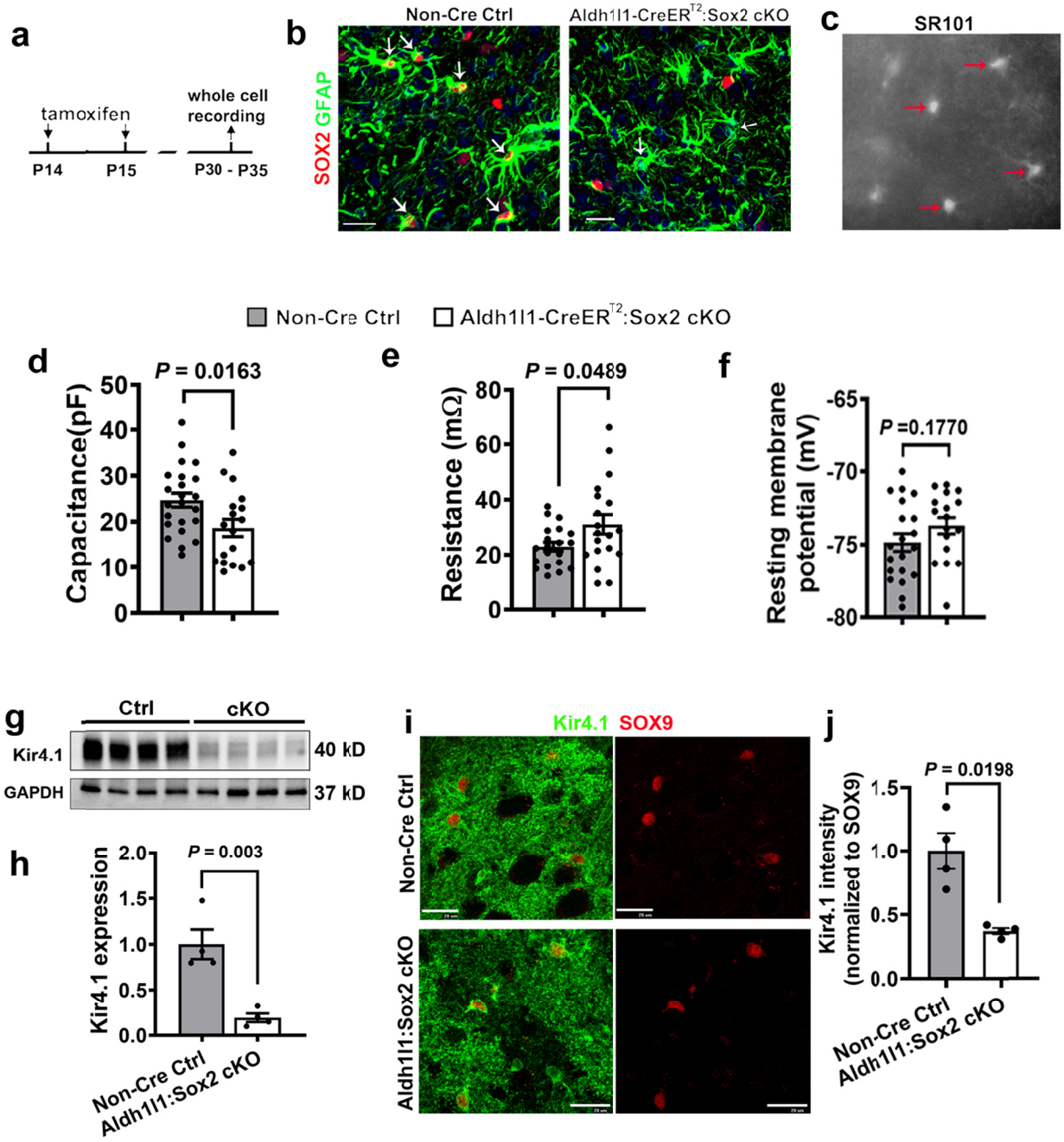

a, experimental design for **b-j**.

b, double IHC showing that SOX2 was expressed in GFAP^{+} astrocytes in the cerebral cortex of non-Cre Ctrl mice and ablated of Aldh1l1:Sox2 cKO mice (arrows). Scale bar = 20 μm.

c, cortical astrocytes visualized by fluorescent dye SR101 (arrows) for whole cell recordings.

d, cell capacitance of *Sox2*-deficient and intact cortical astrocytes Two-tailed Student's t test, $t_{(39)} = 2.511$.

e, input resistance of *Sox2*-deficient and intact cortical astrocytes. Two-tailed Student's t test, Welch's corrected $t_{(25.6)} = 2.068$.

f, resting membrane potential *Sox2*-deficient and intact cortical astrocytes. Two-tailed Student's t test, $t_{(35)} = 1.378$.

g-h, Western blot assay and quantification of Kir4.1 expression (normalized to the internal loading control GAPDH) in the forebrain of Aldh1l1:Sox2 cKO (n=4) and littermate controls (n=4) at P21 (daily 4-hydroxytamoxifen treatment from P4 through P9). Two-tailed Student's t test, $t_{(6)} = 4.792$.

i-j, representative images and quantification of Kir4.1 intensity (normalized to SOX9 intensity) in the cortex of Aldh1l1:Sox2 cKO (n=4) and littermate controls (n=4) at P21 (daily tamoxifen 4-hydroxytamoxifen treatment from P4 through P9). Two-tailed Student's t test, Welch-corrected $t_{(4.4)} = 3.158$. Scale bars=20μm.

Figure 5 – Direct target genes identified by ChIP-seq and transcriptome analysis of SOX2-regulated genes

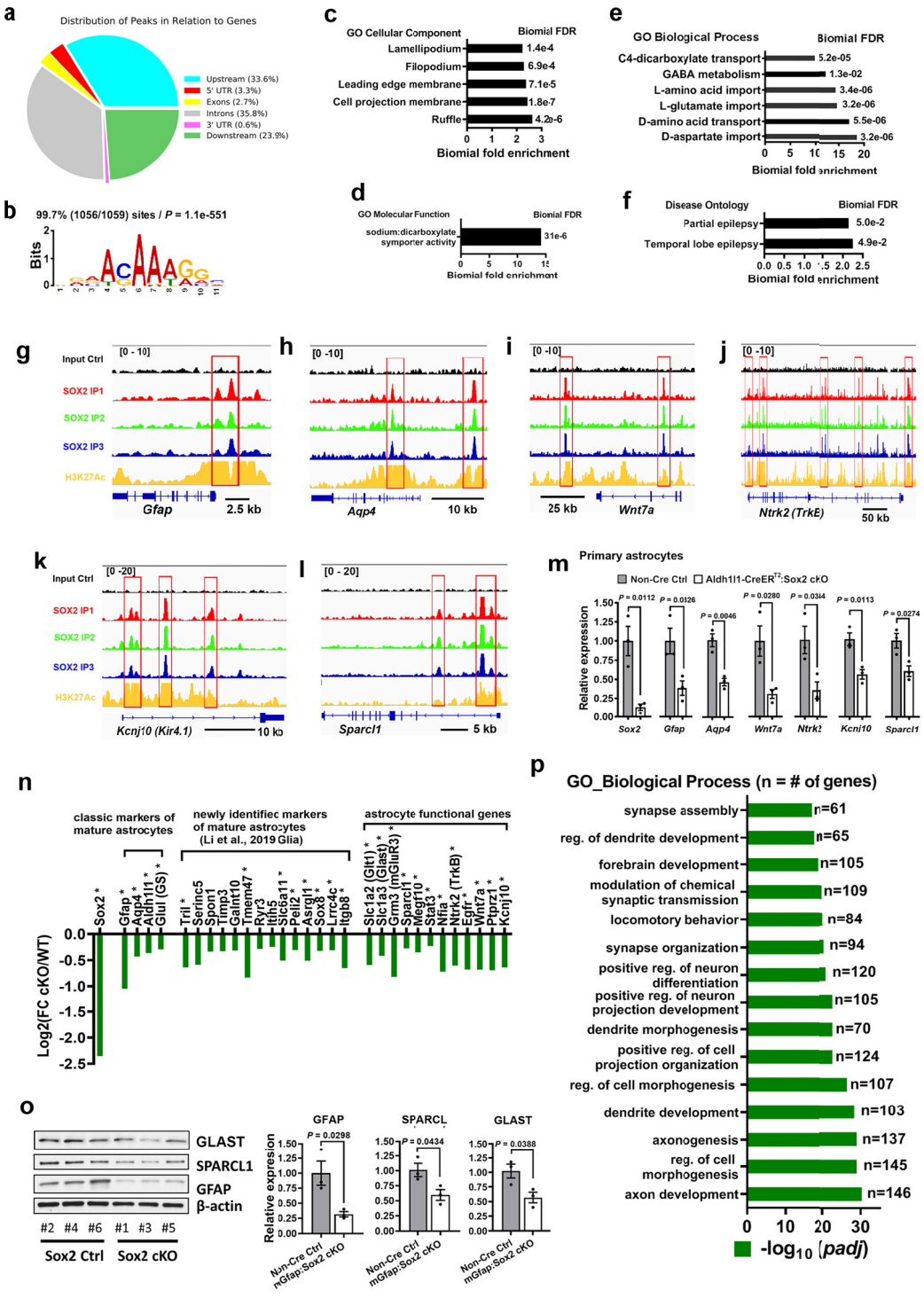

a, distribution of SOX2 peaks relative to the nearest genes.

b, motif enrichment analysis of the top 1059 SOX2-bound sites (Suppl Table 2) showing that 99.7% of the 1059 SOX2-bound regions have the canonical SOX2-binding consensus sequence CAAAG (Table S3).

c-e, gene ontology (GO) terms of significantly enriched cellular components (**c**), molecular function (**d**), and biological processes (**e**) represented by the top1059 SOX2-bound genomic regions.

f, overrepresented disease ontology terms of the top1059 SOX2-bound genomic regions.

g-l, genomic views showing SOX2 binding and overlapping with epigenetic marker H3K27Ac in the astrocytic genes *Gfap*, *Apq4*, *Wnt7a*, *Ntrk2*, *Kcnj10,* and *Sparcl1* (a.k.a. Hevin).

m, RT-qPCR assays of mRNA expression of the astrocyte signature genes in primary cortical astrocytes (DIV21) isolated from neonatal mGfap:Sox2 cKO and non-Cre control mice. Two-tailed Student's *t* test, $t_{(4)} = 4.453$ *Sox2*, $t_{(4)} = 3.210$ *Gfap*, $t_{(4)} = 5.723$ *Aqp4*, $t_{(4)} = 3.396$ *Sparcl1*, $t_{(4)} = 3.372$ *Wnt7a*, $t_{(4)} = 3.154$ *Ntrk2*, $t_{(4)} = 4.448$ *Kcnj10*.

n, RNA-seq identifies representative downregulated genes encoding classic mature astrocytic markers, newly discovered mature astrocytic markers, and key astrocytic functional genes in mGfap:Sox2 cKO spinal cord at P80. Asterisks indicate SOX2-bound downregulated genes (**Table S1**). Y-axis, fold changes (FC) of relative expression in mGfap:Sox2 cKO compared with non-Cre Ctrl.

o, Western blot assay of representative downregulated DEGs GFAP, GLAST, and SPARCL1 in the adult brain of mGfap:Sox2 cKO mice. Two-tailed Student's t test, $t_{(4)} = 2.916$ SPARCL1, $t_{(4)} = 3.304$ GFAP, , $t_{(4)} = 3.030$ GLAST.

p, top 15 significantly enriched GO biological process terms of downregulated genes in mGfap:Sox2 cKO spinal cord. The number of downregulated genes in each term is shown at the right. Padj, adjusted *P* value.

Figure 6 – Downregulation of glutamate transporters and impaired glutamate uptake of *Sox2*-deficient astrocytes

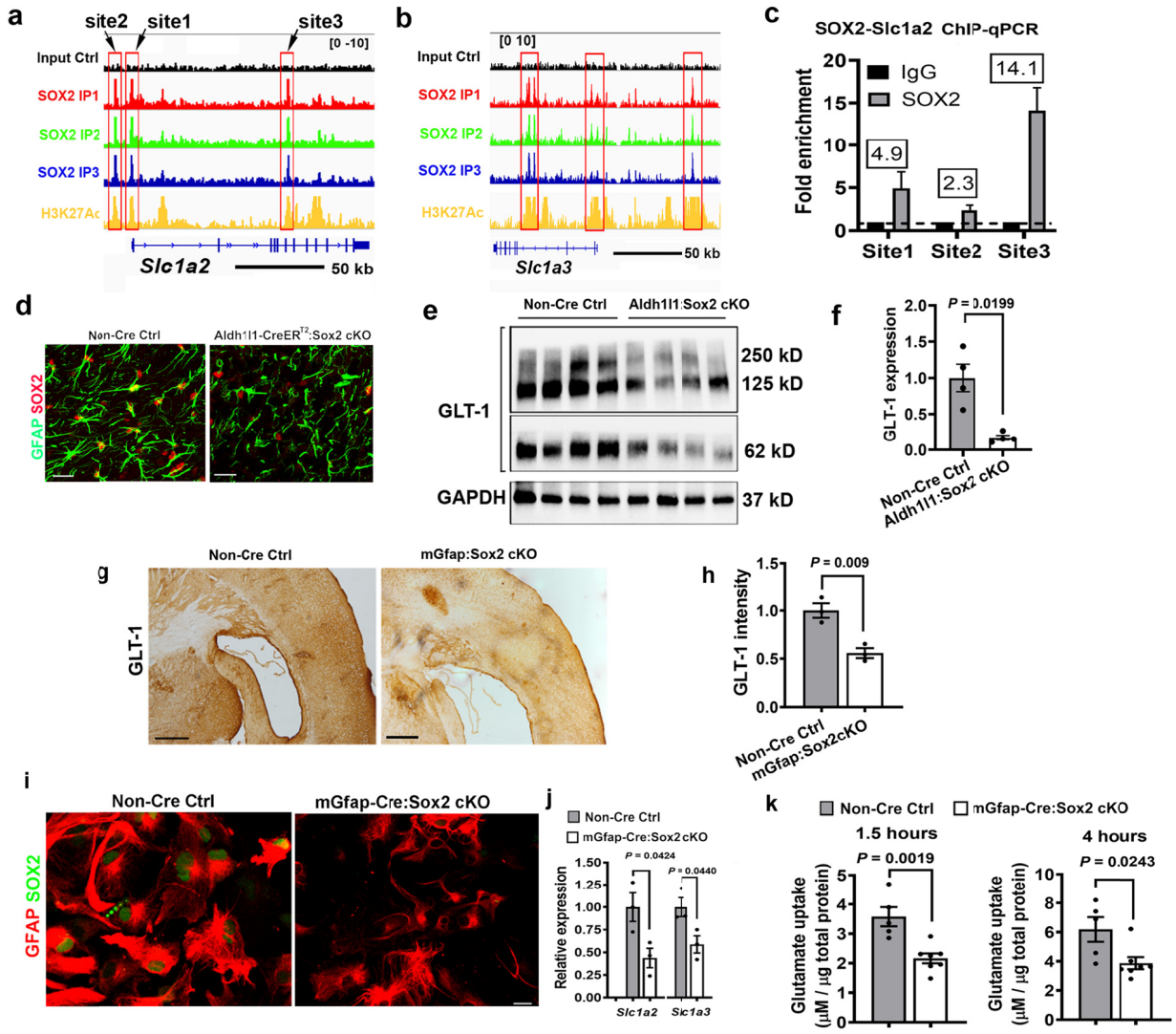

a-b, genomic view of astrocytic glutamate transporter genes Slc1a2 (**a**) and Slc1a3 (**b**) and SOX2-binding sites and genomic occupancy of H3K27Ac, an epigenetic marker of active enhancer/promoter. Note that SOX2-bound sites are occupied by H2K27Ac markers.

c, qPCR of SOX2 (or IgG Ctrl)-immunoprecipitated chromatin confirmation of the SOX2-binding site 1, 2, and 3 in the enhancer/promoter and intronic regions of Slc1a2 gene (a).

d, IHC showing SOX2 is disrupted in GFAP^{+} cortical astrocytes in the brain of P21 Aldh1l1:Sox2 cKO mice which was treated with tamoxifen at P4-P9.

e-f, representative image of Western blot images (e) and quantification (f) of GLT-1 in P21 brain. The quantification was performed based on 62 kD (monomer), 125 kD (dimer), and 250 kD (tetramer) GLT-1. Gray bar, non-Cre Ctrl, white bar, Aldh1l1:Sox2 cKO. Two-tailed Student's *t* test with Welch's correction, corrected $t_{(4.3)} = 3.193$.

g-h, representative DAB histological images (g) and quantification (h) of GLT1 in the forebrain of mGfap:Sox2 cKO and non-Cre Ctrl mice. Scale bar=200µm. Two-tailed Student's *t* test, $t_{(4)}$ = 4.832

i, Representative images of GFAP and SOX2 immunocytochemistry in primary astrocytes at DIV21.

j, RT-qPCR assay of *Slc1a2* and *Slc1a3* in primary astrocytes at DIV21. Two-tailed Student's *t* test, $t_{(4)}$ = 2.940 Slc1a2, $t_{(4)}$ = 2.915 Slc1a3.

k, glutamate uptake at 1.5 h and 4 h after glutamate incubation at DIV21. Two-tailed Student's *t* test, $t_{(10)}$ = 4.188 at 1.5 h and $t_{(10)}$ = 2.650 at 4 h.

Figure 7 – Hyperactivity of astroglial *Sox2*-deficient mice

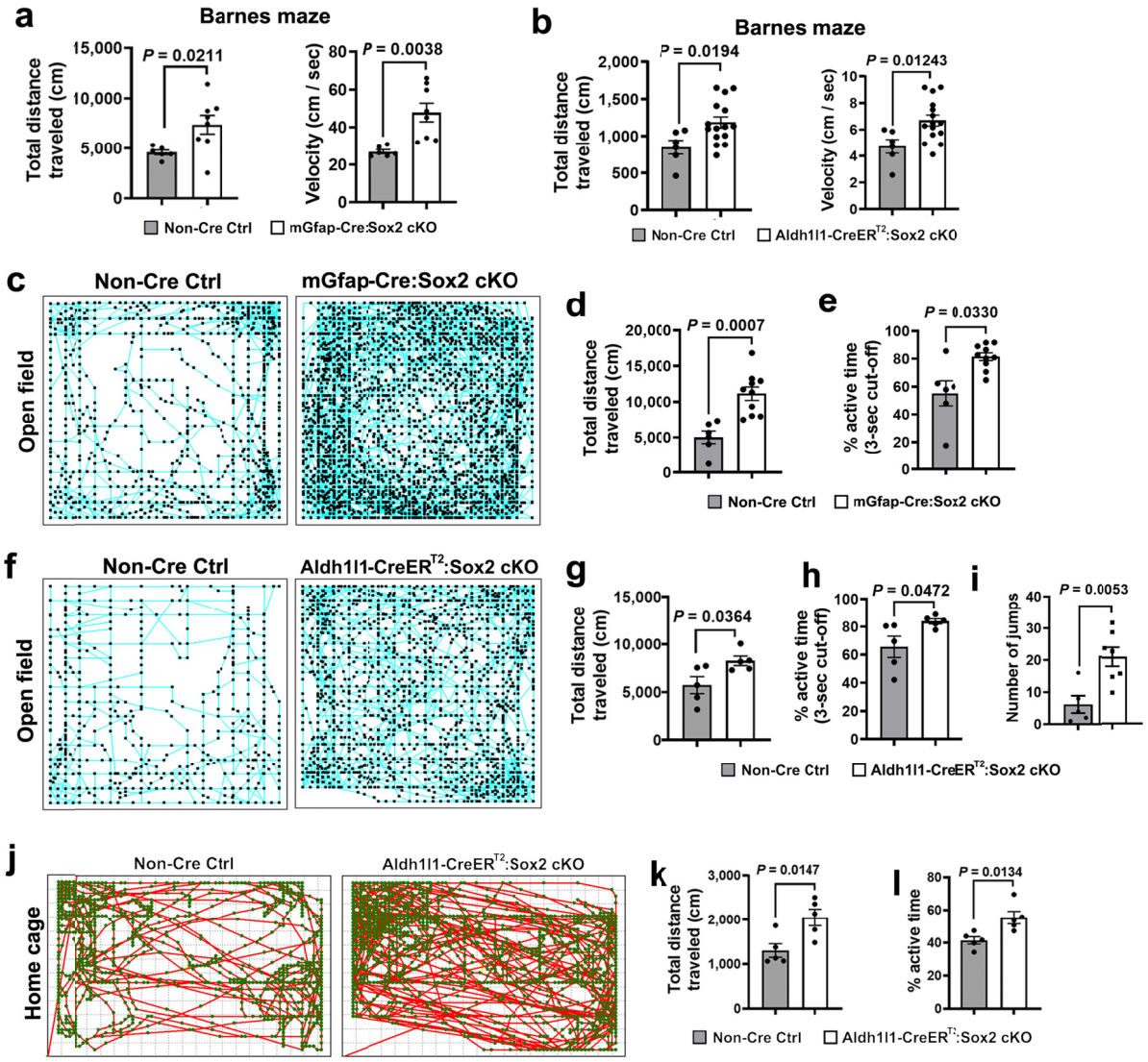

a, total distance traveled (left) and velocity during Barnes maze test. The data was collected on day 6 after 5 consecutive days training. Two months old mGfap:Sox2 mice and non-Cre control littermates were used. Two-tailed Student's t test, Welch's-corrected $t_{(7.9)}$ = 2.873 total distance, Welch's-corrected $t_{(7.6)}$ = 4.097 velocity.

b, total distance traveled (left) and movement velocity. The data was collected on day 6 after 5 consecutive days training. Aldh1l1:Sox2 cKO mice and non-Cre control littermates were treated with tamoxifen to induce SOX2 disruption at P14, P15, and P16 (once a day) and tested on at 2 months old. Two-tailed Student's t test, $t_{(19)}$ = 2.553 total distance, $t_{(19)}$ = 2.695 velocity.

c, representative real-time tracing of movement of two-month old non-Cre Ctrl and mGfap:Sox2 cKO mice in the open field.

d-e, total distance traveled (**d**) and percentage (**e**) of active time in the open field. Two-tailed Student's t test, $t_{(14)}$ = 4.360 total distance, Welch-corrected $t_{(6.0)}$ = 2.759 active time.

f, representative real-time tracing of movement of two-month old non-Cre Ctrl and Aldh1l1:Sox2 cKO mice in the open field. Tamoxifen was administered at P14, P15, and P16 to induce SOX2 disruption in astrocytes.

g-h, total distance traveled (**g**) and percentage (**h**) of active time in the open field. Two-tailed Student's t test, $t_{(8)} = 2.510$ total distance, $t_{(8)} = 2.343$ active time.

i, number of jumps in the open field during 20-minute sessions. Aldh1l1:Sox2 cKO and non-Cre Ctrl littermates were treated with tamoxifen at P14, P15, and P16 and test at two months old. Two-tailed Student's t test, $t_{(10)} = 3.545$.

j-l, representative real-time tracing of animal movement in the home cages (**j**) and quantification of total distance traveled (*k*) and percentage of active time (l) during the 20-minute sessions. Aldh1l1:Sox2 cKO and non-Cre Ctrl littermates were treated with tamoxifen at P14, P15, and P16 and test on 2.5-month old. Two-tailed Student's t test, $t_{(8)} = 3.097$ total distance, $t_{(8)} = 3.159$ active time.

Figure 8 – Astroglial *Sox2* deficiency results in elevated excitability of neurons in the corticostriatal circuit.

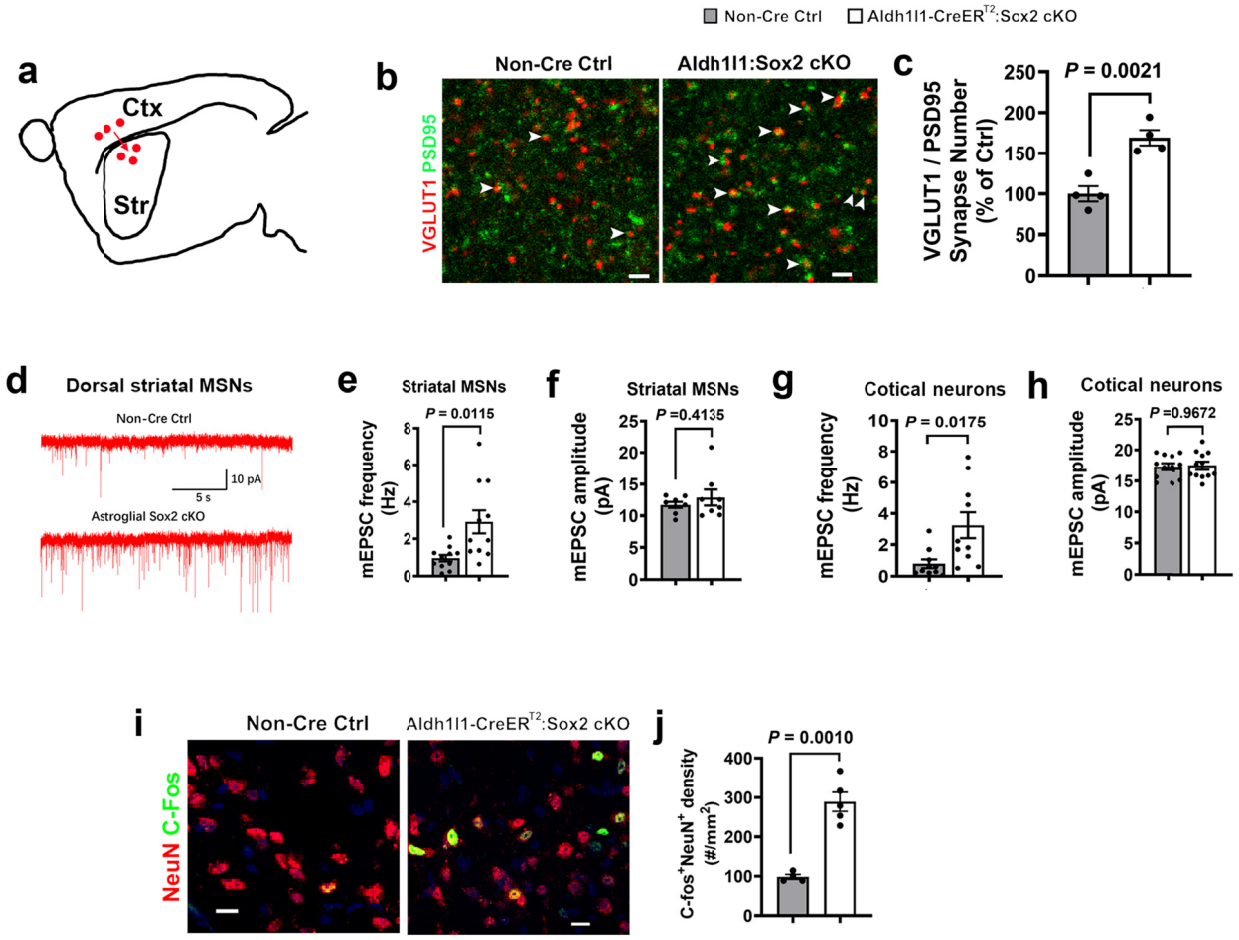

a, schematic drawing depicting cotical neuronal projections onto dorsal striatal medium spinal neurons (MSNs) in the corticostriatal circuitry. Ctx, cortex, Str, striatum.

b, representative IHC confocal images of presynaptic marker vesicular glutamate transporter 1 (VGLUT1) and postsynaptic marker PSD95 in the dorsal striatum of 2-month old Aldh1l1:Sox2 cKO and Ctrl mice which had been injected with tamoxifen at P14, P15, and P16 (once a day). Arrowheads point to VGLUT1/PSD95 co-labeled puncta. Scale bar=1 μm.

c, VGLUT1/PSD95 co-labeled puncta density quantified by Puncta Analyzer plug-in of NIH Image J. Two-tailed Student's t test, $t_{(6)} = 5.177$.

d, current tracing of representative dorsal striatal MSNs from non-Cre Ctrl and Aldh1l1:Sox2 mice at P35 (tamoxifen at P15 and P16).

e-f, mean frequency (**e**) and amplitude (**f**) of mEPSC of MSNs in the dorsal striatum of astroglial *Sox2*-deficient mice (white bar) and *Sox2*-intact mice (gray bar) . Two-tailed Student's t test, Welch-corrected $t_{(11.6)} = 3.001$ frequency; Welch-corrected $t_{(8.9)} = 0.8576$ amplitude.

g-h, mean frequency (**g**) and amplitude (**h**) of mEPSC of the deep layer cortical neurons of astroglial *Sox2*-deficient mice (white bar) and *Sox2*-intact mice (gray bar) . Two-tailed Student's t test, Welch-corrected $t_{(10.99)}$ = 2.793 frequency; $t_{(22)}$ = 0.2997 amplitude.

i-j, representative confocal images of neuron marker NeuN and immediate early gene C-Fos (**i**) and quantification (**j**) in the dorsal striatum of Aldh1l1:Sox2 cKO and non-Cre Ctrl mice at P21 (hydroxy-tamoxifen at P4-P9). Two-tailed Student's t test, Welch-corrected $t_{(4.48)}$ = 7.554

Supplementary Information

Supplementary Figure 1 – Ubiquitous SOX2 deletion downregulates GFAP expression in Sox2-CreER^{T2}:Sox2$^{fl/+}$ mice

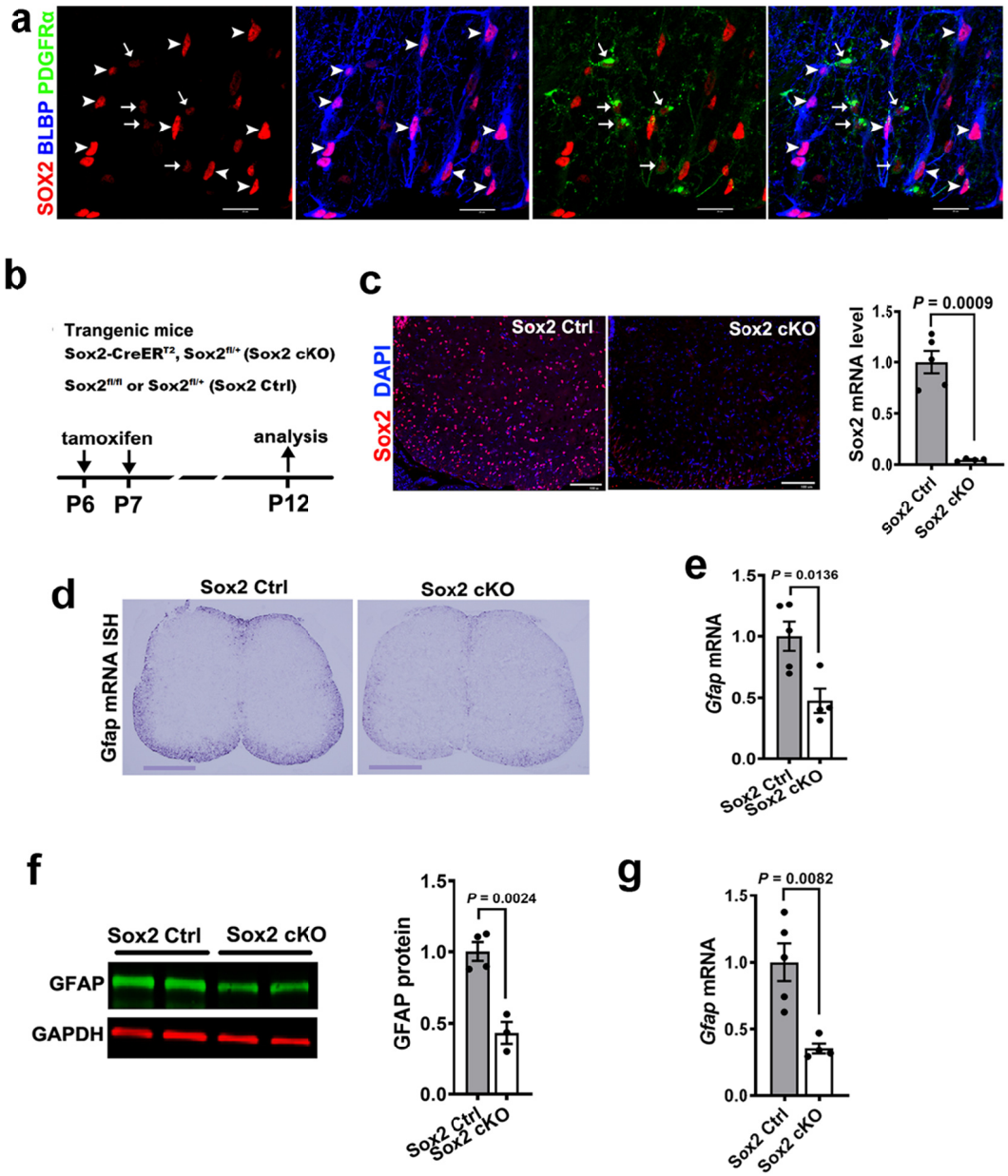

a, confocal images showing Sox2 is expressed at a higher level in brain lipid basic protein (BLBP)$^+$ astrocytic lineage cells (arrowheads) compared with PDGFRα$^+$ oligodendrocyte progenitor cells, OPCs (arrows) in the spinal cord at postnatal day 6 (P6). Scale bar=50μm.

b, experimental designs for panel **c**-**g**.

c, representative images of SOX2 immunostaining and RT-qPCR assay of *Sox2* mRNA in the spinal cord. Two-tailed Student's t test, Welch-corrected $t_{(4.027)}$ = 8.689. Scale bar, 100µm.

d, In situ hybridization showing downregulation of *Gfap* mRNA in the spinal cord. Scale bar=500µm.

e, RT-qPCR assay of *Gfap* mRNA in the spinal cord. Two-tailed Student's t test, $t_{(7)}$ = 3.277.

f, Western blot images and quantification of GFAP in the spinal cord. GAPDH serves as the loading control. Two-tailed Student's t test, $t_{(5)}$ = 5.644.

g, RT-qPCR assay of *Gfap* mRNA in the forebrain. Two-tailed Student's t test, Welch-corrected $t_{(4.639)}$ = 0.0082.

Supplementary Figure 2 – SOX2 cKO does not compromise the functional integrity of the blood brain or spinal cord barriers

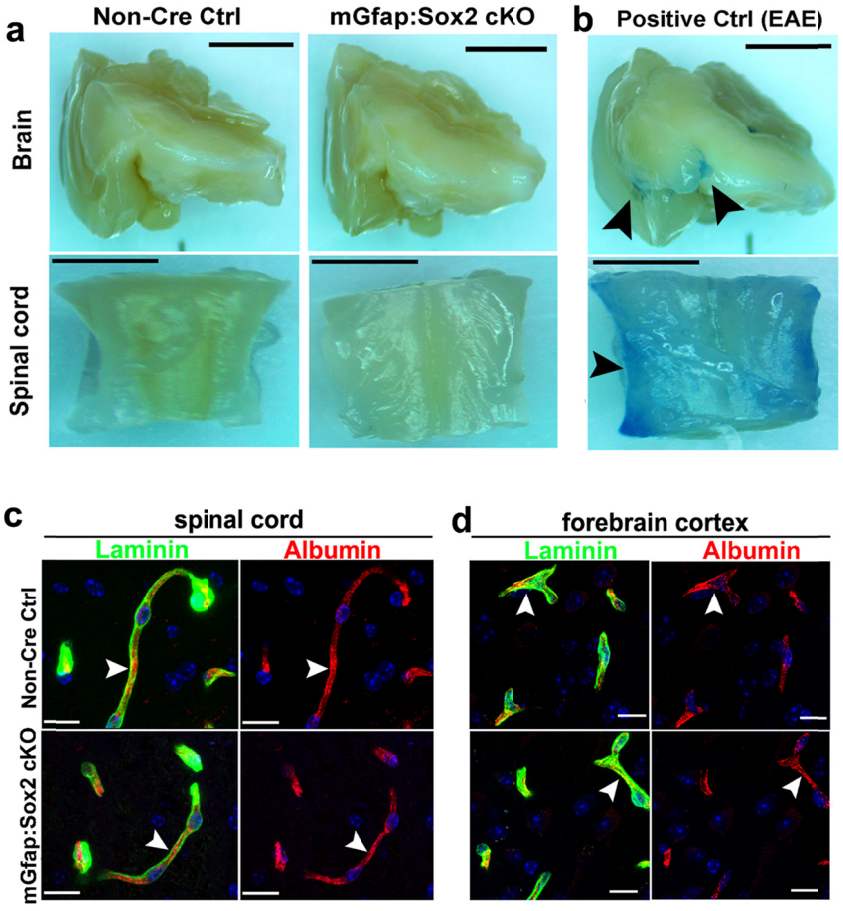

a-b, blood brain (spinal cord) barrier functional assessment by Evans blue dye which was administered thought tail vein injection 30 minutes prior to sacrifice. As a positive control of a leaky barrier, Evans Blue dye was consistently observed in the brain and the spinal cord of mice that had been injured by MOG-peptide$_{35-55}$-induced experimental autoimmune encephalomyelitis

(EAE). Scale bars = 1/8 inch in the brain and 1/16 inch in the spinal cord. Arrowheads in **b** point to Evans blue leakage into the neural tissue.

c-d, confocal images showing the blood-borne macromolecule albumin is strictly confined to the blood vessels labeled by the basement membrane marker Laminin (arrowheads) in the spinal cord (c) and the cerebral cortex (d) of both mGFAP:Sox2 cKO and non-Cre Ctrl mice. Scale bar = 20 um.

Supplementary Figure 3 – whole cell recording of cortical astrocytes in Aldh1l1:Sox2 cKO and non-Cre Ctrl mice at P30-P35 (tamoxifen treatment at P14-P16)

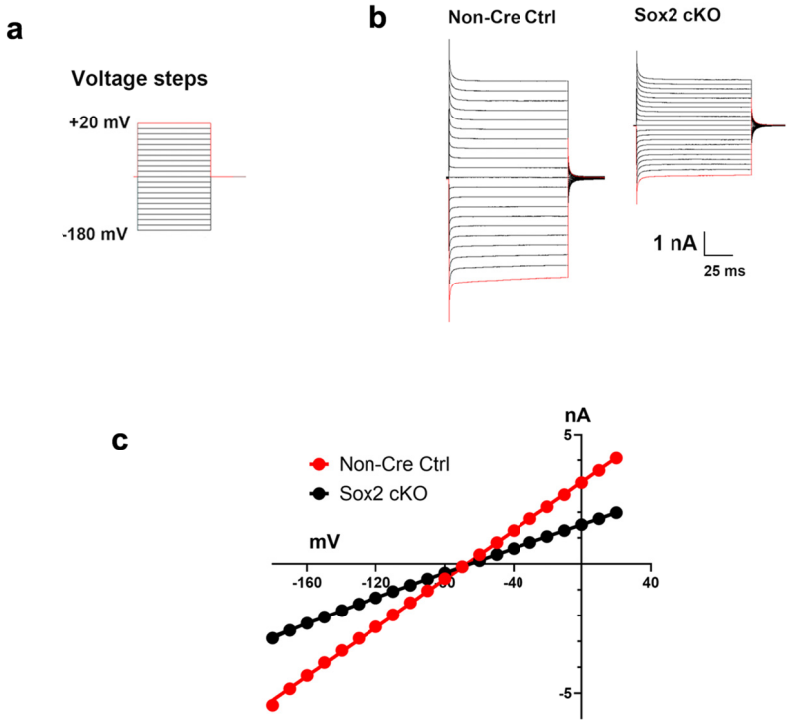

a, voltage step protocol used for astrocyte recording, from -180mV - +20mV with step size of 10mV.

b, representative current tracing of cortical astrocytes from non-Cre Ctrl and Aldh1l1:Sox2 cKO brain.

c, current-voltage (I-V) curve of *Sox2*-deficient (n=21) and *Sox2*-intact (n=15) astrocytes showing passive ion conductance of astrocytes . 3-4 mice were used in each group. Note the nearly linear I-V characteristics of both *Sox2*-intact and deficient astrocytes with apparently different slopes.

Supplementary Figure 4 – transcriptome alteration in the spinal cord of adult mGfap:Sox2 cKO mice

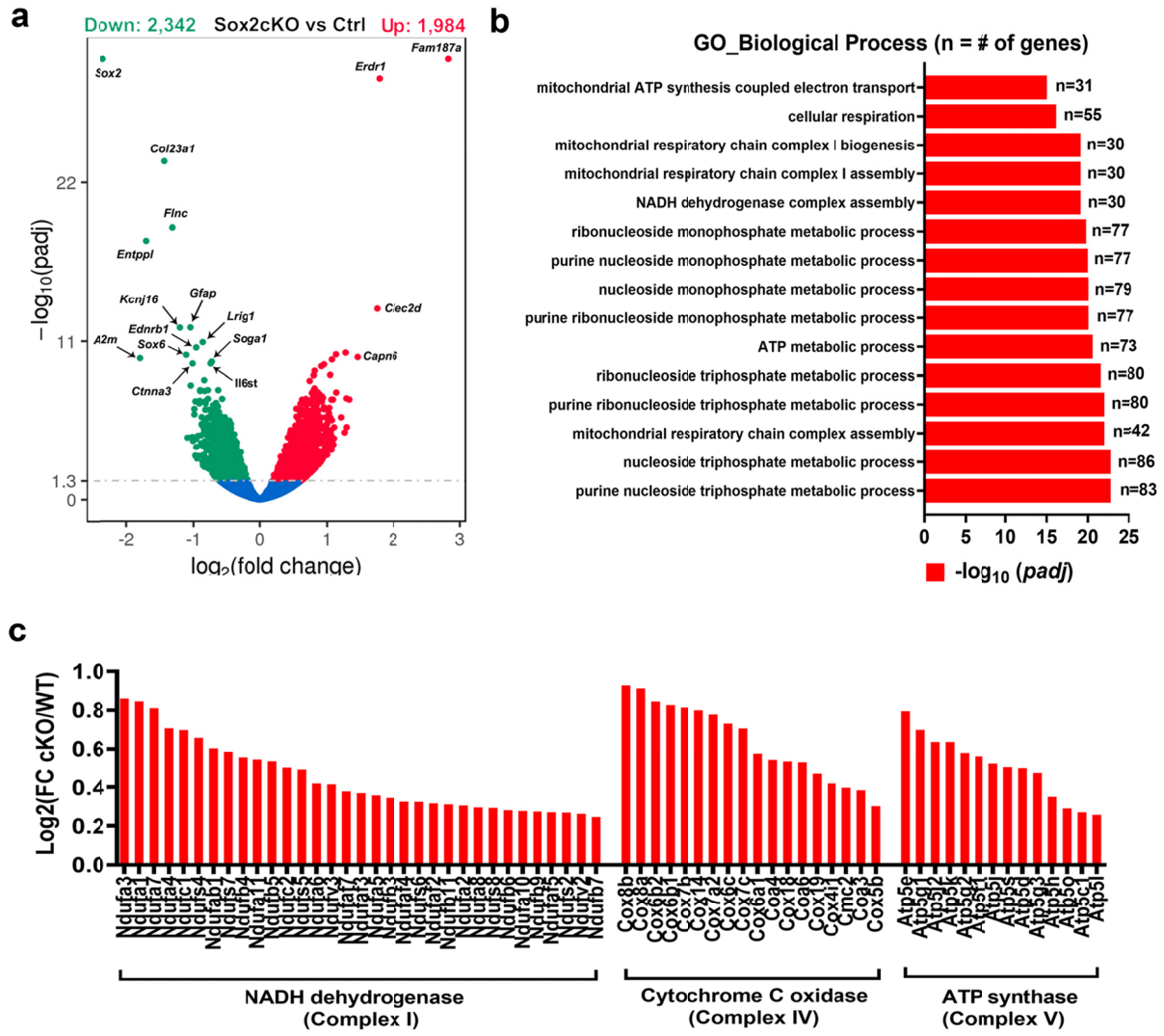

RNA-seq was performed by using total RNA isolated from the adult (P80) spinal cord of mGfap:Sox2 cKO and non-Ce Ctrl mice (n=3 each group).

a, volcanic graph depicting the distribution of 2,324 downregulated and 1,984 upregulated genes.

b, top 15 significantly enriched GO terms of biological process of upregulated DEGs ranked by adjusted P values. The number of genes in each term is shown at the right. Padj, adjusted P value. Note that biological processes involved in ATP biosynthesis are significantly over-represented among the upregulated genes, likely resulting from a secondary adaption to impaired astrocyte maturation.

c, fold changes of upregulated DEGs in mGfap:Sox2 cKO encoding different subunits of Complex I, IV and V of the mitochondrial respiratory chain.

Supplementary Figure 5 – Astroglial *Sox2*-deficent mice develop normal motor skills

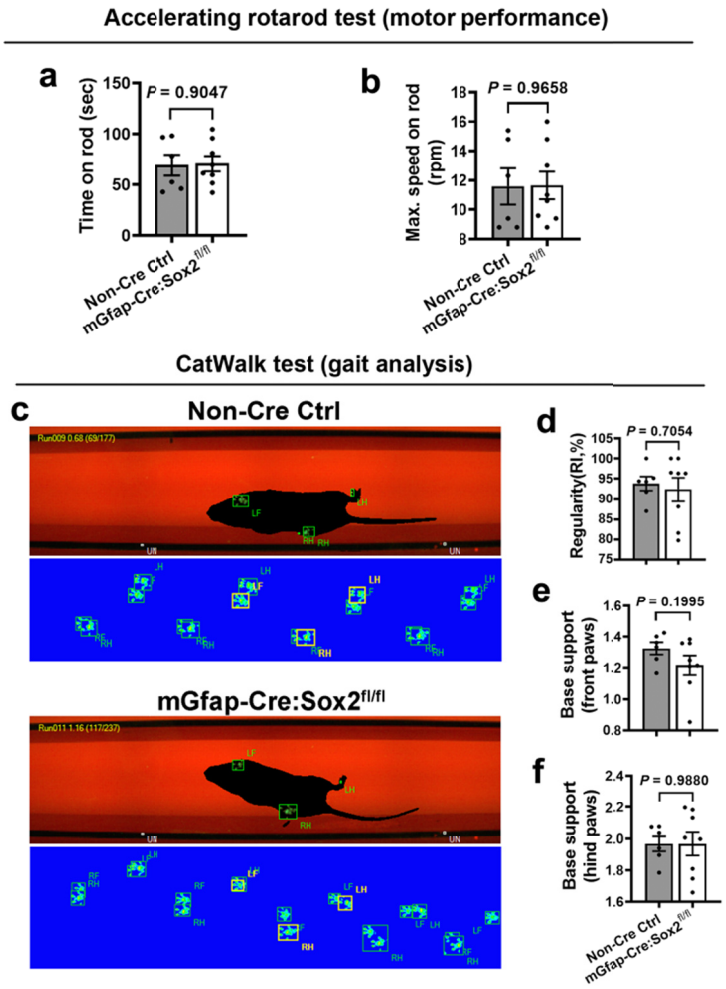

a, retention times on the accelerating rod before falling off. Two-tailed Student's t test, $t_{(12)} = 0.1223$.

b, maximal rotarod speed at the time of falling off. Two-tailed Student's t test, $t_{(12)} = 0.0438$.

c, representative images of footprints and gaits in unforced moving of non-Cre control and mGfap:Sox2 cKO mice.

d, gait analysis by the automatic CatWalk XT equipment (Noldus) showing the gait regularity index, which is the percentage of regular paw placements relative to the total irregular and regular paw placements. Two-tailed Student's t test, $t_{(12)} = 0.7054$.

e, base of support of front paws assessed by the distance (cm) of both forelimbs to each other. Two-tailed Student's t test, $t_{(12)} = 1.358$.

f, base of support of hind paws assessed by the distance (cm) of both hindlimbs to each other. Two-tailed Student's t test, $t_{(12)} = 0.0153$.

Supplementary Figure 6 – Astroglial Sox2-deficent mice develop normal cognitive ability in spatial memory and learning – evidence from Barnes maze test.

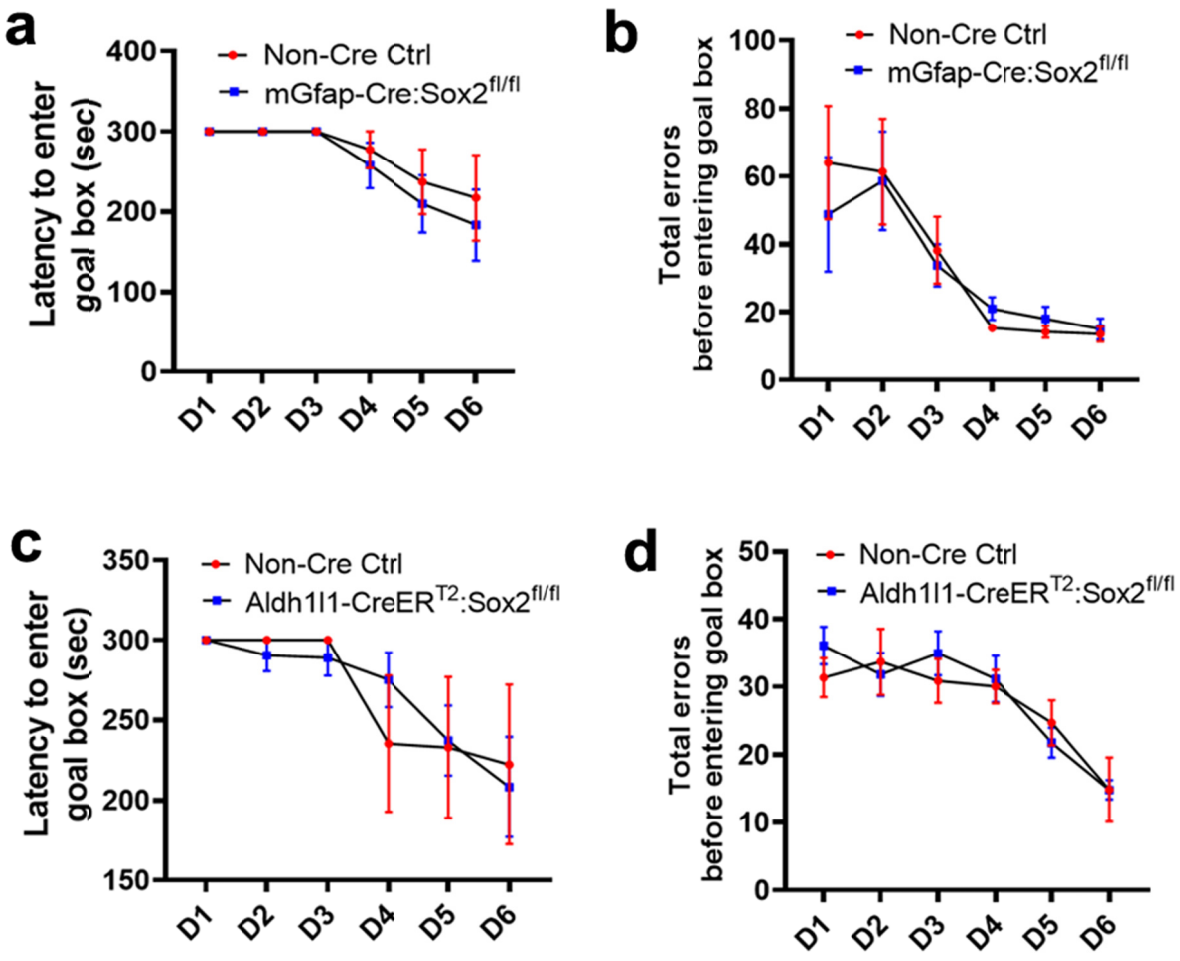

Adult (P60) non-Cre Ctrl and astroglial *Sox2*-deficient animals (mGfap:Sox2 cKO and Aldh1l1:Sox2 cKO) were trained for 5 consecutive days (D1-D5) on Barnes maze for learning and memorizing the goal box with visual cue assistance followed by testing at day 6 (D6).

a, time latency to entering the goal box. If a mouse did not enter the goal box by the end of 5 minutes, the latency was designated as 5 minutes (300 seconds). Two-way ANOVA, $F_{(1, 72)}$ = 0.1052, P = 0.7466 genotype (mGfap:Sox2cKO vs non-Cre Ctrl); $F_{(5, 72)}$ = 5.056, P = 0.0005 time-course. N=6 non-Cre Ctrl, 8 mGfap:Sox2 cKO

b, total errors of non-goal box visits before entering the goal box. Two-way ANOVA, $F_{(1, 72)}$ = 0.1052, P = 0.7466 genotype; $F_{(5, 72)}$ = 8.348, P < 0.0001 time-course.

c, time latency to entering the goal box. Two-way ANOVA, $F_{(1, 114)}$ = 0.0107, P = 0.9178 genotype (Aldh1l1:Sox2 cKO vs non-Cre Ctrl); $F_{(5, 114)}$ = 4.232, P = 0.0015 time-course. N=6 non-Cre Ctrl, 15 Aldh1l1:Sox2 cKO at P60. Tamoxifen were administered to Aldh1l1:Sox2 cKO and non-Cre Ctrl mice at P14-P16.

d, total errors of non-goal box visits before entering the goal box. Two-way ANOVA, $F_{(1, 114)}$ = 0.1738, P = 0.6776 genotype; $F_{(5, 114)}$ = 8.931, P < 0.0001 time-course. Tamoxifen were administered to Aldh1l1:Sox2 cKO and non-Cre Ctrl mice at P14-P16.

Note that mGfap:Sox2 cKO (or Aldh1l1:Sox2 cKO) and their corresponding non-Cre Ctrl mice displayed progressively increasing ability of learning and memory, as evidenced by gradually decreased time latency to enter the goal box (a, c) and reduced total errors before entering the goal box (b, d). However, there was no significant difference in the time latency and total errors between genotypes.

Supplementary Figure 7 – Astroglial *Sox2*-deficiency does not perturb animal social behavior

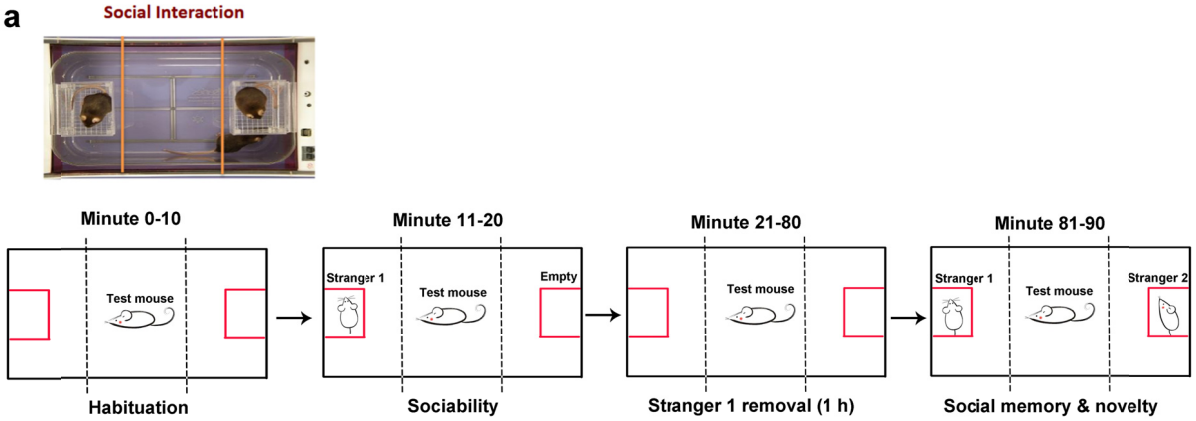

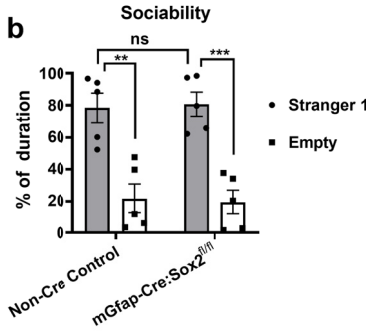

c

Tukey's multiple comparisons test	95.00% CI of diff.	Significant?	Summary	Adjusted P Value
Non-Cre Control:Stranger 1 vs. Non-Cre Control:Empty	22.64 to 90.76	Yes	**	0.0011
Non-Cre Control:Stranger 1 vs. mGfap-Cre:Sox2$^{fl/fl}$:Stranger 1	-36.34 to 31.79	No	ns	0.9974
Non-Cre Control:Stranger 1 vs. mGfap-Cre:Sox2$^{fl/fl}$:Empty	24.92 to 93.04	Yes	***	0.0007
Non-Cre Control:Empty vs. mGfap-Cre:Sox2$^{fl/fl}$:Stranger 1	-93.04 to -24.92	Yes	***	0.0007
Non-Cre Control:Empty vs. mGfap-Cre:Sox2$^{fl/fl}$:Empty	-31.79 to 36.34	No	ns	0.9974
mGfap-Cre:Sox2$^{fl/fl}$:Stranger 1 vs. mGfap-Cre:Sox2$^{fl/fl}$:Empty	27.19 to 95.31	Yes	***	0.0005

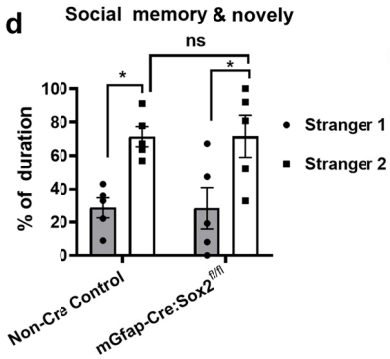

e

Tukey's multiple comparisons test	95.00% CI of diff.	Significant?	Summary	Adjusted P Value
Non-Cre Control:Stranger 1 vs. Non-Cre Control:Stranger 2	-82.65 to -2.759	Yes	*	0.0341
Non-Cre Control:Stranger 1 vs. mGfap-Cre:Sox2$^{fl/fl}$:Stranger 1	-39.71 to 40.17	No	ns	>0.9999
Non-Cre Control:Stranger 1 vs. mGfap-Cre:Sox2$^{fl/fl}$:Stranger 2	-82.88 to -2.989	Yes	*	0.0330
Non-Cre Control:Stranger 2 vs. mGfap-Cre:Sox2$^{fl/fl}$:Stranger 1	2.989 to 82.88	Yes	*	0.0330
Non-Cre Control:Stranger 2 vs. mGfap-Cre:Sox2$^{fl/fl}$:Stranger 2	-40.17 to 39.71	No	ns	>0.9999
mGfap-Cre:Sox2$^{fl/fl}$:Stranger 1 vs. mGfap-Cre:Sox2$^{fl/fl}$:Stranger 2	-83.11 to -3.218	Yes	*	0.0319

a, schematic procedures of mouse social interaction assessed by three-chamber test. Both *mGfap-Cre:Sox2*$^{fl/fl}$ and littermate non-Cre control mice were tested at 2-month old.

b-c, sociability (b) of and multiple comparison results (c) of two-way ANOVA. $F_{(1, 16)}$ = 3.612e-14, P > 0.9999 for genotype; $F_{(1, 16)}$ = 49.08 P < 0.0001 for animals.

d-e, short-term social memory (d) and multiple comparison results (e) of two-way ANOVA. $F_{(1, 16)}$ = 4.104e-12, P > 0.9999 for genotype; $F_{(1, 16)}$ = 18.91 P = 0.0005 for animals.

Note that each group of mice had normal social ability, as demonstrated by significant more time spent in the chamber with a peer mouse (Stranger 1) than the empty chamber (~80% vs ~20%) (b). No significant difference was found between Non-Cre Ctrl and mGfap:Sox2 cKO mice in the

time spent in the chamber with a peer mouse or in the empty chamber (c). When a novel mouse (Stranger 2) and the previously familiar one (Stranger 1) were introduced after a short period of time (a), both non-Cre Ctrl and mGfap:Sox2cKO mice spent significant more time with the novel than the familiar one and no difference was found between the two groups (d, e).

Supplementary Figure 8 – postnatal SOX2 disruption in astrocytes results in long-term hyperactive locomotion.

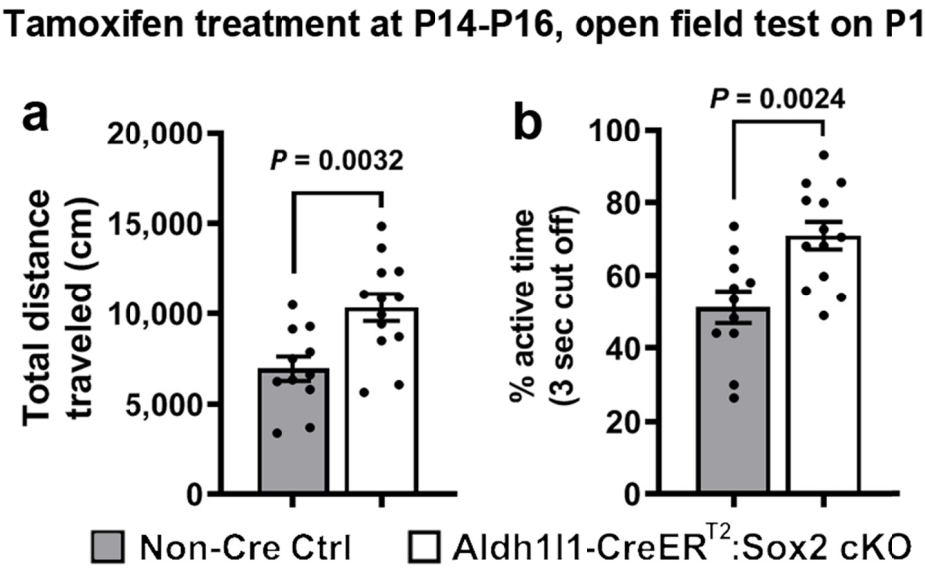

Both Aldh1l1:Sox2 cKO and non-Cre Ctrl mice were received tamoxifen at P14-P16 (three injections, once daily) to induce astroglial SOX2 deletion. Open field test was performed on P150 **a-b**, total distance traveled (**a**) and percentage (**b**) of active time in the open field. Two-tailed Student's t test, $t_{(22)}$ = 3.314 total distance, $t_{(22)}$ = 3.427 active time.

Table S1 – Gene annotations of 9602 SOX2-bound sites

Table S2 – Top 1059 SOX2-bound sites with fold-enrichment greater than 10

Table S3 – SOX2-bound and flanking DNA sequences of top 1059 peaks

Table S4 – Gene ontology analysis of top 1059 SOX2-bound genomic regions

Table S5 – RNA-seq analysis of differentially expressed genes (DEGs) in the spinal cord between adult mGfap:Sox2 cKO and littermate control mice

Table S6 – Gene ontology analysis of downregulated DEGs in the spinal cord between adult mGfap:Sox2 cKO and littermate control mice

Table S7 – Gene ontology analysis of upregulated DEGs in the spinal cord between adult mGfap:Sox2 cKO and littermate control mice

Table S8 – Gene encoding the components of the mitochondrial respiratory chain complexes are upregulated.

Supplementary Video 1 – Jump behavior of an adult non-Cre Ctrl mouse in the open field

Supplementary Video 2 - Jump behavior of an adult Aldh1l1:Sox2 cKO mouse in the open field

(Supplementary Tables and Videos were submitted separately as Supplementary Datasets in the manuscript tracking system)

Reference

1. Lin YP, Ouchi Y, Satoh S, Watanabe S. Sox2 plays a role in the induction of amacrine and Muller glial cells in mouse retinal progenitor cells. Invest Ophthalmol Vis Sci. 2009;50(1):68-74. doi: 10.1167/iovs.07-1619. PubMed PMID: 18719084.
2. Taranova OV, Magness ST, Fagan BM, Wu Y, Surzenko N, Hutton SR, Pevny LH. SOX2 is a dose-dependent regulator of retinal neural progenitor competence. Gene Dev. 2006;20(9):1187-202. Epub 2006/05/03. doi: 10.1101/gad.1407906. PubMed PMID: 16651659; PMCID: 1472477.
3. Heavner WE, Andoniadou CL, Pevny LH. Establishment of the neurogenic boundary of the mouse retina requires cooperation of SOX2 and WNT signaling. Neural Dev. 2014;9:27. doi: 10.1186/1749-8104-9-27. PubMed PMID: 25488119; PMCID: PMC4295269.
4. Bachleda AR, Pevny LH, Weiss ER. Sox2-Deficient Muller Glia Disrupt the Structural and Functional Maturation of the Mammalian Retina. Invest Ophthalmol Vis Sci. 2016;57(3):1488-99. doi: 10.1167/iovs.15-17994. PubMed PMID: 27031842; PMCID: PMC4819558.
5. Surzenko N, Crowl T, Bachleda A, Langer L, Pevny L. SOX2 maintains the quiescent progenitor cell state of postnatal retinal Muller glia. Development. 2013;140(7):1445-56. doi: 10.1242/dev.071878. PubMed PMID: 23462474; PMCID: PMC3596988.
6. Whitney IE, Keeley PW, St John AJ, Kautzman AG, Kay JN, Reese BE. Sox2 regulates cholinergic amacrine cell positioning and dendritic stratification in the retina. J Neurosci. 2014;34(30):10109-21. doi: 10.1523/JNEUROSCI.0415-14.2014. PubMed PMID: 25057212; PMCID: PMC4107400.
7. Pevny LH, Nicolis SK. Sox2 roles in neural stem cells. Int J Biochem Cell Biol. 2010;42(3):421-4. doi: 10.1016/j.biocel.2009.08.018. PubMed PMID: 19733254.
8. Favaro R, Valotta M, Ferri AL, Latorre E, Mariani J, Giachino C, Lancini C, Tosetti V, Ottolenghi S, Taylor V, Nicolis SK. Hippocampal development and neural stem cell maintenance require Sox2-dependent regulation of Shh. Nat Neurosci. 2009;12(10):1248-56. doi: 10.1038/nn.2397. PubMed PMID: 19734891.
9. Ferri A, Favaro R, Beccari L, Bertolini J, Mercurio S, Nieto-Lopez F, Verzeroli C, La Regina F, De Pietri Tonelli D, Ottolenghi S, Bovolenta P, Nicolis SK. Sox2 is required for embryonic development of the ventral telencephalon through the activation of the ventral determinants Nkx2.1 and Shh. Development. 2013;140(6):1250-61. doi: 10.1242/dev.073411. PubMed PMID: 23444355.
10. Ferri AL, Cavallaro M, Braida D, Di Cristofano A, Canta A, Vezzani A, Ottolenghi S, Pandolfi PP, Sala M, DeBiasi S, Nicolis SK. Sox2 deficiency causes neurodegeneration and impaired neurogenesis in

the adult mouse brain. Development. 2004;131(15):3805-19. Epub 2004/07/09. doi: 10.1242/dev.01204. PubMed PMID: 15240551.
11. Zhao C, Ma D, Zawadzka M, Fancy SP, Elis-Williams L, Bouvier G, Stockley JH, de Castro GM, Wang B, Jacobs S, Casaccia P, Franklin RJ. Sox2 Sustains Recruitment of Oligodendrocyte Progenitor Cells following CNS Demyelination and Primes Them for Differentiation during Remyelination. J Neurosci. 2015;35(33):11482-99. doi: 10.1523/JNEUROSCI.3655-14.2015. PubMed PMID: 26290228.
12. Hoffmann SA, Hos D, Kuspert M, Lang RA, Lovell-Badge R, Wegner M, Reiprich S. Stem cell factor Sox2 and its close relative Sox3 have differentiation functions in oligodendrocytes. Development. 2014;141(1):39-50. Epub 2013/11/22. doi: 10.1242/dev.098418. PubMed PMID: 24257626; PMCID: 3865748.
13. Zhang S, Zhu X, Gui X, Croteau C, Song L, Xu J, Wang A, Bannerman P, Guo F. Sox2 is essential for oligodendroglial proliferation and differentiation during postnatal brain myelination and CNS remyelination. J Neurosci. 2018. doi: 10.1523/JNEUROSCI.1291-17.2018. PubMed PMID: 29335358.
14. Zhang S, Rasai A, Wang Y, Xu J, Bannerman P, Erol D, Tsegaye D, Wang A, Soulika A, Zhan X, Guo F. The Stem Cell Factor Sox2 Is a Positive Timer of Oligodendrocyte Development in the Postnatal Murine Spinal Cord. Mol Neurobiol. 2018. Epub 2018/04/07. doi: 10.1007/s12035-018-1035-7. PubMed PMID: 29623612.
15. Guo F, Maeda Y, Ma J, Delgado M, Sohn J, Miers L, Ko EM, Bannerman P, Xu J, Wang Y, Zhou C, Takebayashi H, Pleasure D. Macroglial plasticity and the origins of reactive astroglia in experimental autoimmune encephalomyelitis. J Neurosci. 2011;31(33):11914-28. Epub 2011/08/19. doi: 31/33/11914 [pii]

10.1523/JNEUROSCI.1759-11.2011. PubMed PMID: 21849552.
16. Chen C, Zhong X, Smith DK, Tai W, Yang J, Zou Y, Wang LL, Sun J, Qin S, Zhang CL. Astrocyte-Specific Deletion of Sox2 Promotes Functional Recovery After Traumatic Brain Injury. Cereb Cortex. 2017:1-16. Epub 2017/11/22. doi: 10.1093/cercor/bhx303. PubMed PMID: 29161339.
17. Kautzman AG, Keeley PW, Nahmou MM, Luna G, Fisher SK, Reese BE. Sox2 regulates astrocytic and vascular development in the retina. Glia. 2018;66(3):623-36. Epub 2017/11/28. doi: 10.1002/glia.23269. PubMed PMID: 29178409; PMCID: PMC5767138.
18. Zhuo L, Theis M, Alvarez-Maya I, Brenner M, Willecke K, Messing A. hGFAP-cre transgenic mice for manipulation of glial and neuronal function in vivo. Genesis. 2001;31(2):85-94. Epub 2001/10/23. PubMed PMID: 11668683.
19. Zhang S, Kim B, Zhu X, Gui X, Wang Y, Lan Z, Prabhu P, Fond K, Wang A, Guo F. Glial type specific regulation of CNS angiogenesis by HIFalpha-activated different signaling pathways. Nat Commun. 2020;11(1):2027. doi: 10.1038/s41467-020-15656-4. PubMed PMID: 32332719.
20. Ge WP, Miyawaki A, Gage FH, Jan YN, Jan LY. Local generation of glia is a major astrocyte source in postnatal cortex. Nature. 2012;484(7394):376-80. doi: 10.1038/nature10959. PubMed PMID: 22456708; PMCID: 3777276.
21. Kucukdereli H, Allen NJ, Lee AT, Feng A, Ozlu MI, Conatser LM, Chakraborty C, Workman G, Weaver M, Sage EH, Barres BA, Eroglu C. Control of excitatory CNS synaptogenesis by astrocyte-secreted proteins Hevin and SPARC. Proc Natl Acad Sci U S A. 2011;108(32):E440-9. Epub 2011/07/27. doi: 10.1073/pnas.1104977108. PubMed PMID: 21788491; PMCID: PMC3156217.
22. Muzumdar MD, Tasic B, Miyamichi K, Li L, Luo L. A global double-fluorescent Cre reporter mouse. Genesis. 2007;45(9):593-605. doi: 10.1002/dvg.20335. PubMed PMID: 17868096.
23. Bushong EA, Martone ME, Ellisman MH. Maturation of astrocyte morphology and the establishment of astrocyte domains during postnatal hippocampal development. Int J Dev Neurosci. 2004;22(2):73-86. doi: 10.1016/j.ijdevneu.2003.12.008. PubMed PMID: 15036382.

24. Saunders NR, Dziegielewska KM, Mollgard K, Habgood MD. Markers for blood-brain barrier integrity: how appropriate is Evans blue in the twenty-first century and what are the alternatives? Front Neurosci. 2015;9:385. Epub 2015/11/19. doi: 10.3389/fnins.2015.00385. PubMed PMID: 26578854; PMCID: PMC4624851.
25. Dallerac G, Chever O, Rouach N. How do astrocytes shape synaptic transmission? Insights from electrophysiology. Front Cell Neurosci. 2013;7:159. doi: 10.3389/fncel.2013.00159. PubMed PMID: 24101894; PMCID: PMC3787198.
26. Zhou M, Schools GP, Kimelberg HK. Development of GLAST(+) astrocytes and NG2(+) glia in rat hippocampus CA1: mature astrocytes are electrophysiologically passive. J Neurophysiol. 2006;95(1):134-43. Epub 2005/08/12. doi: 10.1152/jn.00570.2005. PubMed PMID: 16093329.
27. Nimmerjahn A, Kirchhoff F, Kerr JN, Helmchen F. Sulforhodamine 101 as a specific marker of astroglia in the neocortex in vivo. Nat Methods. 2004;1(1):31-7. Epub 2005/03/23. doi: 10.1038/nmeth706. PubMed PMID: 15782150.
28. Olsen ML, Sontheimer H. Functional implications for Kir4.1 channels in glial biology: from K+ buffering to cell differentiation. J Neurochem. 2008;107(3):589-601. doi: 10.1111/j.1471-4159.2008.05615.x. PubMed PMID: 18691387; PMCID: PMC2581639.
29. Bailey TL, Boden M, Buske FA, Frith M, Grant CE, Clementi L, Ren J, Li WW, Noble WS. MEME SUITE: tools for motif discovery and searching. Nucleic Acids Res. 2009;37(Web Server issue):W202-8. doi: 10.1093/nar/gkp335. PubMed PMID: 19458158; PMCID: PMC2703892.
30. Bowles J, Schepers G, Koopman P. Phylogeny of the SOX family of developmental transcription factors based on sequence and structural indicators. Dev Biol. 2000;227(2):239-55. doi: 10.1006/dbio.2000.9883. PubMed PMID: 11071752.
31. Engelen E, Akinci U, Bryne JC, Hou J, Gontan C, Moen M, Szumska D, Kockx C, van Ijcken W, Dekkers DH, Demmers J, Rijkers EJ, Bhattacharya S, Philipsen S, Pevny LH, Grosveld FG, Rottier RJ, Lenhard B, Poot RA. Sox2 cooperates with Chd7 to regulate genes that are mutated in human syndromes. Nat Genet. 2011;43(6):607-11. doi: 10.1038/ng.825. PubMed PMID: 21532573.
32. McLean CY, Bristor D, Hiller M, Clarke SL, Schaar BT, Lowe CB, Wenger AM, Bejerano G. GREAT improves functional interpretation of cis-regulatory regions. Nat Biotechnol. 2010;28(5):495-501. Epub 2010/05/04. doi: 10.1038/nbt.1630. PubMed PMID: 20436461; PMCID: PMC4840234.
33. Schiweck J, Eickholt BJ, Murk K. Important Shapeshifter: Mechanisms Allowing Astrocytes to Respond to the Changing Nervous System During Development, Injury and Disease. Front Cell Neurosci. 2018;12:261. doi: 10.3389/fncel.2018.00261. PubMed PMID: 30186118; PMCID: PMC6111612.
34. Devinsky O, Vezzani A, Najjar S, De Lanerolle NC, Rogawski MA. Glia and epilepsy: excitability and inflammation. Trends Neurosci. 2013;36(3):174-84. doi: 10.1016/j.tins.2012.11.008. PubMed PMID: 23298414.
35. Holt LM, Hernandez RD, Pacheco NL, Torres Ceja B, Hossain M, Olsen ML. Astrocyte morphogenesis is dependent on BDNF signaling via astrocytic TrkB.T1. Elife. 2019;8. doi: 10.7554/eLife.44667. PubMed PMID: 31433295; PMCID: PMC6726422.
36. Creyghton MP, Cheng AW, Welstead GG, Kooistra T, Carey BW, Steine EJ, Hanna J, Lodato MA, Frampton GM, Sharp PA, Boyer LA, Young RA, Jaenisch R. Histone H3K27ac separates active from poised enhancers and predicts developmental state. Proc Natl Acad Sci U S A. 2010;107(50):21931-6. Epub 2010/11/26. doi: 10.1073/pnas.1016071107. PubMed PMID: 21106759; PMCID: PMC3003124.
37. Li J, Khankan RR, Caneda C, Godoy MI, Haney MS, Krawczyk MC, Bassik MC, Sloan SA, Zhang Y. Astrocyte-to-astrocyte contact and a positive feedback loop of growth factor signaling regulate astrocyte maturation. Glia. 2019;67(8):1571-97. doi: 10.1002/glia.23630. PubMed PMID: 31033049; PMCID: PMC6557696.

38. Pajarillo E, Rizor A, Lee J, Aschner M, Lee E. The role of astrocytic glutamate transporters GLT-1 and GLAST in neurological disorders: Potential targets for neurotherapeutics. Neuropharmacology. 2019;161:107559. doi: 10.1016/j.neuropharm.2019.03.002. PubMed PMID: 30851309; PMCID: PMC6731169.
39. Chung WS, Clarke LE, Wang GX, Stafford BK, Sher A, Chakraborty C, Joung J, Foo LC, Thompson A, Chen C, Smith SJ, Barres BA. Astrocytes mediate synapse elimination through MEGF10 and MERTK pathways. Nature. 2013;504(7480):394-400. Epub 2013/11/26. doi: 10.1038/nature12776. PubMed PMID: 24270812; PMCID: PMC3969024.
40. Rimmele TS, Rosenberg PA. GLT-1: The elusive presynaptic glutamate transporter. Neurochem Int. 2016;98:19-28. Epub 2016/05/01. doi: 10.1016/j.neuint.2016.04.010. PubMed PMID: 27129805; PMCID: PMC5070539.
41. Pitts MW. Barnes Maze Procedure for Spatial Learning and Memory in Mice. Bio Protoc. 2018;8(5). Epub 2018/04/14. doi: 10.21769/bioprotoc.2744. PubMed PMID: 29651452; PMCID: PMC5891830.
42. Seibenhener ML, Wooten MC. Use of the Open Field Maze to measure locomotor and anxiety-like behavior in mice. J Vis Exp. 2015(96):e52434. Epub 2015/03/06. doi: 10.3791/52434. PubMed PMID: 25742564; PMCID: PMC4354627.
43. Shepherd GM. Corticostriatal connectivity and its role in disease. Nat Rev Neurosci. 2013;14(4):278-91. Epub 2013/03/21. doi: 10.1038/nrn3469. PubMed PMID: 23511908; PMCID: PMC4096337.
44. Kreitzer AC. Physiology and pharmacology of striatal neurons. Annu Rev Neurosci. 2009;32:127-47. doi: 10.1146/annurev.neuro.051508.135422. PubMed PMID: 19400717.
45. Nagai J, Rajbhandari AK, Gangwani MR, Hachisuka A, Coppola G, Masmanidis SC, Fanselow MS, Khakh BS. Hyperactivity with Disrupted Attention by Activation of an Astrocyte Synaptogenic Cue. Cell. 2019;177(5):1280-92 e20. Epub 2019/04/30. doi: 10.1016/j.cell.2019.03.019. PubMed PMID: 31031006; PMCID: PMC6526045.
46. Ippolito DM, Eroglu C. Quantifying synapses: an immunocytochemistry-based assay to quantify synapse number. J Vis Exp. 2010(45). doi: 10.3791/2270. PubMed PMID: 21113117; PMCID: PMC3159596.
47. Hoffman GE, Smith MS, Verbalis JG. c-Fos and related immediate early gene products as markers of activity in neuroendocrine systems. Front Neuroendocrinol. 1993;14(3):173-213. doi: 10.1006/frne.1993.1006. PubMed PMID: 8349003.
48. Bullitt E. Expression of c-fos-like protein as a marker for neuronal activity following noxious stimulation in the rat. J Comp Neurol. 1990;296(4):517-30. doi: 10.1002/cne.902960402. PubMed PMID: 2113539.
49. Perrin-Terrin AS, Jeton F, Pichon A, Frugiere A, Richalet JP, Bodineau L, Voituron N. The c-FOS Protein Immunohistological Detection: A Useful Tool As a Marker of Central Pathways Involved in Specific Physiological Responses In Vivo and Ex Vivo. J Vis Exp. 2016(110). doi: 10.3791/53613. PubMed PMID: 27167092; PMCID: PMC4941991.
50. Molofsky AV, Deneen B. Astrocyte development: A Guide for the Perplexed. Glia. 2015;63(8):1320-9. Epub 2015/05/13. doi: 10.1002/glia.22836. PubMed PMID: 25963996.
51. Cahoy JD, Emery B, Kaushal A, Foo LC, Zamanian JL, Christopherson KS, Xing Y, Lubischer JL, Krieg PA, Krupenko SA, Thompson WJ, Barres BA. A transcriptome database for astrocytes, neurons, and oligodendrocytes: a new resource for understanding brain development and function. J Neurosci. 2008;28(1):264-78. Epub 2008/01/04. doi: 28/1/264 [pii]

10.1523/JNEUROSCI.4178-07.2008. PubMed PMID: 18171944.

52. Fantes J, Ragge NK, Lynch SA, McGill NI, Collin JR, Howard-Peebles PN, Hayward C, Vivian AJ, Williamson K, van Heyningen V, FitzPatrick DR. Mutations in SOX2 cause anophthalmia. Nat Genet. 2003;33(4):461-3. Epub 2003/03/04. doi: 10.1038/ng1120. PubMed PMID: 12612584.
53. Que J, Okubo T, Goldenring JR, Nam KT, Kurotani R, Morrisey EE, Taranova O, Pevny LH, Hogan BL. Multiple dose-dependent roles for Sox2 in the patterning and differentiation of anterior foregut endoderm. Development. 2007;134(13):2521-31. doi: 10.1242/dev.003855. PubMed PMID: 17522155; PMCID: 3625644.
54. Avilion AA, Nicolis SK, Pevny LH, Perez L, Vivian N, Lovell-Badge R. Multipotent cell lineages in early mouse development depend on SOX2 function. Genes Dev. 2003;17(1):126-40. doi: 10.1101/gad.224503. PubMed PMID: 12514105; PMCID: 195970.
55. Kelberman D, Rizzoti K, Avilion A, Bitner-Glindzicz M, Cianfarani S, Collins J, Chong WK, Kirk JM, Achermann JC, Ross R, Carmignac D, Lovell-Badge R, Robinson IC, Dattani MT. Mutations within Sox2/SOX2 are associated with abnormalities in the hypothalamo-pituitary-gonadal axis in mice and humans. J Clin Invest. 2006;116(9):2442-55. Epub 2006/08/26. doi: 10.1172/JCI28658. PubMed PMID: 16932809; PMCID: PMC1551933.
56. Eichenbaum H. Hippocampus: cognitive processes and neural representations that underlie declarative memory. Neuron. 2004;44(1):109-20. Epub 2004/09/29. doi: 10.1016/j.neuron.2004.08.028. PubMed PMID: 15450164.
57. Sweatt JD. Hippocampal function in cognition. Psychopharmacology (Berl). 2004;174(1):99-110. Epub 2004/06/19. doi: 10.1007/s00213-004-1795-9. PubMed PMID: 15205881.
58. Shoneye T, Orrego AT, Jarvis R, Men Y, Chiang MSR, Yang Y. Differential Proliferation and Maturation of Subcortical Astrocytes During Postnatal Development. Front Neurosci. 2020;14:435. Epub 2020/05/28. doi: 10.3389/fnins.2020.00435. PubMed PMID: 32457572; PMCID: PMC7225521.
59. Golowasch J, Thomas G, Taylor AL, Patel A, Pineda A, Khalil C, Nadim F. Membrane capacitance measurements revisited: dependence of capacitance value on measurement method in nonisopotential neurons. J Neurophysiol. 2009;102(4):2161-75. Epub 2009/07/03. doi: 10.1152/jn.00160.2009. PubMed PMID: 19571202; PMCID: PMC2775376.
60. Tong X, Ao Y, Faas GC, Nwaobi SE, Xu J, Haustein MD, Anderson MA, Mody I, Olsen ML, Sofroniew MV, Khakh BS. Astrocyte Kir4.1 ion channel deficits contribute to neuronal dysfunction in Huntington's disease model mice. Nat Neurosci. 2014;17(5):694-703. doi: 10.1038/nn.3691. PubMed PMID: 24686787; PMCID: PMC4064471.
61. Hagey DW, Klum S, Kurtsdotter I, Zaouter C, Topcic D, Andersson O, Bergsland M, Muhr J. SOX2 regulates common and specific stem cell features in the CNS and endoderm derived organs. PLoS Genet. 2018;14(2):e1007224. Epub 2018/02/13. doi: 10.1371/journal.pgen.1007224. PubMed PMID: 29432416; PMCID: PMC5825159.
62. Rothstein JD, Dykes-Hoberg M, Pardo CA, Bristol LA, Jin L, Kuncl RW, Kanai Y, Hediger MA, Wang Y, Schielke JP, Welty DF. Knockout of glutamate transporters reveals a major role for astroglial transport in excitotoxicity and clearance of glutamate. Neuron. 1996;16(3):675-86. doi: 10.1016/s0896-6273(00)80086-0. PubMed PMID: 8785064.
63. Kang P, Lee HK, Glasgow SM, Finley M, Donti T, Gaber ZB, Graham BH, Foster AE, Novitch BG, Gronostajski RM, Deneen B. Sox9 and NFIA coordinate a transcriptional regulatory cascade during the initiation of gliogenesis. Neuron. 2012;74(1):79-94. Epub 2012/04/17. doi: 10.1016/j.neuron.2012.01.024. PubMed PMID: 22500632; PMCID: PMC3543821.
64. Huang AY, Woo J, Sardar D, Lozzi B, Bosquez Huerta NA, Lin CJ, Felice D, Jain A, Paulucci-Holthauzen A, Deneen B. Region-Specific Transcriptional Control of Astrocyte Function Oversees Local Circuit Activities. Neuron. 2020. doi: 10.1016/j.neuron.2020.03.025. PubMed PMID: 32320644.

65. Tiwari N, Pataskar A, Peron S, Thakurela S, Sahu SK, Figueres-Onate M, Marichal N, Lopez-Mascaraque L, Tiwari VK, Berninger B. Stage-Specific Transcription Factors Drive Astrogliogenesis by Remodeling Gene Regulatory Landscapes. Cell Stem Cell. 2018;23(4):557-71 e8. Epub 2018/10/06. doi: 10.1016/j.stem.2018.09.008. PubMed PMID: 30290178; PMCID: PMC6179960.
66. Higashimori H, Schin CS, Chiang MS, Morel L, Shoneye TA, Nelson DL, Yang Y. Selective Deletion of Astroglial FMRP Dysregulates Glutamate Transporter GLT1 and Contributes to Fragile X Syndrome Phenotypes In Vivo. J Neurosci. 2016;36(27):7079-94. Epub 2016/07/08. doi: 10.1523/JNEUROSCI.1069-16.2016. PubMed PMID: 27383586; PMCID: PMC4938857.
67. Risher WC, Patel S, Kim IH, Uezu A, Bhagat S, Wilton DK, Pilaz LJ, Singh Alvarado J, Calhan OY, Silver DL, Stevens B, Calakos N, Soderling SH, Eroglu C. Astrocytes refine cortical connectivity at dendritic spines. Elife. 2014;3. Epub 2014/12/18. doi: 10.7554/eLife.04047. PubMed PMID: 25517933; PMCID: PMC4286724.
68. Guo F, Bannerman P, Mills Ko E, Miers L, Xu J, Burns T, Li S, Freeman E, McDonough JA, Pleasure D. Ablating N-acetylaspartate prevents leukodystrophy in a Canavan disease model. Ann Neurol. 2015;77(5):884-8. Epub 2015/02/26. doi: 10.1002/ana.24392. PubMed PMID: 25712859.
69. Hull V, Wang Y, Burns T, Zhang S, Sternbach S, McDonough J, Guo F, Pleasure D. Antisense Oligonucleotide Reverses Leukodystrophy in Canavan Disease Mice. Ann Neurol. 2020;87(3):480-5. doi: 10.1002/ana.25674. PubMed PMID: 31925837.
70. Khroyan TV, Zhang J, Yang L, Zou B, Xie J, Pascual C, Malik A, Xie J, Zaveri NT, Vazquez J, Polgar W, Toll L, Fang J, Xie X. Rodent motor and neuropsychological behaviour measured in home cages using the integrated modular platform SmartCage. Clin Exp Pharmacol Physiol. 2012;39(7):614-22. Epub 2012/05/01. doi: 10.1111/j.1440-1681.2012.05719.x. PubMed PMID: 22540540; PMCID: PMC5567678.
71. Yang L, Zou B, Xiong X, Pascual C, Xie J, Malik A, Xie J, Sakurai T, Xie XS. Hypocretin/orexin neurons contribute to hippocampus-dependent social memory and synaptic plasticity in mice. J Neurosci. 2013;33(12):5275-84. Epub 2013/03/22. doi: 10.1523/JNEUROSCI.3200-12.2013. PubMed PMID: 23516292; PMCID: PMC3640412.

Figures

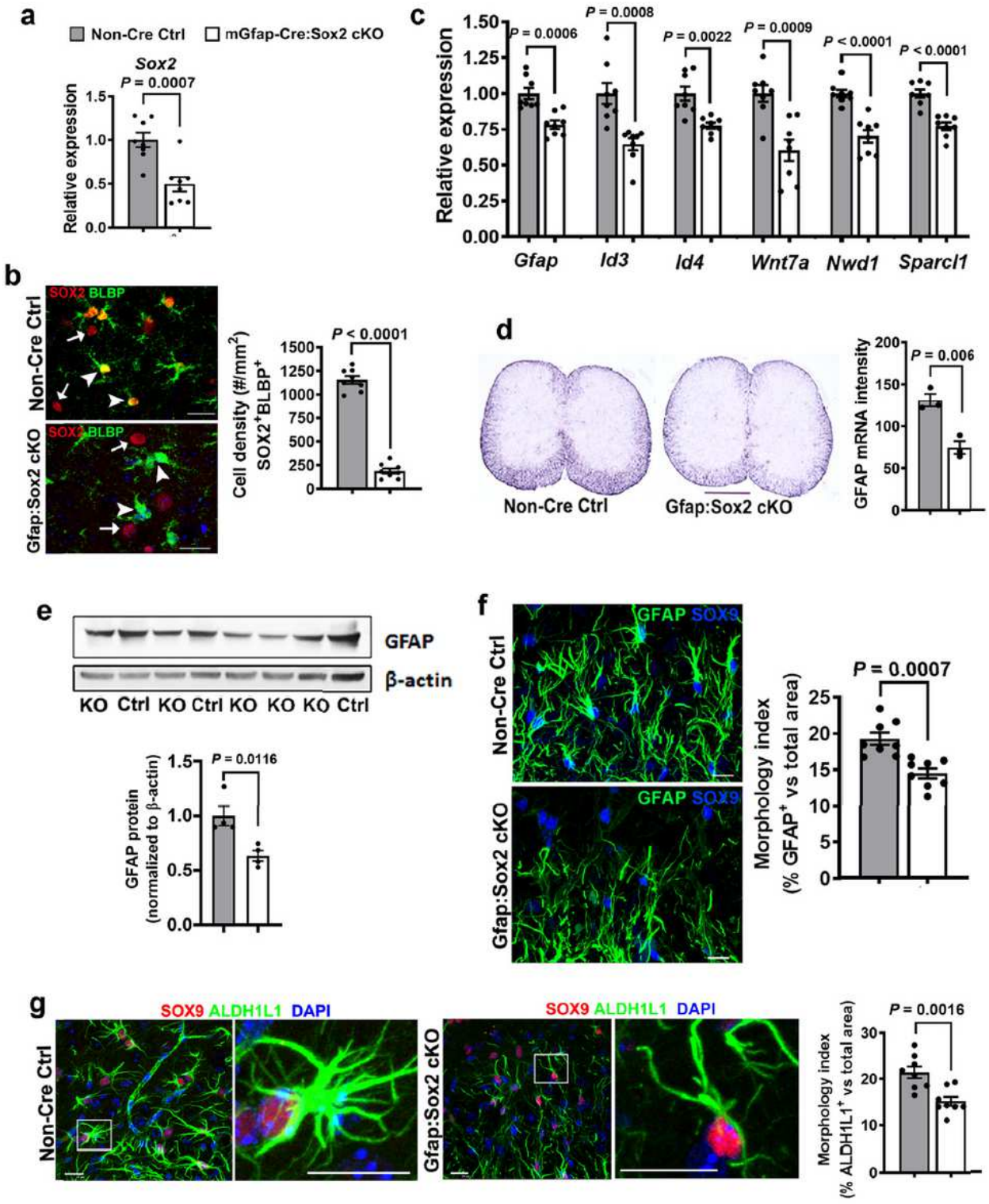

Figure 1

SOX2 conditional knockout (cK O) inhibits astrocyte maturation in mGfap- Cre:Sox2fl/fl mice. Data were collected from the spinal cord of two litters of mGfap-Cre:Sox2fl/fl (mG fap:Sox2 cKO) and non-Cre littermate control mice at P14. a, RT-qPCR assay of Sox2 mRNA. Two-tailed Student's t test, t(14)=4.312.

b, immunohistochemistry (IHC) and quantification in the spinal cord. SOX2 is expressed in BLBP+ astrocytes in Ctrl and is deleted in cKO (arrowheads). Arrows points to SOX2-expressing non-astrocytic cells. Two-tailed Student's t test, t(14)=19.44. Scale bar = 20 μm. c, RT-qPCR assay of astrocyte-enriched genes. Two- tailed Student's t test, t(14) = 4.448 Gfap, t(14) = 4.228 Id3, t(14) = 4.181 Id4, t(14) = 4.220 Wnt7a, t(14) = 5.826 Nwd1, and t(14) = 6.013 Sparcl1. d, Gfap mRNA in situ hybridization (ISH) and quantification. Two-tailed Student's t test, t(4) = 5.313. Scale bar=500μm. e, Western blot and quantification of GFAP protein level. Two-tailed Student's t test, t(6) = 3.584. f, representative images of GFAP and astrocyte nuclear marker SOX9 and the percentage of GFAP+ area among total assessed area. Two-tailed Student's t test, t(14) = 4.348. Scale bar = 10 μm. g, representative images of astrocytic process marker ALDH1L1 and SOX9 and the percentage of ALDH1L1+ area among total assessed area. Two-tailed Student's t test, t(14) = 3.889. Scale bar = 10 μm.

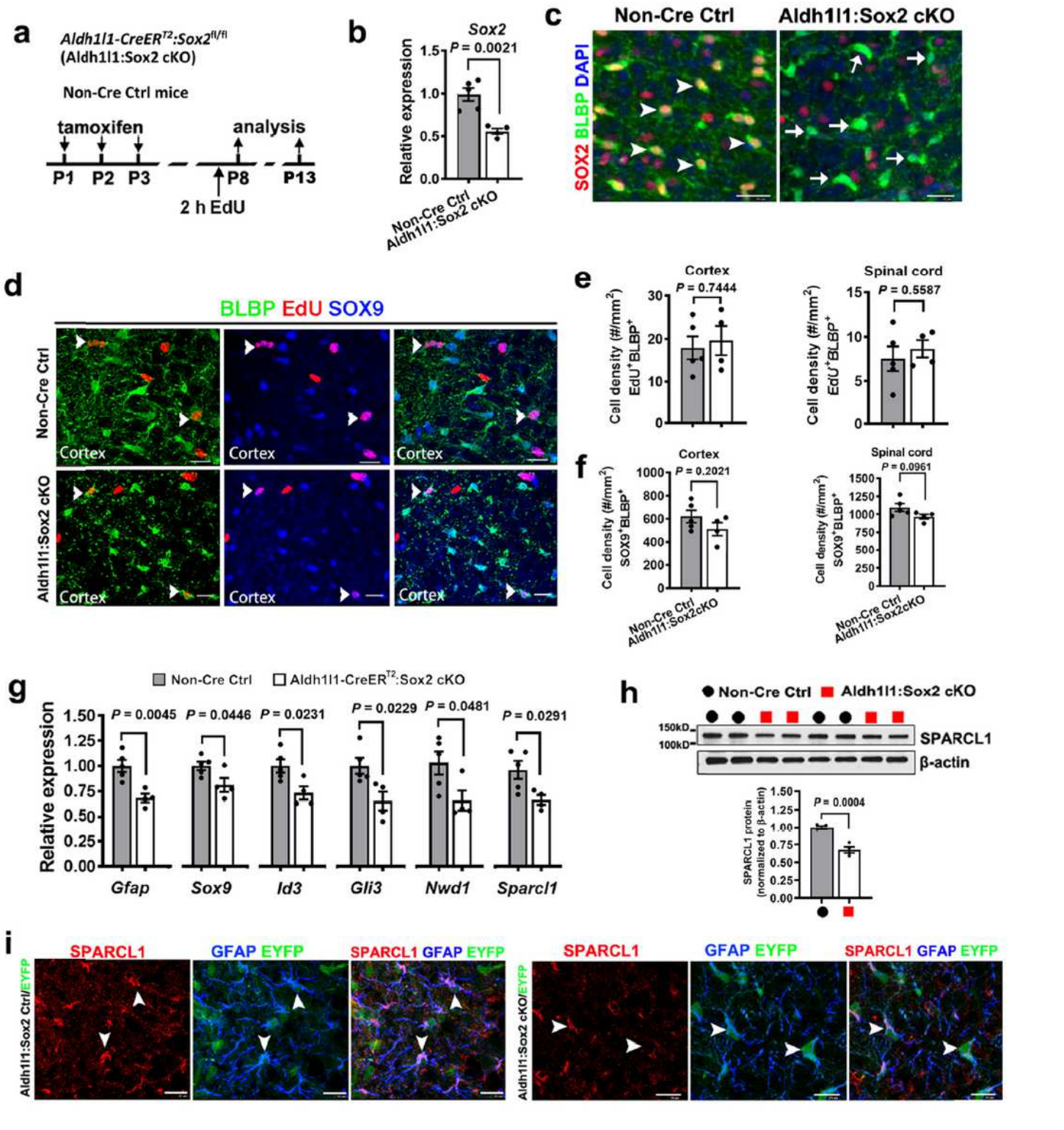

Figure 2

SOX2 cK O inhibits molecular maturation without perturbing astrocyte proliferation in the early postnatal CNS. a, experimental design. Neonatal mice carrying Aldh1l1- CreERT2:So x2fl/fl (Aldh1l1:Sox2 cK O) and Sox 2fl/fl or Sox2 fl/+ (non-Cre Ctrl) were injected with tamoxifen at P1, P2, and P3 (once a day), and analyzed at P8 (b-f) and P13 (g-i). Two hours before sacrifice at P8, thymidine analogy EdU was administered for astrocyte proliferation assay. b, RT-qP CR assay of Sox2 mRN A in the spinal cord. Two-

tailed Stu dent's t test, t(14) = 4.742. c, confocal images showing SOX2 expression in BLBP+ astrocytes in the cerebral cortex of non-Cre control mice (arrowheads, left) and absent in Aldh1l1:Sox2 cKO mice (arrows, right). Scale bar = 25 um. d, representative confocal images of BLBP, SOX9, and EdU immunostaining in the cerebral cortex. Arrowheads point to triple positive astrocytes. Scale bar = 20 um. e, density of EdU+BLBP+ proliferating astrocytes. Two-tailed Student's t test, t(7) = 0.3392 cerebral cortex and t(7) = 1.922 spinal cord. f, density of SOX9+BLBP+ astrocytes. Two-tailed Student's t test, t(7) = 1.407 cerebral cortex and t(7) = 3.481 spinal cord. g, expression of astrocyte-enriched genes in the forebrain. Two-tailed Student's t test, t(7) = 4.110 Gfap, t(7) = 2.440 Sox9, t(7) = 2.896 Id3, t(7) = 2.902 Gli3, t(7) = 2.391 Nwd1, and t(7) = 2.736 Sparcl1. h, Western blot images and quantification of mature astrocyte enriched protein SPARCL1 in the forebrain. Two-tailed Student's t test, t(6) = 6.996. i, Triple IHC of SPARCL1, SOX9, and EYFP in the cerebral cortex of Aldh1l1-CreERT2:Rosa26-EYFP and Aldh1l1-CreERT2:Sox2fl/fl:Rosa26-EYFP mice at P13.

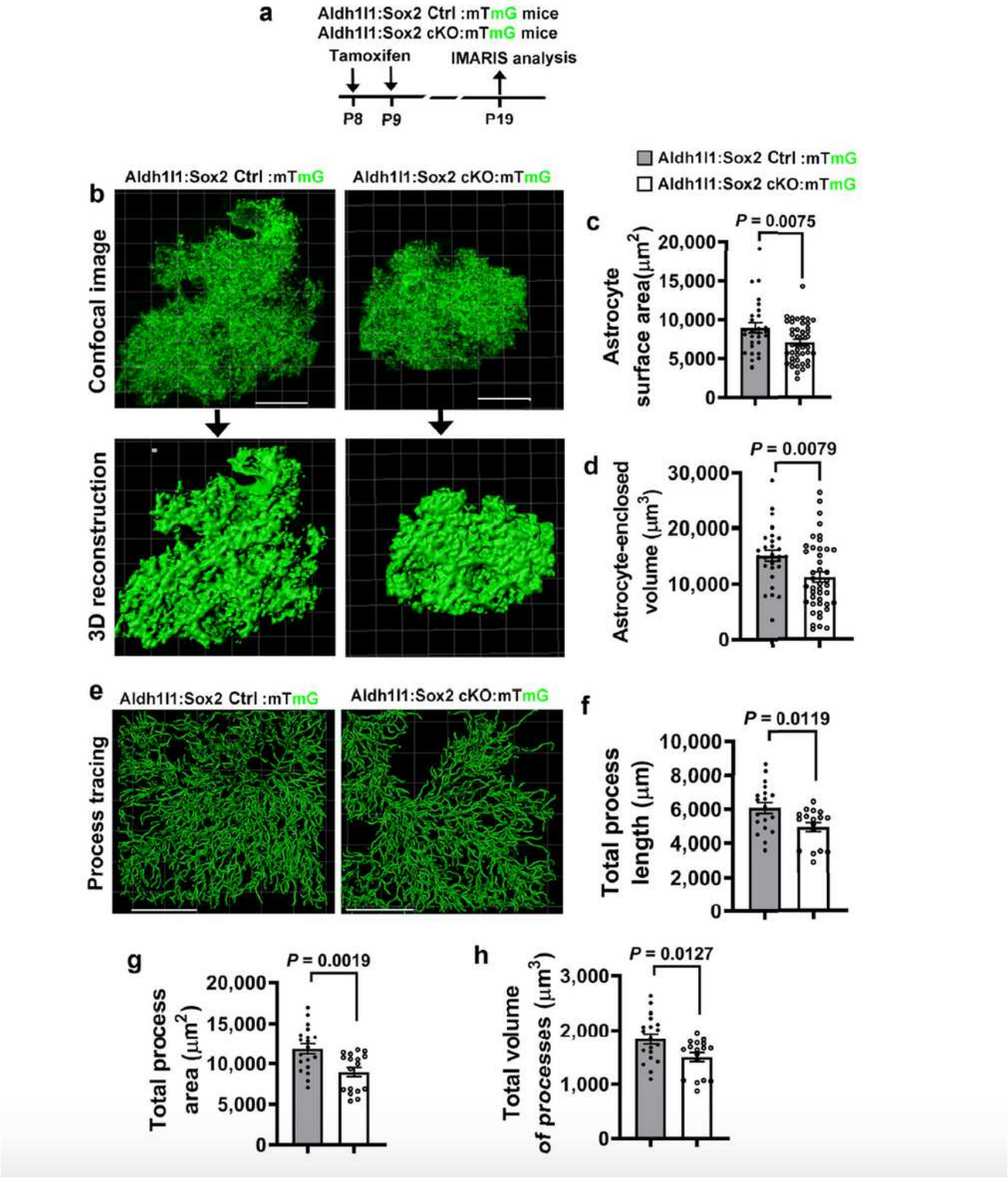

Figure 3

SOX2 regulates astrocyte morphological maturation. a, experimental design. b, maximal projection of confocal images showing mG- expressing astrocytes (upper) and 3D reconstruction of mG signals by IMARIS (lower). Scale bar = 20μm. c-d, surface area (c) and enclosed volume (d) of mG-positive astrocytes. Two-tailed Student's t test, t(69) = 2.753 surface area, t(69) = 2.737 volume. n=28 astrocytes from 3 Aldh1l1:Sox2 WT:mTmG mice and 43 astrocytes from Aldh1l1:Sox2 cKO:mTmG mice. e,

automatic tracing of mG+ astrocyte processes by the Filament Tool of IMARIS. Scale bar = 20μm. f-h, length (f), surface area (g), and volume (h) of mG+ processes of astrocytes. Two -tailed Student's t test, , t(34) = 2.658 length, t(34) = 3.376 area, and t(34) = 2.632 volume. n=17 and 19 astrocytes from 3-4 Aldh1l1:Sox2 WT:mTmG and Aldh1l1:Sox2 cKO:mTmG mice.

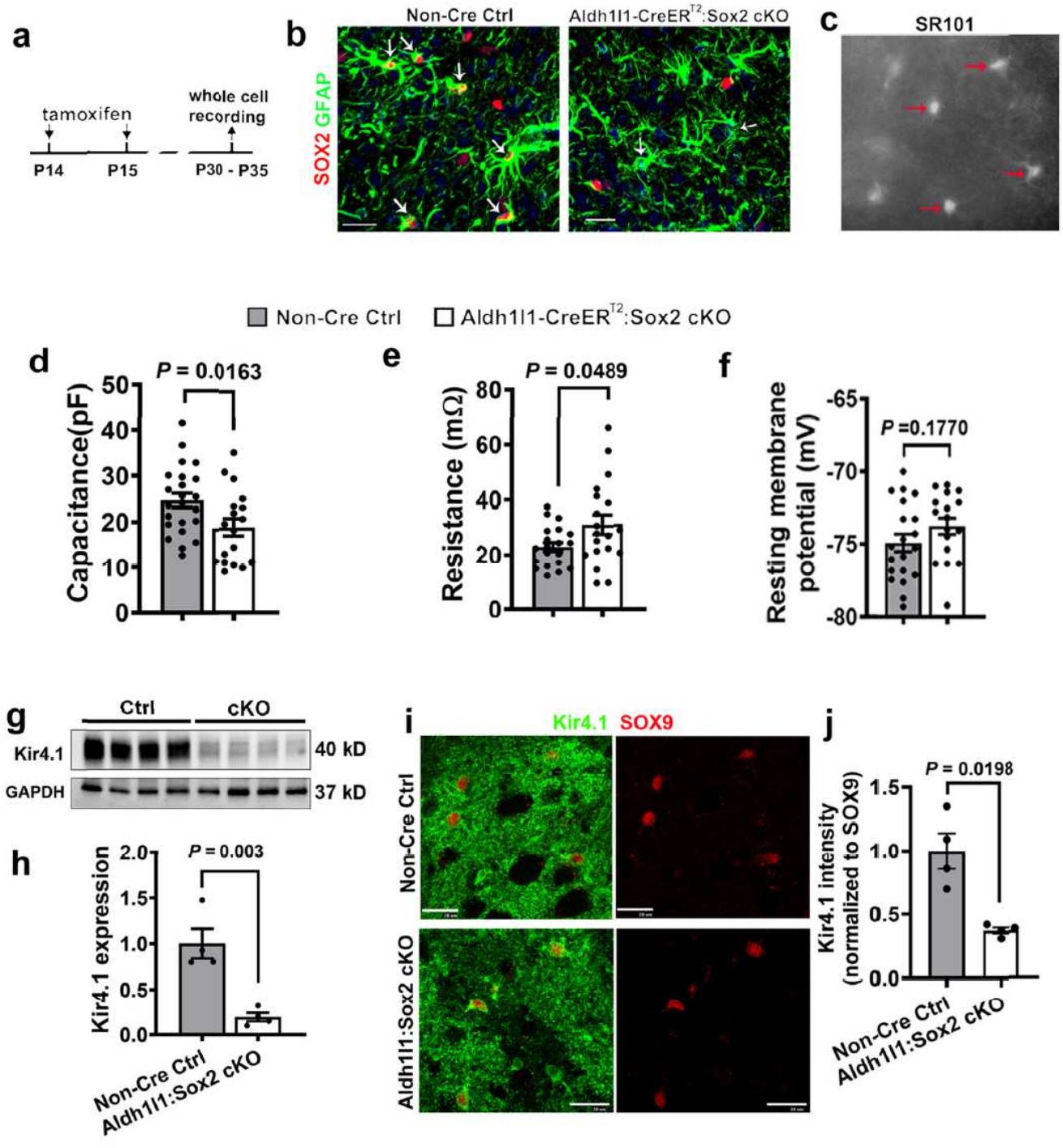

Figure 4

SOX2 disruption impairs astrocyte electrophysiological properties. a, experimental design for b-j. b, double IHC showing that SOX 2 was expressed in GFAP+ astrocytes in the cerebral cortex of non-Cre Ctrl mice and ablated of Aldh1l1:Sox2 cKO mice (arrows). Scale bar = 20 μm. c, cortical astrocytes visualized

by fluorescent dye SR1 01 (arrows) for whole cell recordings. d, cell capacitance of Sox2-deficient and intact cortical astrocytes Two-tailed Student's t test, t(39) = 2.511. e, input resistance of Sox2-deficient and intact cortical astrocytes. Two-tailed Student's t test, Welch's corrected t(25.6) = 2.068. f, resting membrane potential Sox2-deficient and intact cortical astrocytes. Two-tailed Student's t test, t(35) = 1.378. g-h, Western blot assay and quantification of Kir4.1 expression (normalized to the internal loading control GAPDH) in the forebrain of Aldh1l1:Sox2 cKO (n=4) and littermate controls (n=4) at P21 (daily 4-hydroxytamoxifen treatment from P4 through P9). Two-tailed Student's t test, t(6) = 4.792. i-j, representative images and quantification of Kir4.1 intensity (normalized to SOX9 intensity) in the cortex of Aldh1l1:Sox2 cKO (n=4) and littermate controls (n=4) at P21 (daily tamoxifen 4-hydroxytamoxifen treatment from P4 through P9). Two-tailed Student's t test, Welch-corrected t(4.4) = 3.158. Scale bars=20μm.

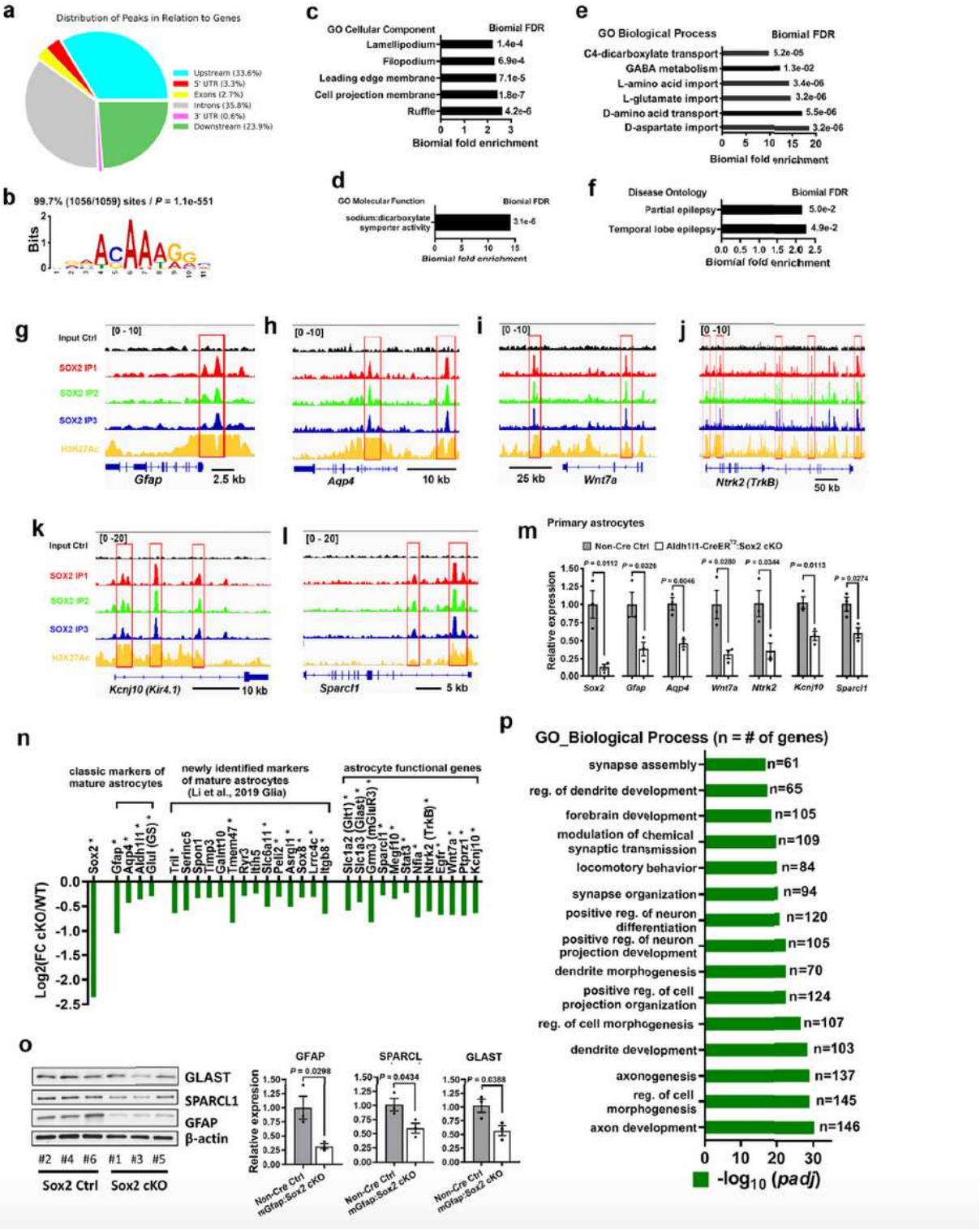

Figure 5

Direct target genes identified by ChIP-seq and transcriptome analysis of SOX2-regulated genes. a, distribution of SO X2 peaks relative to the nearest genes. b, motif enrichment analysis of the top 1059 SOX2-bound sites (Suppl Table 2) showing that 99.7% of the 1059 SOX2-bound regions have the canonical SOX2-binding consensus sequence CAAAG (Table S3). c-e, gene ontology (GO) terms of significantly enriched cellular components (c), molecular function (d), and biological processes (e)

represented by the top1059 SOX2-bound genomic regions. f, overrepresented disease ontology terms of the top1059 SOX2-bound genomic regions. g-l, genomic views showing SOX2 binding and overlapping with epigenetic marker H3K27Ac in the astrocytic genes Gfap, Apq4, Wnt7a, Ntrk2, Kcnj10, and Sparcl1 (a.k.a. Hevin). m, RT-qPCR assays of mRNA expression of the astrocyte signature genes in primary cortical astrocytes (DIV21) isolated from neonatal mGfap:Sox2 cKO and non-Cre control mice. Two-tailed Student's t test, t(4) = 4.453 Sox2, t (4) = 3.210 Gfap, t(4) = 5.723 Aqp4, t(4) = 3.396 Sparcl1, t(4) = 3.372 Wnt7a, t(4) = 3.154 Ntrk2, t(4) = 4.448 Kcnj10. n, RNA-seq identifies representative downregulated genes encoding classic mature astrocytic markers, newly discovered mature astrocytic markers, and key astrocytic functional genes in mGfap:Sox2 cKO spinal cord at P80. Asterisks indicate SOX2-bound downregulated genes (Table S1). Y-axis, fold changes (FC) of relative expression in mGfap:Sox2 cKO compared with non-Cre Ctrl. o, Western blot assay of representative downregulated DEGs GFAP, GLAST, and SPARCL1 in the adult brain of mGfap:Sox2 cKO mice. Two-tailed Student's t test, t(4) = 2.916 SPARCL1, t(4) = 3.304 GFAP, , t(4) = 3.030 GLAST. p, top 15 significantly enriched GO biological process terms of downregulated genes in mGfap:Sox2 cKO spinal cord. The number of downregulated genes in each term is shown at the right. Padj, adjusted P value.

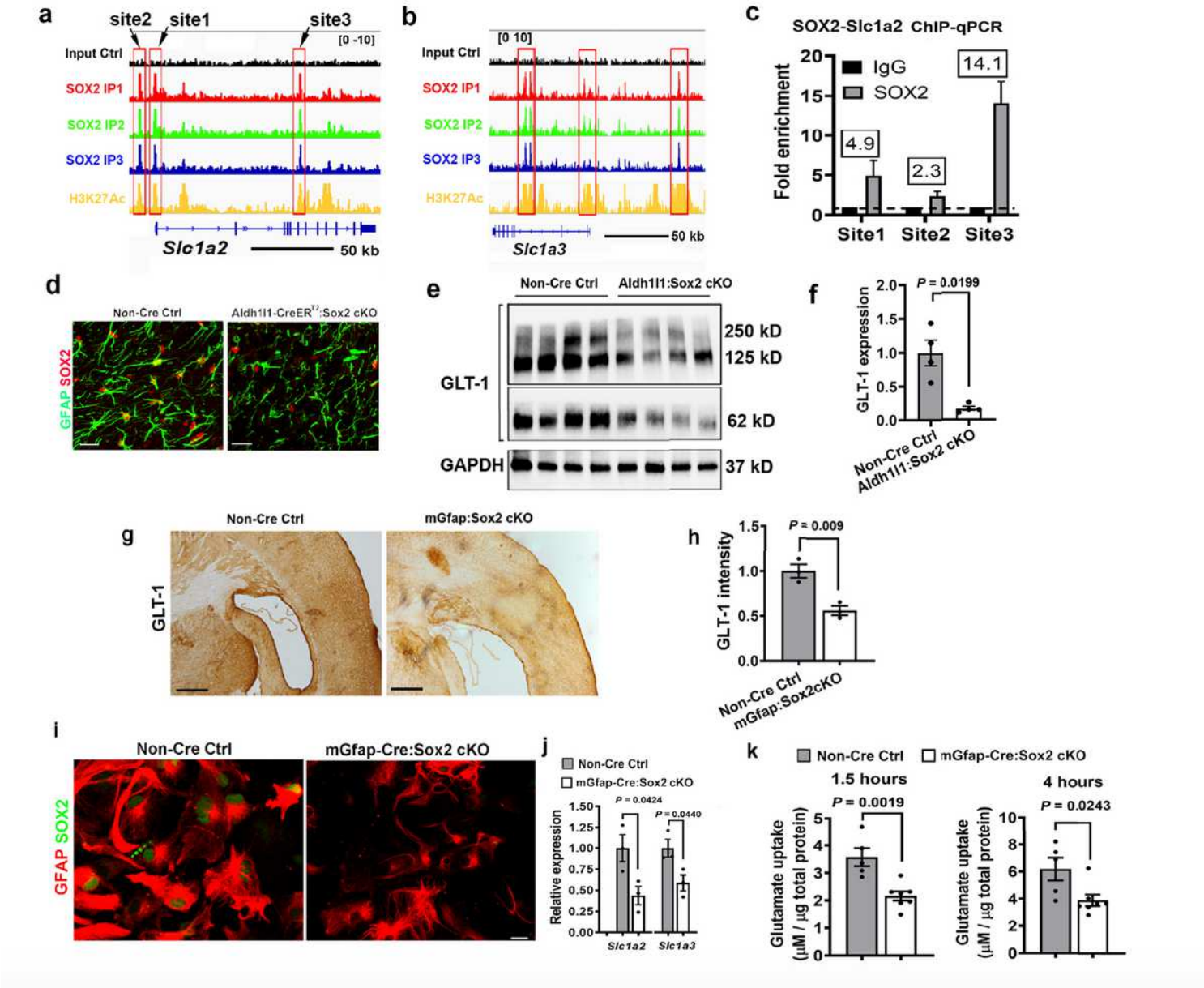

Figure 6

Downregulation of glutamate transporters and impaired glutamate uptake of Sox2-deficient astrocytes. a-b, genomic view of astrocytic glutamate transporter genes Slc1a2 (a) and Slc1a3 (b) and SOX2-binding sites and genomic occupancy of H3K27Ac, an epigenetic marker of active enhancer/promoter. Note that S OX2-bound sites are occupied by H2K27Ac markers. c, qPCR of SOX2 (or IgG Ctrl)-immunoprecipitated chromatin confirmation of the SOX2-binding site 1, 2, and 3 in the enhancer/ promoter and intronic regions of Slc1a2 gene (a). d, IHC showing SOX 2 is disrupt ed in GFAP+ cortical astrocytes in the brain of P 21 Aldh1l1:Sox2 cKO mice which was treated wit h tamoxifen at P4-P9. e-f, representative image of Wes tern blot images (e) and quantification (f) of GL T-1 in P21 brain. The quantification was performed based on 62 kD (monomer), 125 kD (dimer), and 250 kD (tetramer) GLT-1. Gray bar, non-Cre Ctrl, white bar, Ald h1l1:Sox2 cKO. Two-tailed Student's t test with Welch's correction, corrected t(4.3) = 3.193. g-h, representative DAB histological images (g) and quantification (h) of GLT1 in the forebrain of mGfap:Sox2

cKO and non-Cre Ctrl mice. Scale bar=200μm. Two-tailed Student's t test, t(4) = 4.832 i, Representative images of GFAP and SOX2 immunocytochemistry in primary astrocytes at DIV21. j, RT-qPCR assay of Slc1a2 and Slc1a3 in primary astrocytes at DIV21. Two-tailed Student's t test, t(4) = 2.940 Slc1a2, t(4) = 2.915 Slc1a3. k, glutamate uptake at 1.5 h and 4 h after glutamate incubation at DIV21. Two-tailed Student's t test, t(10) = 4.188 at 1.5 h and t(10) = 2.650 at 4 h.

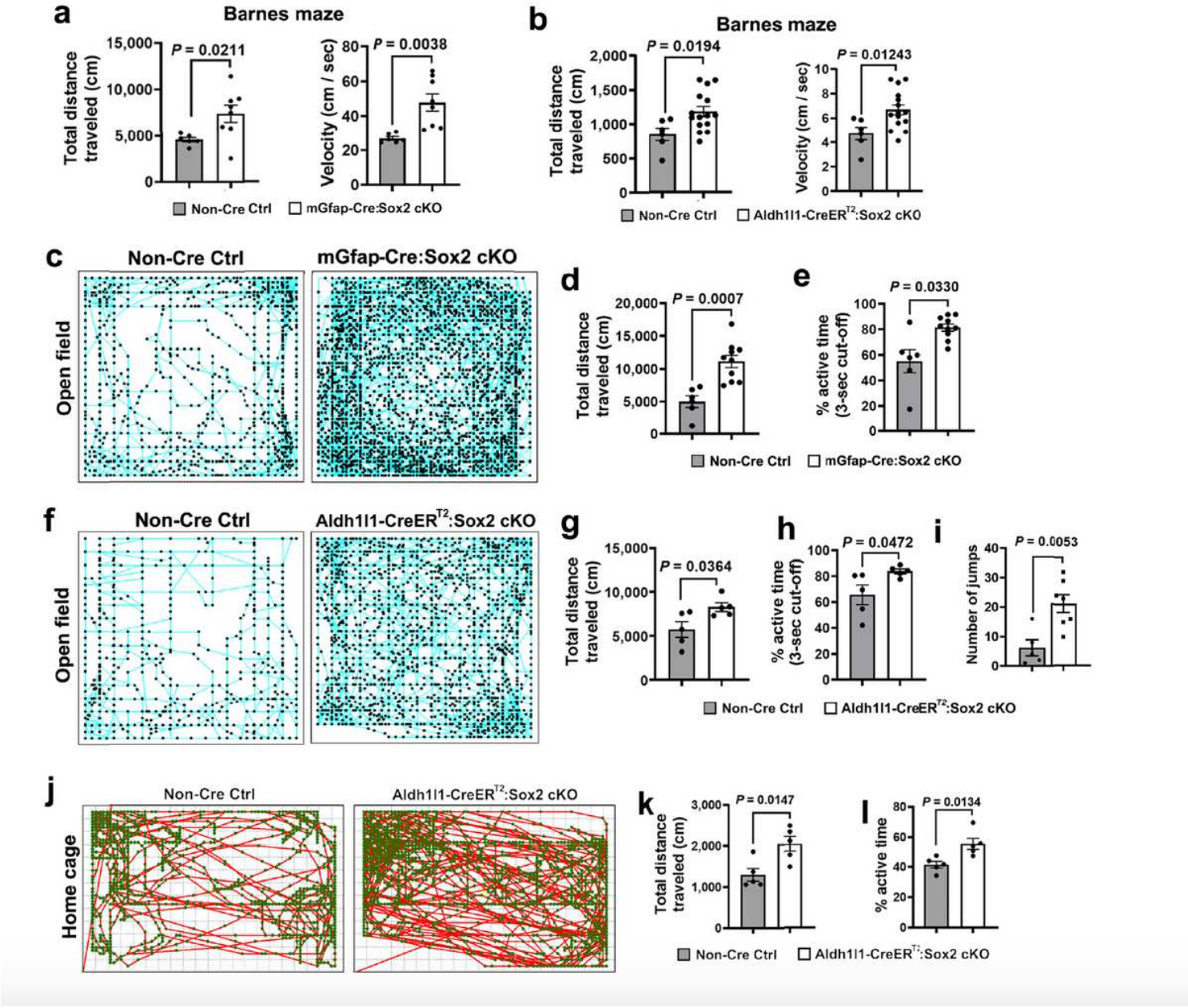

Figure 7

Hyperactivity of astroglial Sox 2-deficient mice. a, total distance traveled (left) and velocity during Barnes maze test. The data was collected on day 6 after 5 consecutive days training. Two months old mGfap:Sox 2 mice and non-Cre control littermate s were used. Two-tailed Student's t test, Welch 's-corrected t(7.9) = 2.873 total distance, Welch's-corrected t(7.6) = 4.097 velocity. b, total distance traveled (left) and movement velocity. T he data was collected on day 6 aft er 5 consecutive days training.

Aldh1l1:Sox2 cK O mice and non -Cre control littermates were treated with tamoxifen to induce SOX2 disruption at P14, P15, and P16 (once a day) and tested on at 2 months old. Two-tailed Student' t test, t(19) = 2.553 total distance, t(19) = 2.695 velocity. c, representative real- time tracing of movement of two-month old non-Cre Ctrl and mGfap:S ox2 cKO mice in the open field. d-e, total distance traveled (d) and percentage (e) of active time in the open field. Two-tailed Student' s t test, t(14) = 4.360 total distance, Welch-correc ted t(6.0) = 2.759 active time. f, representative real-time tracing of movement of two-month old non-Cre Ctrl and Aldh1l1:Sox2 cKO mice in the open field. Tamoxifen was administered at P14, P15, and P16 to induce SOX2 disruption in astrocytes. g-h, total distance traveled (g) and percentage (h) of active time in the open field. Two-tailed Student's t test, t(8) = 2.510 total distance, t(8) = 2.343 active time. i, number of jumps in the open field during 20-minute sessions. Aldh1l1:Sox2 cKO and non-Cre Ctrl littermates were treated with tamoxifen at P14, P15, and P16 and test at two months old. Two-tailed Student's t test, t(10) = 3.545. j-l , representative real-time tracing of animal movement in the home cages (j) and quantification of total distance traveled (k) and percentage of active time (l) during the 20- minute sessions. Aldh1l1:Sox2 cKO and non -Cre Ctrl littermates were treated with tamoxifen at P14, P15, and P16 and test on 2.5-month old. Two-tailed Student's t test, t(8) = 3.097 total distance, t(8) = 3.159 active time.

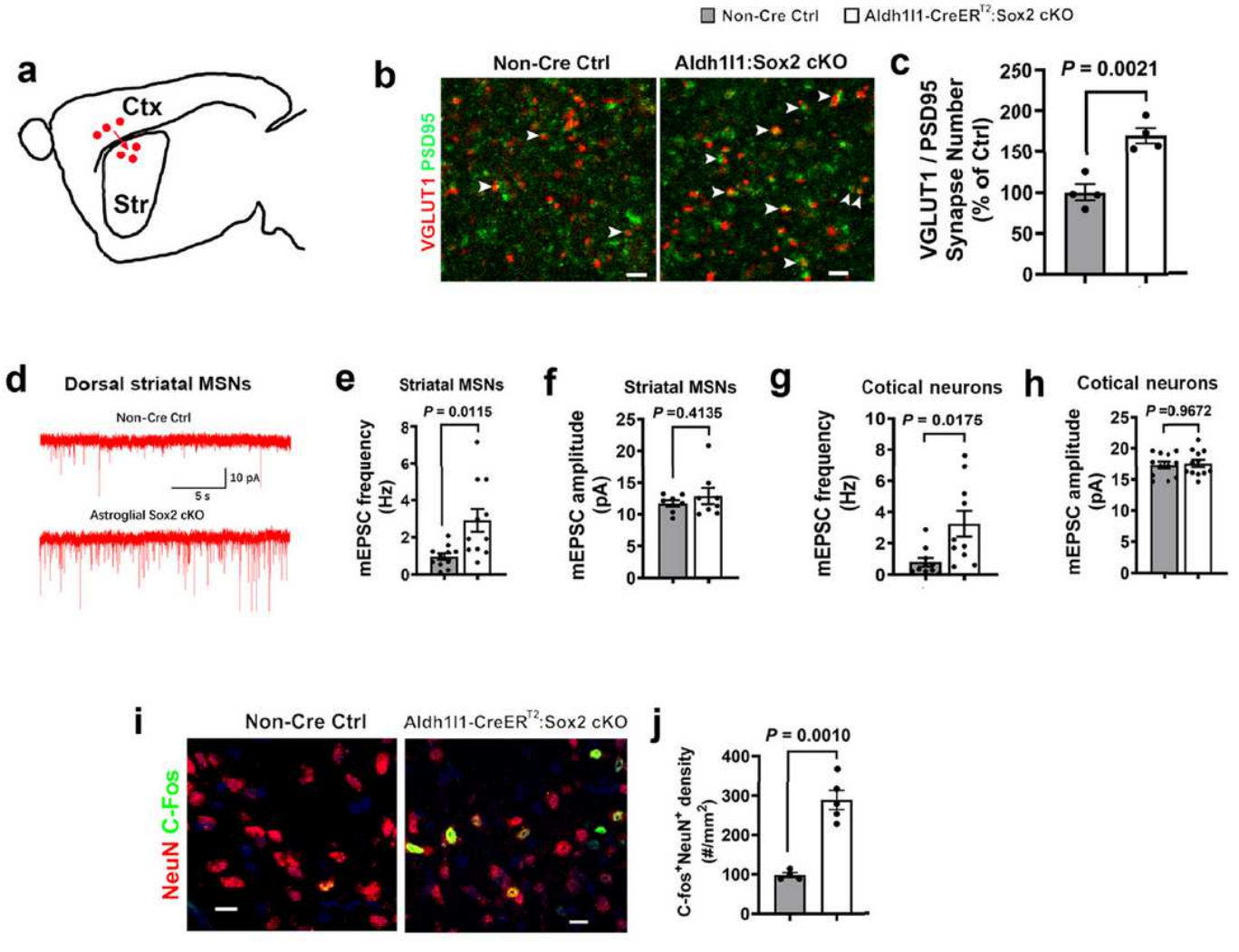

Figure 8

Astroglial Sox2 deficiency results in elevated excitability of neurons in the corticostriatal circuit. a, schematic drawing depicting cotical neuronal projections onto dorsal striatal medium spin al neurons (MSNs) in the corticostriatal circuitry. Ctx, cortex, Str, striatum. b, representative IH C confocal images of presynaptic marker vesicular glutamate transport er 1 (VGLUT 1) and postsynaptic marker PSD95 in the dorsal striatum of 2-month old Aldh1l1:S ox2 cKO and Ctrl mice which had been injected with tamoxifen at P14, P15, and P16 (once a d ay). Arrowheads point to VGLUT1/P SD95 co-labeled puncta. Scale bar= 1 μm. c, VGLUT1/PSD95 c o-labeled puncta density quantified by Puncta Analyzer plug-in of NIH Image J. Two-tailed Student's t test, t(6) = 5. 177. d, current tracing of representative dorsal striatal MSNs from non-Cre Ctrl and Aldh1l1:Sox 2 mice at P 35 (tamoxifen at P15 and P16). e-f, mea n frequency (e) and amplitude (f) of mEPSC of MSNs in the dorsal striatum of astroglial Sox2-deficient mice (white bar) and Sox2 -in tact mice (g ray bar) . Two-tailed Student's t test , Welch-corrected t(11. 6) = 3.001 frequency; Welch-correct ed t(8.9) = 0.8 576 amplitude. g-h, mean frequency (g) and amplitude (h) of mEPSC of the deep layer cortical neurons of astroglial Sox2-deficient mice (white bar) and Sox2 -intact mice (gray bar) . Two-tailed Student's t test, Welch-corrected t(10.99) = 2.793 frequency; t(22) = 0.2997 amplitude. i-j, representative confocal images of neuron marker NeuN and immediate early gene C-Fos (i) and quantification (j) in the dorsal striatum of Aldh1l1:Sox2 cKO and non-Cre Ctrl mice at P21 (hydroxy-tamoxifen at P4-P9). Two-tailed Student's t test, Welch-corrected t(4.48) = 7.554